

Passive Safety Optimization in Liquid Sodium-Cooled Reactors Final Report

Nuclear Engineering Division

About Argonne National Laboratory

Argonne is a U.S. Department of Energy laboratory managed by UChicago Argonne, LLC under contract DE-AC02-06CH11357. The Laboratory's main facility is outside Chicago, at 9700 South Cass Avenue, Argonne, Illinois 60439. For information about Argonne, see www.anl.gov.

Availability of This Report

This report is available, at no cost, at <http://www.osti.gov/bridge>. It is also available on paper to the U.S. Department of Energy and its contractors, for a processing fee, from:

U.S. Department of Energy

Office of Scientific and Technical Information

P.O. Box 62

Oak Ridge, TN 37831-0062

phone (865) 576-8401

fax (865) 576-5728

reports@adonis.osti.gov

Disclaimer

This report was prepared as an account of work sponsored by an agency of the United States Government. Neither the United States Government nor any agency thereof, nor UChicago Argonne, LLC, nor any of their employees or officers, makes any warranty, express or implied, or assumes any legal liability or responsibility for the accuracy, completeness, or usefulness of any information, apparatus, product, or process disclosed, or represents that its use would not infringe privately owned rights. Reference herein to any specific commercial product, process, or service by trade name, trademark, manufacturer, or otherwise, does not necessarily constitute or imply its endorsement, recommendation, or favoring by the United States Government or any agency thereof. The views and opinions of document authors expressed herein do not necessarily state or reflect those of the United States Government or any agency thereof, Argonne National Laboratory, or UChicago Argonne, LLC.

Passive Safety Optimization in Liquid Sodium-Cooled Reactors Final Report

by

J.E. Cahalan¹ and D. Hahn²

¹Nuclear Engineering Division, Argonne National Laboratory

²Korea Atomic Energy Research Institute

December 2005

TABLE OF CONTENTS

	<u>Page</u>
Project Summary.....	1
Project Organization.....	3
Task 1: Computational Methods for Analysis of Passive Safety Design Features.....	5
Research Objective.....	5
Research Progress Overview.....	5
Design Specifications.....	5
Model Interface with SASSYS-1 and SSC-K.....	6
Formulation – Conservation Equations.....	7
Formulation – Constitutive Equations.....	11
Code Implementation.....	15
Code Document.....	15
Code Verification.....	16
Code Archive.....	20
Planned Activities.....	20
Task 2: Comparative Analysis and Evaluation of Innovative Design Features.....	23
Research Objective.....	23
Research Progress Overview.....	23
KALIMER-150 Design and State-of-the-Art Modeling for Baseline Analysis.....	23
Accident Sequences.....	26
Reactivity Feedback Effects.....	27
Baseline Analysis Results.....	27
Enhanced Analysis Application.....	30
Enhanced Safety Design Features.....	33
Planned Activities.....	35
Task 3: Safety Implications of Advanced Technology Power Conversion and Design Innovations and Simplifications.....	37
Research Objective.....	37
Research Progress Overview.....	37
Supercritical CO ₂ Cycle Performance without IHTS.....	37
Heat Exchanger Design.....	40
Pressure Relief System Design.....	42
Coupled KALIMER-150/S-CO ₂ Brayton Cycle Configuration Studies.....	45
Cycle/Plant Efficiency Optimization Study.....	47
Na-CO ₂ Heat Exchanger Design Optimization.....	48

TABLE OF CONTENTS (cont.)

	<u>Page</u>
Overpressure Protection System Development	48
Assessment of HX Failure Consequences	50
Overpressure Protection System Conceptual Design	51
Gas Turbine Performance Analysis	53
Planned Activities	54
Task 4: Post-Accident Heat Removal and In-Vessel Retention	55
Research Objective	55
Research Progress Overview	55
Task 4.1 Test Plan for Measurement of Metallic Fuel Liquidus/Solidus and Mobilization Temperatures	55
Task 4.2 Test Plan for Measurement of Metallic Fuel and Fuel/Steel Alloy Freezing Behavior	58
Task 4.3 Test Plan for Measurement of CO ₂ /Sodium Mixing Consequences in Pool Geometry	63
Planned Activities	66
Project Publications	73
References: Project Technical Reports	74

LIST OF FIGURES

<u>No.</u>		<u>Page</u>
1	Coolant Sub-Channels in a 19 Pin Hex.....	6
2	Sub-Channels Grouped by Row and Sector.....	6
3	Coolant Sub-Channel Variables.....	8
4	Radial Node Structure Used for a Fuel Pin, with Coolant and Structure	10
5	Sub-channel Configuration and Temperature Distribution Along the Elevation	12
6	Comparison of the CFX Data with Analytical Conduction Shape Factor Data	13
7	Comparison of the CFX Data with Existing Correlations on Turbulent Mixing.....	14
8	Results for a Scram with a Delayed Pump Trip.....	17
9	XX09 Instrumentation	18
10	Steady-State Top of Core Coolant Temperatures Across the XX09 Subassembly	18
11	Transient Peak Coolant Temperatures Near the Top of the Core as a Function of Time..	19
12	Lateral Coolant Temperature Distribution Near the Top of the Core at 85 Seconds into the Transient	20
13	Transient Flow Rates in XX09	21
14	KALIMER-150 Conceptual Design	24
15	KALIMER-150 Core Loading Pattern.....	25
16	Unprotected Transient Overpower Accident Power History	28
17	Unprotected Loss of Flow Accident Power and Flow History	28
18	Unprotected Loss-of-Heat-Sink Accident Power History	29
19	Summary of Peak Temperatures Calculated by SASSYS-1 and SSC-K.....	29
20	UTOP Case Power Comparison.....	31
21	UTOP Case Core Radial Expansion Comparison.....	31
22	ULOHS Case Power Comparison.....	32
23	ULOHS Case Control Rod Driveline Expansion Reactivity Comparison.....	32
24	UTOP Radial Expansion Reactivity Feedback for Core Restraint Modification	34
25	UTOP Reactor Power for Core Restraint Modification.....	35
26	UTOP Control Rod Driveline Reactivity Feedback for Core Restraint and CRDL Modification.....	36
27	UTOP Reactor Power for Core Restraint and CRDL Modification	36
28	Schematic Illustration of Temperature and Pressure Conditions for KALIMER-150 Coupled to a Supercritical Carbon Dioxide Gas Turbine Brayton Cycle Power Converter.....	38
29	Design Concepts of Sodium-to-Supercritical CO ₂ Heat Exchanger.....	40
30	Schematic Drawing of SWRPRS for KALIMER-150.....	42
31	Design Concept of Pressure Relief System for BREST-300	43
32	Design Concept of Pressure Relief System for KALIMER-150 without IHTS	44
33	Schematic of S-CO ₂ Brayton Cycle Coupled to KALIMER-150.....	45
34	Cycle Efficiency Dependencies	46
35	T-s Diagram for the Cycle	46
36	IHX Design Comparison.....	47
37	KALIMER-150 Coupled to the S-CO ₂ Brayton Cycle with Optimized HXs	49
38	Temperature Behaviors of SG and OPS	50

LIST OF FIGURES (cont.)

<u>No.</u>		<u>Page</u>
39	System Pressure Behavior with Rupture Disk Set Pressure Variations.....	51
40	Design Concept of Overpressure Protection System for KALIMER-150 Coupled with S-CO ₂ Brayton Cycle Power Conversion System.....	52
41	Pressure Distributions in Axial Locations and Mass Flow Rates and Mach Numbers in Broken Pipe and Drain Pipe.....	52
42	Pressure and Temperature Distribution and Velocity Vectors in 1-Stage Stator and Rotor of Turbine.....	53
43	Performance Curve of a Turbine.....	54
44	Heating and Cooling DTA Curves at 10 K/mm for U-19.5 Pu-3.3 Zr (at. %) Alloy	57
45	Thermal Gravimetric Method for Determination of Mobilization Temperature	57
46	Fuel Melt Freezing and Interaction Apparatus	60
47	Cross-Section of Freezing/Plugging Test Section	61
48	Chemical Interaction Test Section.....	62
49	Schematic of Test Apparatus	64
50	CO ₂ Gas Injection Device.....	64
51	Assembly Drawing of Test Section	65
52	Project Schedule Gantt Chart.....	71

LIST OF TABLES

<u>No.</u>		<u>Page</u>
1	Organization Responsibilities by Task	3
2	KALIMER-150 Design Parameters.....	25
3	Pressure Drops and Required Pumping Power	48
4	Design Summary of Na-CO ₂ Heat Exchanger.....	49
5	Overpressure Protection System Design Summary	53
6	Project Task/Milestone/Deliverable Summary	67

Project Summary

This report summarizes the results of a three-year collaboration between Argonne National Laboratory (ANL) and the Korea Atomic Energy Research Institute (KAERI) to identify and quantify the performance of innovative design features in metallic-fueled, sodium-cooled fast reactor designs. The objective of the work was to establish the reliability and safety margin enhancements provided by design innovations offering significant potential for construction, maintenance, and operating cost reductions. The project goal was accomplished with a combination of advanced model development (Task 1), analysis of innovative design and safety features (Tasks 2 and 3), and planning of key safety experiments (Task 4).

Task 1. Computational Methods for Analysis of Passive Safety Design Features. An advanced three-dimensional subassembly thermal-hydraulic model was developed jointly and implemented in ANL and KAERI computer codes. The objective of the model development effort was to provide a high-accuracy capability to predict fuel, cladding, coolant, and structural temperatures in reactor fuel subassemblies, and thereby reduce the uncertainties associated with lower fidelity models previously used for safety and design analysis. The project included model formulation, implementation, and verification by application to available reactor tests performed at EBR-II.

Task 2. Comparative Analysis and Evaluation of Innovative Design Features. Integrated safety assessments of innovative liquid metal reactor designs were performed to quantify the performance of inherent safety features. The objective of the analysis effort was to identify the potential safety margin enhancements possible in a sodium-cooled, metal-fueled reactor design by use of passive safety mechanisms to mitigate low-probability accident consequences. The project included baseline analyses using state-of-the-art computational models and advanced analyses using the new model developed in Task 1.

Task 3. Safety Implications of Advanced Technology Power Conversion and Design Innovations and Simplifications. Investigations of supercritical CO₂ gas turbine Brayton cycles coupled to the sodium-cooled reactors and innovative concepts for sodium-to-CO₂ heat exchangers were performed to discover new designs for high efficiency electricity production. The objective of the analyses was to characterize the design and safety performance of equipment needed to implement the new power cycle. The project included considerations of heat transfer and power conversion systems arrangements and evaluations of systems performance.

Task 4. Post Accident Heat Removal and In-Vessel Retention. Test plans were developed to evaluate 1) freezing and plugging of molten metallic fuel in subassembly geometry, 2) retention of metallic fuel core melt debris within reactor vessel structures, and 3) consequences of intermixing of high pressure CO₂ and sodium. The objective of the test plan development was to provide planning for measurements of data needed to characterize the consequences of very low probability accident sequences unique to metallic fuel and CO₂ Brayton power cycles. The project produced three test plans ready for execution.

Project Organization

The individual task responsibilities of ANL and KAERI are indicated in Table 1. For Tasks 1 and 2, where ANL and KAERI share both leadership and technical performance responsibilities, each of the activities is planned and executed with a high degree of coordination between the two organizations. For Task 3, ANL and KAERI share the responsibility for execution of activities. ANL leads Task 4, and KAERI actively contributes to all the activities by supplying phenomenological test requirements and reviewing test plans.

Table 1. Organization Responsibilities by Task.

Task No.	Lead	ANL Responsibilities	KAERI Responsibilities
1.0	Joint	Manage ANL modeling effort	Manage KAERI modeling effort
1.1	Joint	Plan project activities, coordinate with KAERI, prepare document contribution. Maintain project definition document.	Plan project activities, coordinate with ANL, prepare document contribution. Maintain project definition document.
1.2	Joint	Specify model design based on US analysis needs, coordinate with KAERI, prepare report contribution.	Specify model design based on Korean analysis needs, coordinate with ANL, prepare report contribution.
1.3	Joint	Formulate model. Write conservation equations, integrate with constitutive relations, design numerical solution strategy.	Formulate model. Write constitutive equations, evaluate correlations, integrate with conservation equations.
1.4	Joint	Specify code architecture and data management for model integration with SAS4A/SASSYS-1.	Specify code architecture and data management for model integration with SSC-K.
1.5	Joint	Implement code modules in SAS4A/SASSYS-1.	Implement code modules in SSC-K.
1.6	Joint	Write code description report	Write code description report
1.7	Joint	Verify code performance	Verify code performance
1.8	Joint	Maintain ANL code archive	Maintain KAERI code archive
2.0	Joint	Manage ANL analysis effort	Manage KAERI analysis effort
2.1	Joint	Plan project activities, coordinate with KAERI, prepare document contribution. Maintain project definition document.	Plan project activities, coordinate with ANL, prepare document contribution. Maintain project definition document.
2.2	Joint	Specify US passive safety design features. Coordinate design selection with KAERI. Prepare contribution to report.	Specify Korean passive safety design features. Coordinate design selection with ANL. Prepare contribution to report.
2.3	Joint	Identify ANL analysis methods. Coordinate analysis modeling assumptions with KAERI. Prepare	Identify KAERI analysis methods. Coordinate analysis modeling assumptions with ANL. Prepare

		contribution to report.	contribution to report.
2.4	Joint	Assemble model input data for ANL analysis.	Assemble input data for KAERI analysis.
2.5	Joint	Identify accident analysis scenarios. Specify evaluation criteria. Coordinate scenario and evaluation criteria selection with KAERI. Prepare contribution to report	Identify accident analysis scenarios. Specify evaluation criteria. Coordinate scenario and evaluation criteria selection with ANL. Prepare contribution to report.
2.6	Joint	Perform baseline analysis	Perform baseline analysis
2.7	Joint	Perform enhanced analyses	Perform enhanced analyses
2.8	Joint	Prepare final report	Prepare final report
3.0	ANL	Manage ANL effort	Manage KAERI effort
3.1	ANL	Assess CO2 system performance	Review ANL results
3.2	ANL	Assess HX design	Review ANL assessment
3.3	ANL	Develop innovative HX design	Develop innovative HX design
3.4	ANL	Develop innovative system des.	Develop innovative system des.
3.5	Joint	Analyze HX failure	Analyze HX failure
3.6	ANL	Prepare annual report (1)	Contribute to annual report
3.7	ANL	Develop analysis computer code	Review ANL code
3.8	Joint	Analyze accident scenarios	Analyze accident scenarios
3.9	Joint	Assess performance upgrades	Assess performance upgrades
3.10	ANL	Prepare annual report (2)	Contribute to annual report
3.11	ANL	Assess HX failure consequences	Review analysis results
3.12	ANL	Analyze plant safety	Review analysis results
3.13	Joint	Identify plant safety upgrades	Identify plant safety upgrades
3.14	ANL	Prepare annual report (3)	Contribute to annual report
4.0	ANL	Manage ANL effort	Manage KAERI effort
4.1	ANL	Fuel/steel mobility test plan	Develop test requirements
4.2	ANL	CAMEL metallic fuel test plan	Develop test requirements
4.3	ANL	CO2/sodium test plan	Develop test requirements

Narrative

Task 1: Computational Methods for Analysis of Passive Safety Design Features

Research Objective

ANL and KAERI collaborate in the planning, management, construction and documentation of the development, implementation and testing of a detailed three-dimensional fuel subassembly thermal-hydraulic model. This model computes steady-state and transient fuel, cladding and coolant temperatures in each fuel pin and coolant sub-channel of the core. Also, coolant flow rates for each sub-channel, lateral flow between adjacent sub-channels, and duct wall temperatures for each flat of each subassembly are calculated. The model provides accurate and reliable data for calculations of reactivity feedbacks and safety margins.

Research Progress Overview

In 2003, ANL and KAERI agreed on Task 1 scope and issued a joint project document [3] defining activities, responsibilities, and schedule (Milestone 1.1). The desired modeling capabilities were documented as a set of design specifications [7] necessary to fulfill the requirements for passive safety design evaluation (Milestone 1.2). In 2004, the mathematical formulation of the model was completed [13], with ANL assuming the responsibility for the conservations equations and KAERI taking the responsibility for developing the constitutive relations (Milestone 1.3). The source code architecture for the model was developed [16] with the flexibility to be easily implemented in the ANL SASSYS-1 code as well as the KAERI SSC-K code (Milestone 1.4). In 2005, model implementation in SASSYS-1 and SSC-K [22] was completed (Milestone 1.5), and a code model documentation report [23] was issued (Milestone 1.6). Model validation and code verification [27] was completed by analysis of the EBR-II SHRT-17 test (Milestone 1.7). The model source code, testing results, and all documentation are maintained in archives at ANL and KAERI (Milestone 1.8).

Design Specifications

The design specifications for the new detailed subassembly thermal hydraulic model were determined jointly by ANL and KAERI. The new model uses a coolant sub-channel treatment similar to that used in COBRA-4C or SUPERENERGY-2. Figure 1 illustrates the sub-channels for a 19 pin subassembly with a triangular array of pins. There are options to either treat every sub-channel, as in Fig. 1, or to group sub-channels by row and sector, as in Fig. 2.

The coolant treatment includes axial coolant flow parallel to the pins and cross flow between sub-channels driven by pressure differences and wire wrap sweeping. Both forced convection and buoyancy-driven natural circulation are handled. There is an option to conserve computer time and reduce computer memory requirements by treating some subassemblies with a detailed sub-channel treatment while other subassemblies are treated in less detail. In addition to a detailed sub-channel analysis within each subassembly, the new model accounts for subassembly-to-subassembly heat transfer by conduction through the subassembly duct walls and through the coolant between subassemblies.

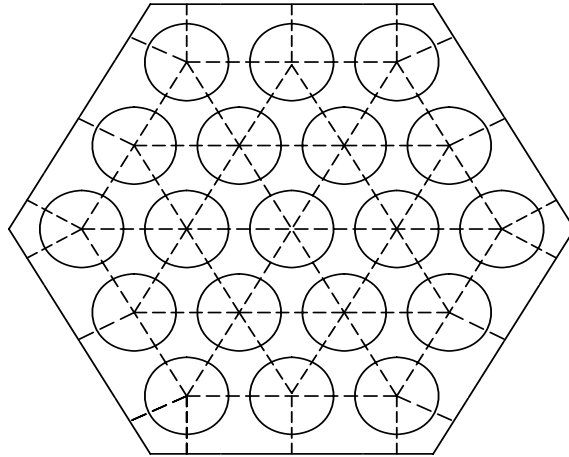


Fig. 1. Coolant Sub-Channels in a 19 Pin Hex.

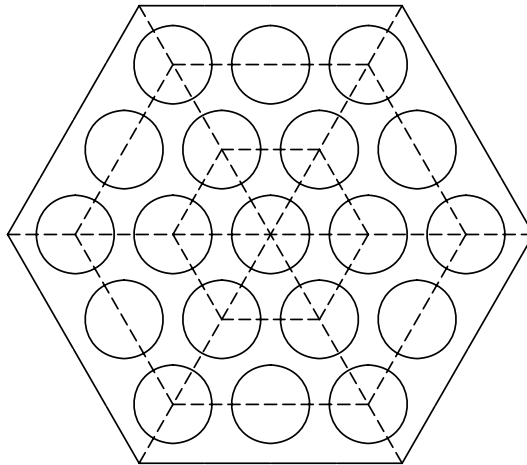


Fig. 2. Sub-Channels Grouped by Row and Sector.

Model Interface with SASSYS-1 and SSC-K

The model was specifically designed for integration into the ANL SASSYS-1 code as well as the KAERI SSC-K code. Although there are some differences between the SASSYS-1 and SSC-K features, the thermal-hydraulic model was developed to satisfy the interface with both of the codes. The interfacing requirements for coupling with modules in the SASSYS-1 code were determined at ANL. These include the input processing, data management, and printed output service modules, and the phenomenological modules that perform analysis of reactor kinetics, reactivity feedback, metallic fuel element performance, and coolant systems thermal hydraulics. The interface data requirements derived by ANL for SAS4A were reviewed by KAERI and additional requirements for SSC-K were suggested. The input/output module for SSC-K was modified. The core thermal-hydraulic model is linked to the SSC-K primary loop model for steady state and transient calculations. The interface requirements were updated in parallel with the modification of the SSC-K code. Integration of the whole-core thermal hydraulic model with the SSC-K code was performed with initial proof testing.

Formulation – Conservation Equations

The basic conservations equations used in the new model include continuity, momentum and energy equations for the coolant. An energy equation is used for the fuel pin. In addition, equations were determined for calculating the pressure driven and the wire-wrap sweeping cross-flow between adjacent coolant sub-channels and for calculating the heat flow between adjacent sub-channels due to turbulent mixing and thermal conduction.

Figure 3 shows the main coolant sub-channel variables used in the model for an axial node. As indicated in Fig. 3 the main coolant variables are:

- \bar{p}_{ji} = coolant pressure at the middle of node j in channel I,
- \bar{T} = average coolant temperature for the node,
- w_{ji} = coolant flow rate in the axial direction at the bottom of node j in sub-channel I,
- w_{Ljik} = lateral flow rate from sub-channel I to sub-channel k at node j,
- z_j = axial location at the bottom of node j.

The basic continuity equation for the coolant in an axial node of a sub-channel is

$$\frac{d}{dt}(\bar{\rho}_{ji} A_{ji} \Delta z_j) = w_{ji} - w_{j+1,i} - \sum_k w_{Ljik} \quad (1)$$

The coolant momentum equation is

$$\begin{aligned} \frac{1}{2} \left(\frac{\Delta z_j}{A_{ji}} + \frac{\Delta z_{j-1}}{A_{j-1,i}} \right) \frac{dw_{ji}}{dt} = & \bar{p}_{j-1,i} - \bar{p}_{ji} - \Delta p_{fji} - \frac{w_{ji} |w_{ji}| K_{orji}}{2 \rho_{ji} A_{ji}^2} - \rho_{ji} g (\Delta z_j + \Delta z_{j-1}) / 2 \\ & - \frac{w_{ji}^2}{\rho_{ji} A_{ji}^2} + \frac{w_{ji}^2}{\rho_{ji} A_{ji}^2} - \frac{w_{ji}^2}{\rho_{ji} A_{j-1,i}^2} + \frac{w_{j-1,i}^2}{\rho_{j-1,i} A_{j-1,i}^2} - \frac{1}{2} \sum_k [(1 - S_{wjik}) w_{Ljik} \left(\frac{w_{jk}}{\rho_{jik} A_{ji} A_{jk}} \right. \\ & \left. - \frac{w_{ji}}{\rho_{jik} A_{ji}^2} \right) + (1 - S_{wj-1,ik}) w_{Lj-1,ik} \left(\frac{w_{j-1,k}}{\rho_{j-1,ik} A_{j-1,i} A_{j-1,k}} - \frac{w_{j-1,k}}{\rho_{j-1,ik} A_{j-1,i}^2} \right)] \end{aligned} \quad (2)$$

The energy equation for the coolant is

$$\begin{aligned} V_{cji} C_{prefji} \frac{d}{dt} [\bar{\rho}_{ji} (\bar{T}_{ji} - T_r)] = & \sum_{in} w_{inji} (T_{inji} - T_r) C_{prefji} - \sum_{out} w_{outji} (T_{out} - T_r) C_{prefji} \\ & + \phi_{ji} \end{aligned} \quad (3)$$

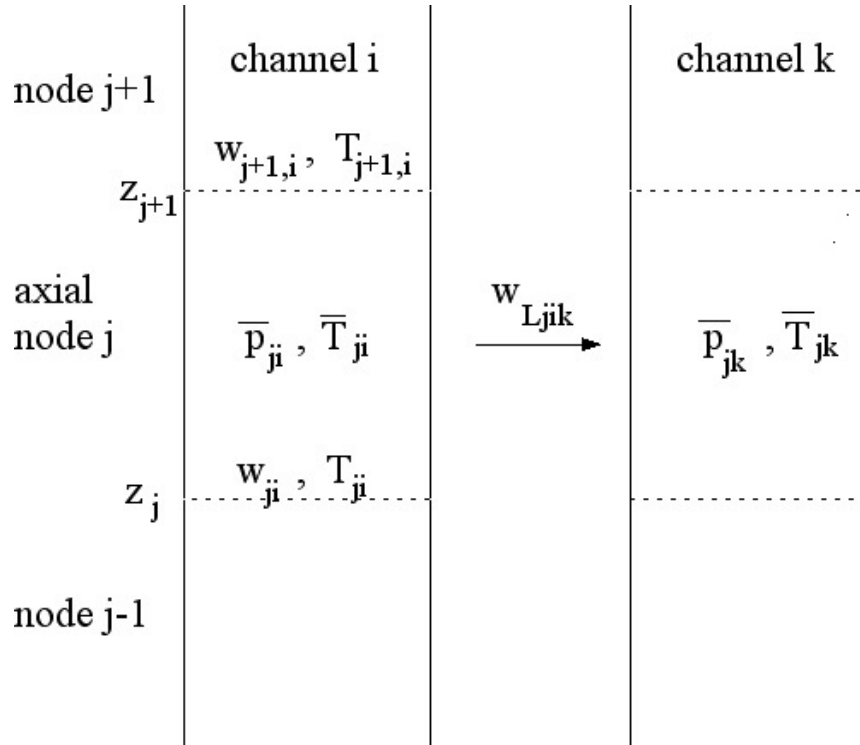


Fig. 3. Coolant Sub-Channel Variables.

The energy equation in the fuel is

$$\rho_f C_f \frac{dT_f}{dt} = \frac{1}{r} \frac{d}{dr} \left(k_f r \frac{dT_f}{dr} \right) + Q \quad (4)$$

A similar equation is used for the cladding, and a bond gap conductance is used between the fuel outer surface and the cladding inner surface. In the above equations:

- A = coolant flow area in the sub-channel
- C_f = heat capacity of the fuel
- C_{pref} = coolant heat capacity, evaluated at T_r
- g = acceleration of gravity
- I = sub-channel number
- j = axial node number
- k = sub-channel number of a connecting sub-channel
- k_f = fuel thermal conductivity
- K_{or} = orifice coefficient
- Δp_{fji} = friction pressure drop in the bottom half of node j and the top half of node j-1
- Q = heat source per unit volume in the fuel
- $S_{wjik} = 1$ if $w_{jik} \geq 0$,
- $= 0$ otherwise

t = time
 T_f = fuel temperature
 T_{in} = temperature of coolant entering the node, either from another axial node in the same sub-channel or from a connecting sub-channel
 T_{out} = temperature of coolant leaving the node
 T_r = reference temperature. \bar{T} at the beginning of the time step is used for T_r .
 V_c = coolant volume in the axial node
 Z = axial distance
 ρ_j = coolant density at the bottom of node j
 $\bar{\rho}_j$ = coolant density at the middle of node j
 ρ_f = fuel density
 ϕ_{ji} = heat source to the coolant node

$$\phi_{ji} = \phi_{cji} + \phi_{\gamma ji} + \phi_{scji} + \phi_{chchji} \quad (5)$$

ϕ_{cji} = heat source from the cladding and structure surfaces to the coolant
 $\phi_{\gamma ji}$ = direct heat source to the coolant from neutrons and gamma rays
 ϕ_{scji} = heat source from turbulent mixing and conduction from adjacent sub-channels
 ϕ_{chchj} = heat source to the coolant from channel-to-channel heat transfer

Also,

$$\phi_{scji} = \sum_k [u_{1ik} k_j + u_{2ik} C_j (\bar{w}_{ji} + \bar{w}_{jk})] (\bar{T}_{jk} - \bar{T}_{ji}) \quad (6)$$

where

u_{1ik} = geometry factor for conduction from sub-channel i to sub-channel k
 u_{2ik} = turbulent mixing factor

The coolant lateral flow rate is given by

$$w_{Ljik} = K_{sik} \frac{(w_{ji} + w_{j+1,i})}{2} + w_{Lpjik} \quad (7)$$

K_{sik} = wire wrap sweeping factor

In this equation the first term is the net flow due to wire wrap sweeping, and the second term is the pressure driven sub-channel to sub-channel flow. Note that $K_{sik} = 0$ unless there is net sweeping from sub-channel i to sub-channel k . For a gap between an inner sub-channel and another inner sub-channel or between an inner sub-channel and an edge sub-channel there are

For an interior fuel node, $1 < I < NT$, the conduction equation (Equation 4) becomes:

$$m_{fi} C_{fi} \frac{dT_{fi}}{dt} = 2\pi r_{i+1} \bar{k}_{i,i+1} (T_{i+1} - T_i) + 2\pi r_i \bar{k}_{i-1,i} (T_{i-1} - T_i) + Q_i \quad (10)$$

where

m_{fi} = fuel mass per unit height in node i

Q_i = heat source per unit height in node i

$\bar{k}_{i,i+1}$ = effective average thermal conductivity for heat flow from node i to $i+1$

Similar equations are used for node 1, for node NT and for the cladding.

Formulation – Constitutive Equations

Thermal Conduction Model

One of the critical parameters determining the thermal-hydraulic behavior of coolant in the sub-channels is the heat conduction between two neighboring sub-channels. This portion of heat transfer becomes more important when the flow rate is very low in case of such as a loss of flow accident. Detailed analyses were performed at KAERI with the CFX code to determine a correlation that could be applied in the new model formulation to account for local heat flux effects. The local heat flux due to conduction through the gap in the control volume is described as follows:

$$q''_{cond,local} = k \left(\frac{\Delta T}{\Delta x} \right)_S, \quad (11)$$

where S is the gap size between the sub-channels, and k is the thermal conductivity. In the existing sub-channel codes, the heat conduction through the coolant is approximated with the channel average temperature and the channel center-to-center distance as the characteristic length. That is,

$$q''_{cond,approx} = C \frac{k}{L_c} (\bar{T}_1 - \bar{T}_2), \quad (12)$$

where C is a factor correcting the difference between the local heat flux and the heat flux based on the average temperature. L_c is the centroid distance between two adjacent sub-channels.

The value of the correction factor, C , is usually selected arbitrarily by the code users based on their own judgments. However, it is reasonable to determine this factor considering the influence of physical parameters. Therefore, it is meaningful to generate an advanced thermal conduction model including the dependency on material properties and/or the channel geometries. The latest version of CFX 5.6 is used for the calculation. Typical triangular sub-channel geometry with 50 cm of length is constructed. The gap size is 1.5 mm and the centroid distance between the sub-channels is 5.1384 mm. Water is selected as a fluid flowing the sub-channels. Figure 5 depicts the channel geometry used in the simulation. The temperature difference between the sub-

channels is 70 K. The inlet temperature for sub-channel 1 (left side) and sub-channel 2 (right side) are 363 K and 293 K, respectively.

When one simulation for a certain fluidic condition is completed, the elevation of concern is selected and two surfaces against the gap between two sub-channels at that elevation are constructed. These surfaces are used to get the average temperatures. To calculate the local heat flux through the gap, S , much effort is exerted to extract useful data from CFX prediction results. At first, one imaginary line is constructed along the x-coordinate in Fig. 5 at a certain point of the y-coordinate and channel elevation, z-coordinate. Then, the local temperature distribution along the line shown in Fig. 5 is exported as a data file. Repeating this procedure, the gap averaged local heat flux can be obtained.

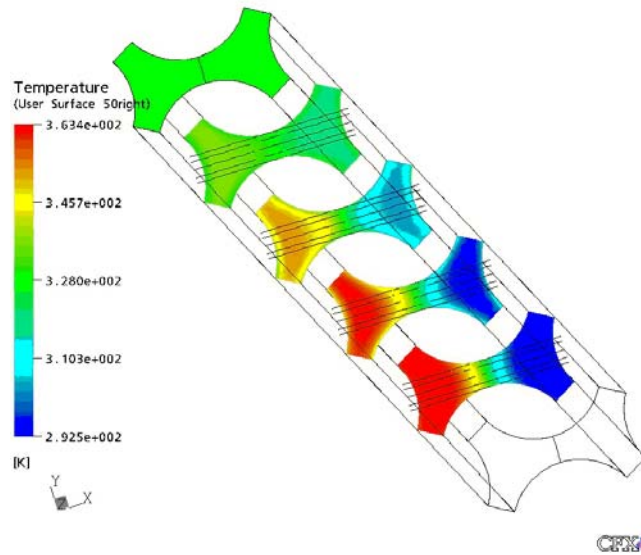


Fig. 5. Sub-channel Configuration and Temperature Distribution Along the Elevation.

Through the studies during the first year of the program, the analysis methodology was prepared and a sample calculation was completed to get the correction factor data. The data for various Reynolds numbers, temperature differences, and channel elevations are incorporated into a well-formulated correlation, which is applicable for the coolant and geometry of concern.

The CFX code calculations have been performed at KAERI and a correlation is suggested, which is applicable to the new model formulation to account for local heat flux effects in the gap between two subchannels. Figure 6 compares the evaluated data with the previous analytical data of the conduction geometry factor.

The CFX data of conduction geometry factor is best correlated with the following equations:

$$u_{1ik} = 0.7774 \left(\frac{s}{L_c} \right) \left(\frac{P}{D} \right) \left(\frac{s}{D} \right)^{-0.2627} \quad (13)$$

where

s = gap size between subchannels

L_c = centroid distance between subchannels.

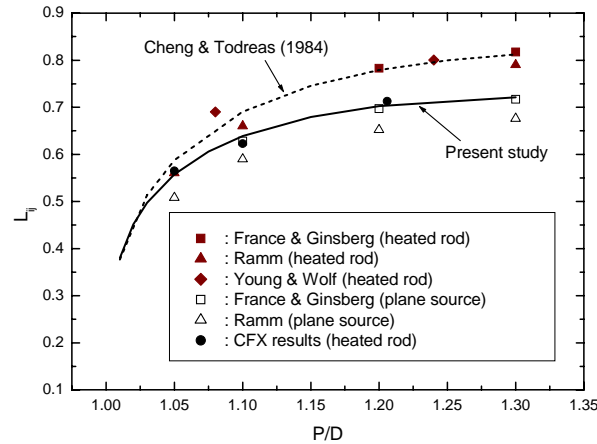


Fig. 6. Comparison of the CFX Data with Analytical Conduction Shape Factor Data.

Turbulent Mixing Model

The turbulent mixing between the sub-channels affects directly the momentum transfer and heat transfer, thus, the overall temperature distribution in the sub-channels. In most traditional sub-channel codes, the turbulent mixing is highly dependent on user input selection. In the present activity, data for turbulent mixing coefficient are generated from CFX calculation and the accuracy of existing mixing models is evaluated based on the data.

Usually, the turbulent mixing flow rate through the interface of the subchannels is defined using the turbulent mixing coefficient, β as follows:

$$W' = \rho u_{eff} S_{ij} \equiv \beta S_{ij} \bar{G}. \quad (14)$$

where W' is the mixing flow rate per unit length between two subchannels through the gap S_{ij} , and \bar{G} is the average axial mass flux flowing along the subchannels. The effective mean mixing velocity is denoted as u_{eff} . Therefore, the turbulent mixing coefficient means the ratio of effective mean velocity to axial velocity. This mixing coefficient is essentially the same as the gap Stanton number, St_g , defined as follows:

$$St_g \equiv \frac{Q_{ij}}{c_p \Delta T S_{ij} \bar{G}}, \quad (15)$$

where Q_{ij} is the heat rate due to turbulent mixing per unit length through the gap, S_{ij} .

Now, to obtain the turbulent mixing coefficient it is required to calculate the heat rate due to turbulence mixing. This heat rate is evaluated from the total heat transfer rate calculated from

CFX results considering the heat balance. Then, the heat flux through the gap is expressed as follows:

$$q''_{tot} = Q_{tot} / (S \cdot 2\Delta z), \quad (16)$$

where Δz is the infinitesimal axial length for which the total heat rate has been evaluated. Then, we can calculate the turbulent mixing heat flux by subtracting the conduction heat flux from total heat flux as follows:

$$q''_{turb,mix} = q''_{tot} - k \frac{\Delta T}{\Delta x}. \quad (17)$$

Now, the heat rate due to turbulence mixing through the gap S_{ij} can be evaluated as follows:

$$Q_{ij} = q''_{turb,mix} \cdot S \quad (18)$$

The turbulent mixing coefficient is determined by comparing the turbulent mixing heat rate with the axial heat rate as follows:

$$\beta = \frac{q''_{turb,mix}}{\bar{c}_p \bar{G} \Delta T} = \frac{q''_{turb,mix}}{\bar{c}_p \bar{\rho} \bar{v} \Delta T}. \quad (19)$$

The data obtained from the CFX calculation lie within the reasonable ranges of other experimental data at higher P/D ratio. However, CFX underestimates the turbulent mixing at lower P/D ratio due to the lack of anisotropic component of turbulence as shown in Fig. 7. The effect of wire-wrap spacer on turbulent mixing is not included in the present assessment because it is not possible to differentiate the mixing flow due to turbulence from the diversion flow generated directly by the existence of wire-wrap.

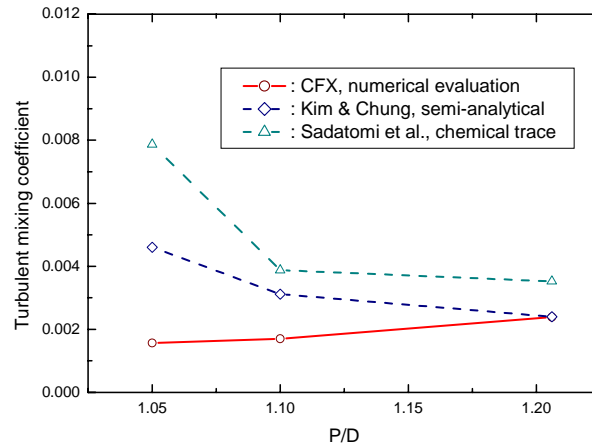


Fig.7. Comparison of the CFX Data with Existing Correlations on Turbulent Mixing.

Judging from the above results, the direct application of CFX results to predict the turbulent mixing in rod arrays is not appropriate. Therefore, the most accurate turbulent mixing model is suggested for the use in the three-dimensional thermal-hydraulic model to exclude the user dependency. Through the evaluation of existing correlations of turbulent mixing it is recommended that the following correlation suggested by Kim and Chung (S. Kim and B. J. Chung, "A Scale Analysis of the Turbulent Mixing Rate for Various Prandtl Number Flow Fields in Rod Bundles," *Nucl. Eng. Des.*, Vol. 205, pp. 281-294, 2001) is the most appropriate to model the turbulent mixing in subchannel flow of liquid metal:

$$u_{2ik} = \left[St_{g,IT} + St_{g,FP} \right] \frac{S}{(A_{ji} + A_{jk})}, \quad (20)$$

where $St_{g,IT}$ and $St_{g,FP}$ are the mixing due to an isotropic turbulence and the mixing from a periodic flow pulsation, respectively, which are expressed as follows:

$$St_{g,IT} = \frac{2}{\gamma^2} \sqrt{\frac{\alpha}{8}} \frac{D_h}{S_{ij}} \frac{1}{Pr} \frac{S_{ij}}{b\delta} Re^{-\beta/2} \quad (21)$$

$$St_{g,FP} = \frac{2}{\gamma^2} \sqrt{\frac{\alpha}{8}} \frac{D_h}{S_{ij}} \cdot a_x \cdot \frac{z_{FP}}{d} \cdot Str \cdot Re^{-\beta/2} \quad (22)$$

The definitions of the variables are found in the work of Kim and Chung.

Code Implementation

Implementation of the advanced three-dimensional model in the SASSYS-1 codes was completed in June, 2005 (Milestone 1.5). Preliminary testing of the implementation was completed through construction and execution of two nineteen-pin subassembly test problems. The test problems were designed with power skews across the subassemblies and heat transfer through the hexcan walls of adjoining flats. The results of the implementation testing indicated that all modeling features were operating as designed.

The advanced three-dimensional model was also implemented in the SSC-K code (Milestone 1.5). The momentum, energy and reactivity calculation routines of detailed core sub-channel model were coupled with those of SSC-K code. Preliminary testing of the implementation was performed through the steady-state calculation of two nineteen-pin subassembly test problem. The results of the testing indicated that all modeling features were operating as designed. Transient calculation of the test problem is being performed, which will complete the implementation and testing.

Code Document

A detailed code documentation report was prepared and issued, fulfilling the requirement for Milestone 1.6. The report includes a description of modeling features, both in words and in

detailed mathematical formulations. The numerical procedures used to obtain solutions are described. Interfaces with other code models are described, including connections to the input and output data routines, the coolant loops thermal-hydraulics model, the reactivity feedback and reactor kinetics model, and the fuel pin mechanics model. The model data management techniques and a source code architecture overview are described to aid future additions and modifications. The report also contains a detailed user's guide, including descriptions of required computer capabilities, overview of the flexible modeling techniques available, input preparation, and output data with an example problem. A detailed input data description is also provided.

KAERI revised the code document report including the description of detailed constitutive relations for the subassembly model. More information related to the modified SSC-K code have been added, which describe the modeling features, numerical procedures, interfaces with other models, data management techniques, detailed user's guide and detailed input data description.

Code Verification

Code verification and model validation activities proceeded with construction and execution of multiple test problems. These activities fulfilled the requirements for Milestone 1.7, Code Verification.

Figure 8 shows output from a sample problem run with the new model. This test case uses two 19 pin subassemblies with subassembly-to-subassembly heat transfer between them. Coolant temperatures from one of the subassemblies are shown in Figure 8. The transient was a simulated scram with a delayed pump trip and little natural circulation head in the primary loop. Temperatures drop rapidly due to the scram and then rise after the pump trip until enough buoyancy is established in the subassemblies to increase the flow rate and stop the temperature rise. Flow reversal occurred in the center sub-channels from 22.5 seconds to 83.5 seconds in the transient. Flow reversal occurred in the edge sub-channels from 22.0 seconds to 111.25 seconds.

The case described above used two subassemblies, each containing 19 pins and 42 coolant sub-channels in the pin section. Four axial nodes were used in a lower reflector below the pin section, 24 axial nodes were used in the core, 6 axial nodes were used in the gas plenum region above the core, and 5 axial nodes were used in a reflector above the pins. A null transient of 50 steps with a time step of 1.0 second was used for each subassembly separately. Then a 50 step null transient using both subassemblies and subassembly-to-subassembly heat transfer was run with a time step of 0.5 seconds. Finally the regular transient was run for 1200 steps using a time step of 0.25 seconds. The null transients started with 35 iterations per step and got down to 2 iterations per step as they converged on a steady-state solution. The regular transient required between 12 and 21 iterations per step. The total running time was 867 seconds on a Sun Blade computer with a 500 MHz processor.

Code verification activities continued with the construction and execution of simulation of the Shutdown Heat Removal Test 17 (SHRT-17) performed in the EBR-II reactor at Argonne National Laboratory-West (H. P. Planchon, et al., "The Experimental Breeder Reactor II Inherent Shutdown and Heat Removal Tests – Results and Analysis," *Nucl. Eng. Des.*, Vol. 91, pp. 287-

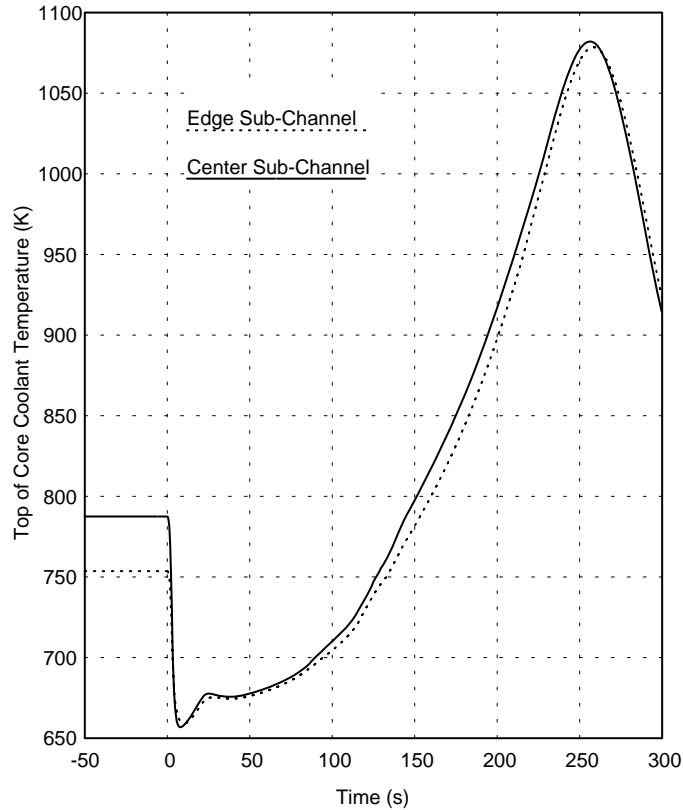


Fig. 8. Results for a Scram with a Delayed Pump Trip.

296, 1986). SHRT-17, one of a series of EBR-II tests conducted to demonstrate passive safety characteristics of sodium-cooled reactors, was a simulation of a protected loss-of-flow accident.

For the purpose of validating the sub-channel model, the most useful information from this test is the flow meter data and the detailed thermocouple data from the instrumented subassembly XX09 in the core. XX09 was a driver subassembly in which many of the wire wrap spacers on the fuel pins were replaced by thermocouple leads. The thermocouples were placed in the coolant near the cladding at the locations shown in Fig. 9. Two electromagnetic flow meters were placed in series below the fuel pins.

The whole EBR-II core was modeled for SASSYS-1 calculations. Also, the whole primary heat transfer loop and the intermediate heat transfer loop were modeled. For XX09 and its six neighbors a detailed representation was used. For these subassemblies every coolant sub-channel and every fuel pin were modeled. Also, the XX09 thimble flow region, as shown in Fig. 9, was included in the model. The other subassemblies in the core were modeled with single channel representations. Axially, 15 nodes were used for the fuel region, 6 nodes were used for the gas plenum region, 7 nodes were used for the axial shield region below the fuel pins, and 11 nodes were used for the axial shield region above the fuel pins.

The calculated and measured steady-state coolant temperatures at the TTC locations near the top of the core in a line going diagonally across the XX09 subassembly are shown in Fig. 10. The

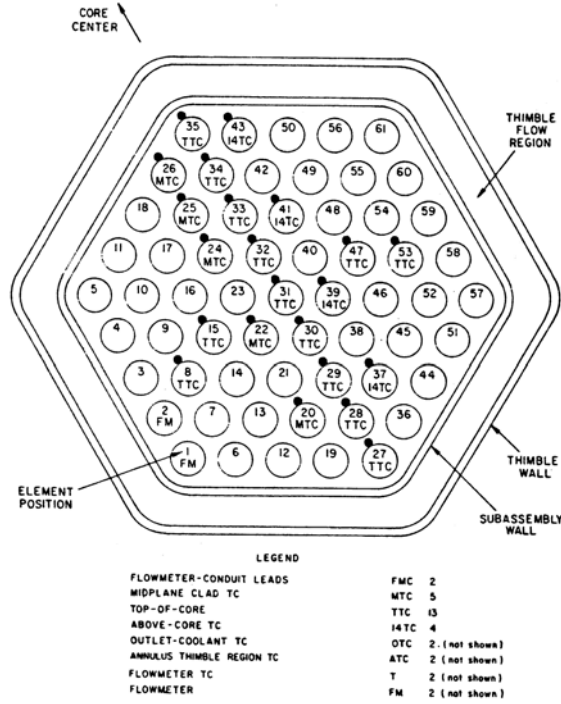


Fig. 9. XX09 Instrumentation.

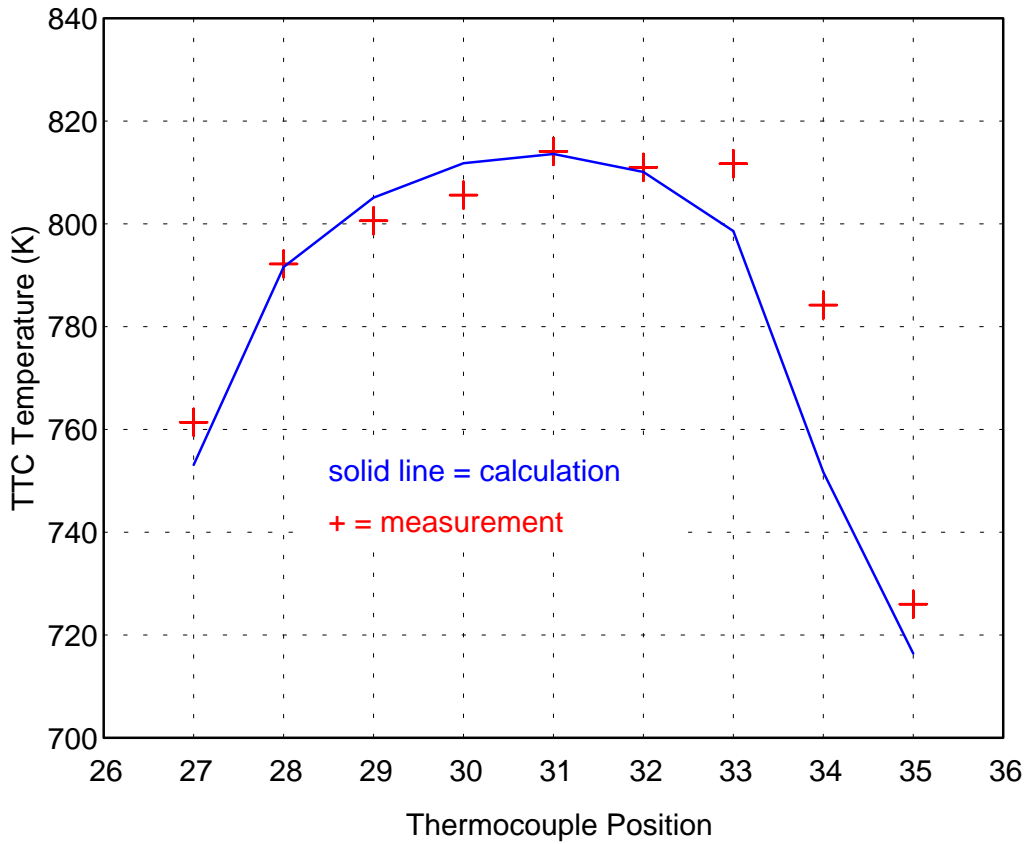


Figure 10. Steady-State Top of Core Coolant Temperatures Across the XX09 Subassembly.

Agreement between measured and calculated temperatures is quite good, but the results demonstrate the difference between the idealized perfectly spaced pins in the calculations and the actual imperfect pin spacing in the reactor. In an irradiated subassembly the wire wrap spacers or thermocouple leads tend to hold the pin spacing near the design value, but duct wall bowing, pin bowing, thermal expansion and irradiation swelling tend to distort the coolant channels and coolant temperature distributions to some extent.

Transient peak coolant temperatures near the top of the core as a function of time are shown in Fig. 11. After the control rods scram at time zero the power drops very rapidly, leading to a rapid drop in coolant temperature. Then, as the pumps coast down and stop the flow rate drops, leading to higher coolant temperatures until natural circulation heads build up and increase coolant flow rates, leading to a drop in coolant temperatures. The calculated and measured coolant temperatures are almost identical during the pump coast-down phase of the transient. Later in the transient the calculated and measured temperatures still agree well, although the measured peak near 75 seconds is somewhat higher than the calculated peak.

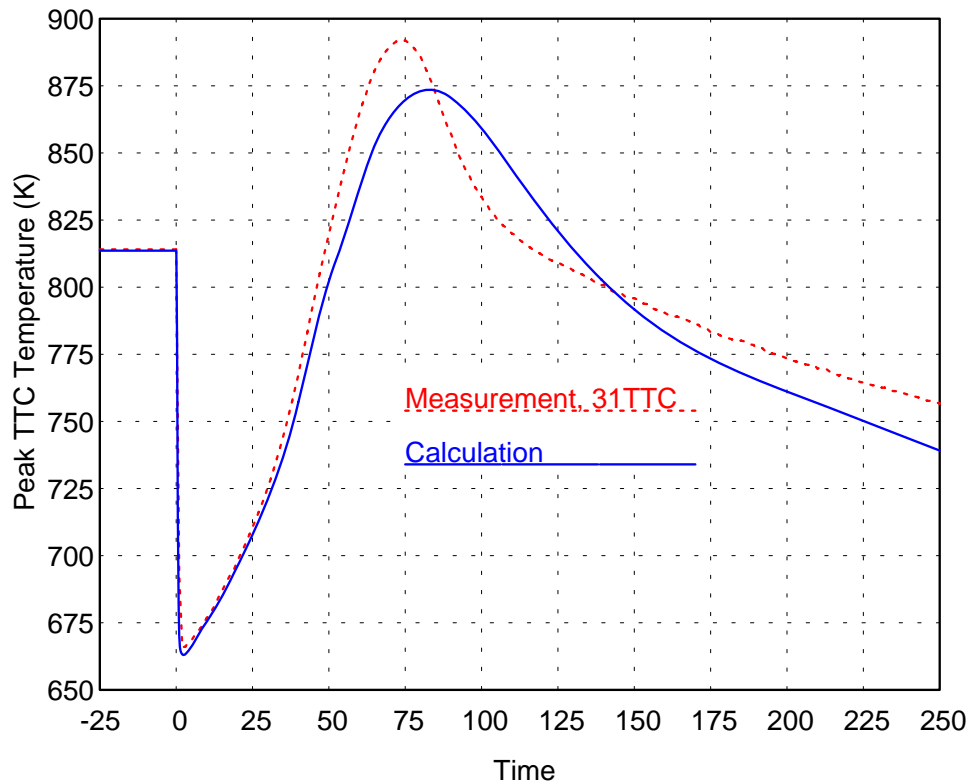


Fig. 11. Transient Peak Coolant Temperatures Near the Top of the Core, as a Function of Time.

The lateral coolant temperature profile near the top of the core at 85 seconds into the transient is shown in Fig. 12. Agreement between measured and calculated temperatures in this figure is good, although these results indicate that at low flow rates the calculated lateral heat flow to the thimble flow region and the neighboring subassemblies may be somewhat over-estimated.

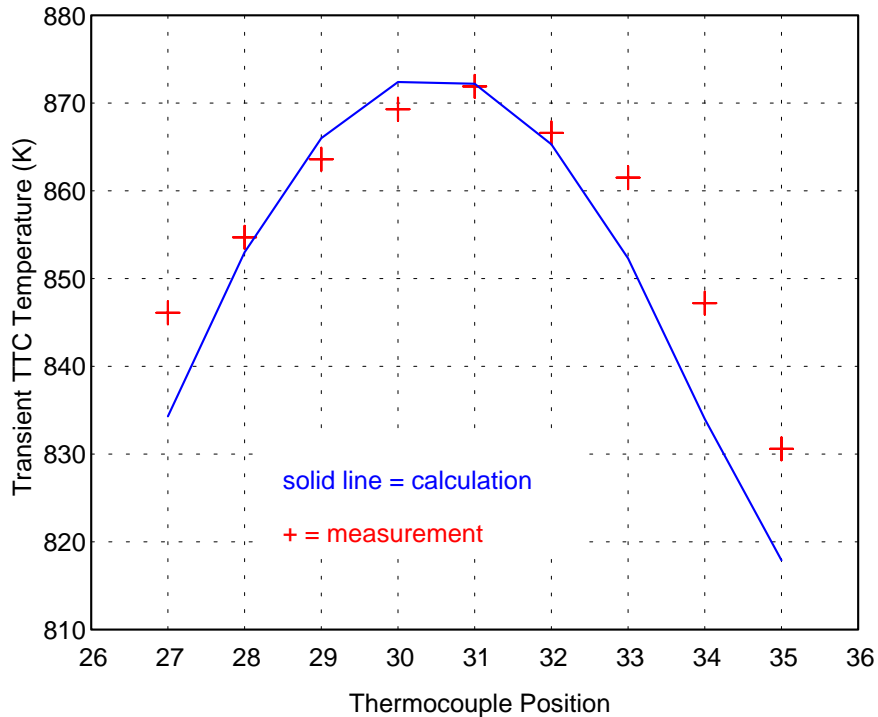


Fig. 12. Lateral Coolant Temperature Distribution Near the Top of the Core at 85 Seconds into the Transient

Figure 13 shows the transient coolant flow rates in XX09. There were two flow meters in series below the pin section in XX09. These flow meters measured the same flow. During the early part of the transient, during most of the pump coast-down, these two flow meters gave almost identical readings; and the computed flow rate agreed well with the measured flow rate. By the time that the pumps stopped turning, at 50.5 seconds, the readings from the two pumps differed significantly. Also, at low flows there was considerable noise in the flow meter signals. At low flows the width of the scatter band in each flow meter reading was about 10% of the reading, and the readings of the two flow meters differed by 30-50%. There was apparently a small DC voltage offset in the readings from at least one of the flow meters. At low flows the computed flow rate agreed with the measured flow rates as well as the two flow meters agreed with each other.

Code Archive

In accordance with the requirements for Milestone 1.8, archives of the updated SASSYS-1 and SSC-K codes are being maintained at ANL and KAERI, respectively, in compliance with each organization’s software quality assurance requirements for configuration control and retrieval.

Planned Activities

The reported activities complete the scope planned for Task 1.

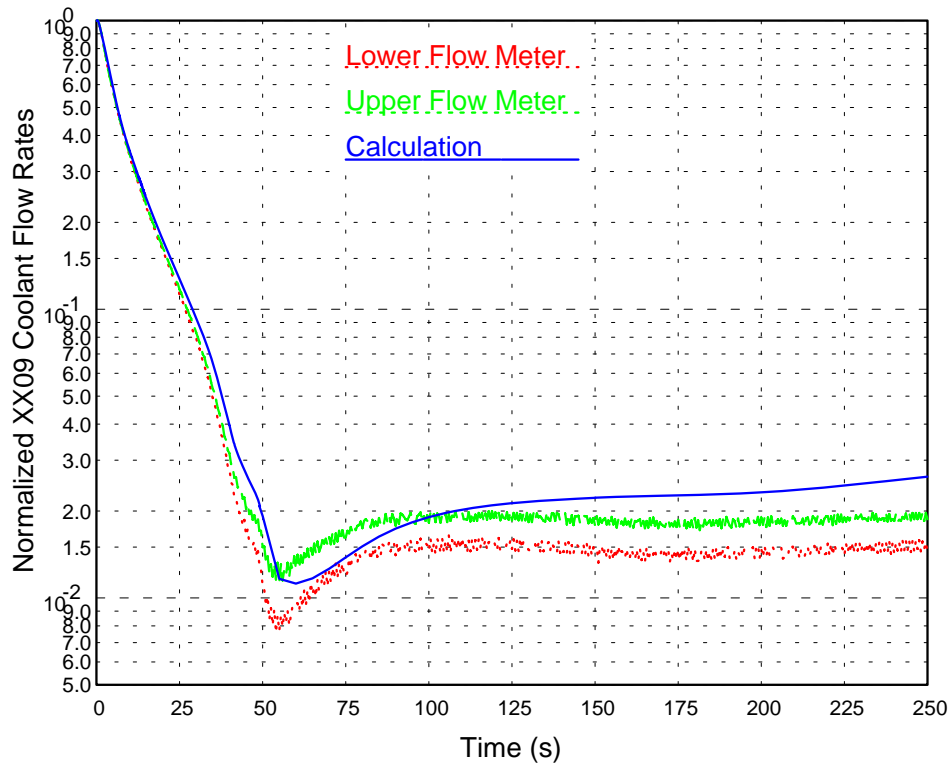


Fig. 13. Transient Flow Rates in XX09.

Narrative

Task 2: Comparative Analysis and Evaluation of Innovative Design Features

Research Objective

ANL and KAERI collaborate in the planning, management, performance, and documentation of comparative analyses of innovative safety design features. The analyses are performed with state-of-the-art capabilities available at KAERI and ANL, as well as the advanced model developed in Task 1. The objectives of these analyses are to identify the passive safety margins provided by innovative design features, to quantify the reliability and safety margin enhancement provided by design innovations offering significant potential for construction, maintenance, and operating cost reductions, and to establish a basis for selection of design features for inclusion in an optimized conceptual design. The increased safety margins provided by these new analyses and design features may permit simplification of the overall reactor design concept, and reduction of reliance on engineered safety systems.

Research Progress Overview

In 2003, ANL and KAERI agreed on Task 2 scope and issued a joint project document [3] defining activities, responsibilities, and schedule (Milestone 2.1). The KALIMER-150 conceptual reactor design developed by the KALIMER Technology Development Team at KAERI was selected [5] to serve as a basis for simulation of innovative safety design features and evaluation of enhanced safety margins (Milestone 2.2). The ANL SASSYS-1 and KAERI SSC-K computer codes were selected [10] as the state-of-the-art computational methods for performance of the baseline analyses (Milestone 2.3). In 2004, KAERI and ANL cooperated in baseline safety analyses of the KALIMER-150 conceptual design. Design specifications of KALIMER-150 were provided by KAERI, and input data for SASSYS-1 and SSC-K were assembled [12] (Milestone 2.4). ANL and KAERI agreed to perform transient simulations of unprotected (e.g. without scram) transient overpower (UTOP), loss-of-flow (ULOF), and loss-of-heat-sink (ULOHS) accident sequences [12] (Milestone 2.5). Baseline safety analyses were performed [17] using the SASSYS-1 and SSC-K computer codes (Milestone 2.6). In 2005, advanced analyses [28] were performed to complete the task activities. The advanced three-dimensional subassembly model developed in Task 1 was employed to re-analysis the baseline transients, and specific design features were investigated to demonstrate passive safety margin enhancements (Milestone 2.7). Advanced analysis results were documented in a deliverable report, and Task 2 was concluded with the completion of this final report (Milestone 2.8).

KALIMER-150 Design and State-of-the-Art Modeling for Baseline Analysis

The KALIMER design is depicted in Fig. 14. KALIMER is a pool-type, sodium-cooled, metallic-fuelled fast reactor that serves as a prototypic demonstration for future commercial liquid metal-cooled reactor (LMR) designs. The principal design objectives for KALIMER are enhanced safety, competitive economics, proliferation resistance, and environmental friendliness.

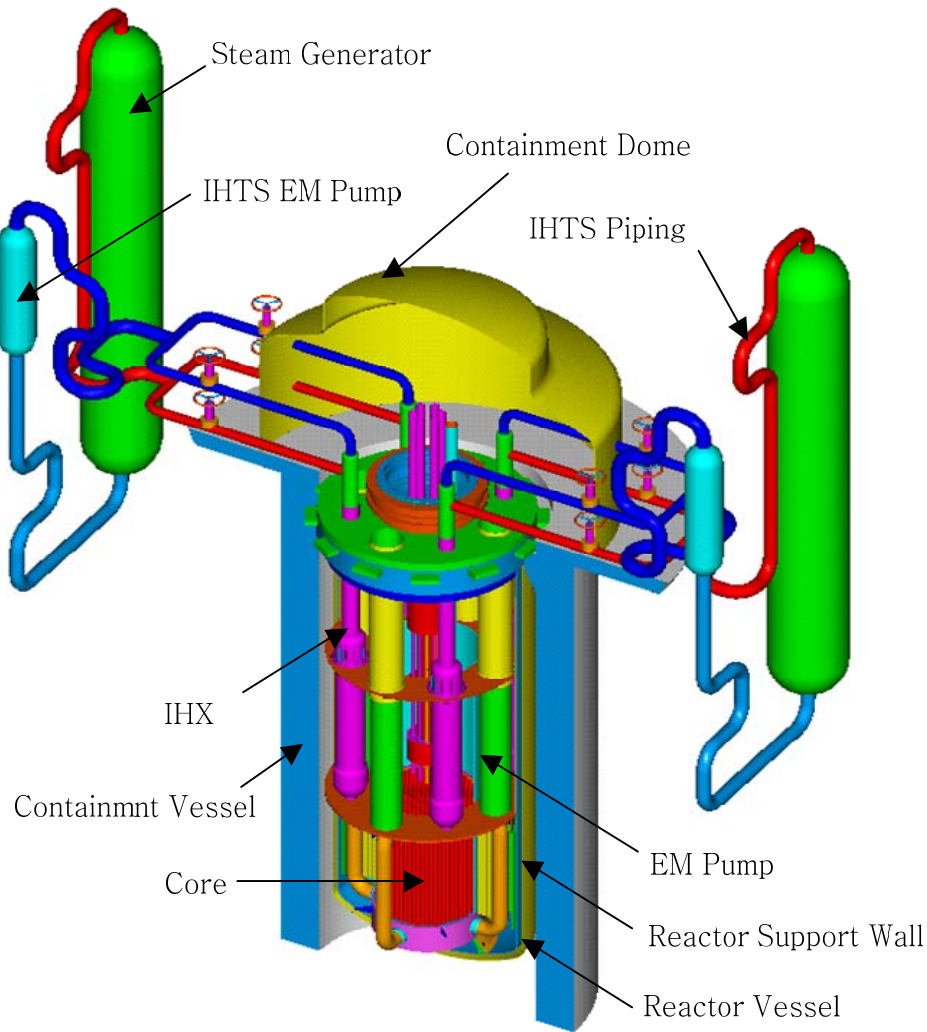


Fig. 14. KALIMER-150 Conceptual Design.

The KALIMER-150 core loading pattern is shown in Fig. 15. Metallic fuel is selected as the most appropriate fuel for KALIMER because of its in-reactor performance, nuclear characteristics, proliferation resistance, and inherent safety performance. KALIMER-150 design parameters are given in Table 2.

In the baseline analyses, the thermal/hydraulic performance of the reactor core is represented with a single-pin model in multiple channels. Each channel represents a single fuel pin and the associated coolant and structure. The structure field may be used to represent some part of the hex-can and the pin spacers. One-dimensional, radial heat transfer calculations are performed at many axial locations to model heat transfer from the fuel through the cladding to the coolant, and from the coolant to the structure, the gas plenum, and the reflectors. One-dimensional (axial) coolant flow is modeled with a momentum equation solution for the axial pressure profile, and convective heat transfer conditions are assumed at the interfaces between the coolant and the

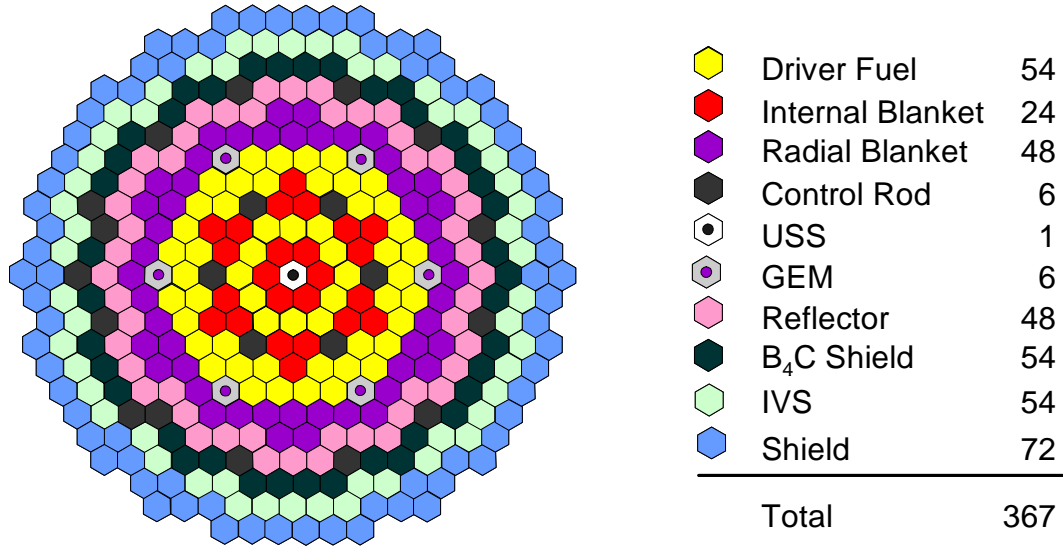


Fig. 15 KALIMER-150 Core Loading Pattern.

Table 2. KALIMER-150 Design Parameters

OVERALL			
Net Plant Power, MWe	150	Cladding Material	HT9
Core Power, MWt	392.2	Refueling Interval, months	18
Gross Plant Efficiency, %	41.5	PHTS	
Net Plant Efficiency, %	38.2	Reactor Core I/O Temp., °C	386.2 / 530.0
Reactor Type	Pool	Total PHTS Flow Rate, kg/s	2143.1
Number of IHTS Loops	2	Primary Pump Type	Electromagnetic
Safety Shutdown Heat Removal	PSDRS	Number of Primary Pumps	4
Seismic Design	Seismic Isolation Bearing	IHTS	
CORE		IHX I/O temp., °C	339.7 / 511.0
Core Configuration	Heterogeneous	IHTS Total Flow Rate, kg/s	1803.6
Core Height, mm	1000	IHTS Pump Type	Electromagnetic
Axial Blanket Thickness, mm	0	Number of IHXs	4
Maximum Core Diameter, mm	3373	Number of SG	2
Fuel Form	U-Pu-10%Zr	STEAM SYSTEM	
Feed Fuel Enrichment (Total TRU)	30.0	Steam Flow Rate, kg/s	175.45
Assembly Pitch, mm	161.0	Steam Temperature, °C	483.2
Fuel/Blanket Pins per Assembly	271 /127	Steam Pressure, MPa	15.5

cladding, the reflectors, and the structure. Temperatures are calculated at multiple radial nodes in the fuel, the cladding, the reflectors, and the structure. The coolant has a single temperature at each axial location. Axial heat conduction is neglected.

For the whole-core model, each channel represents a single, average pin in a sub-assembly, and several sub-assemblies are grouped together, so that a single channel may represent all the pins in a number of similar sub-assemblies. In the KALIMER-150 baseline model, four channels were used to represent 1) the hottest driver sub-assembly, 2) the remaining driver sub-assemblies, 3) the internal blanket sub-assemblies, and 4) the radial blanket sub-assemblies.

Accident Sequences

For the UTOP sequence, it is assumed that a control system failure results in the inadvertent withdrawal of a control rod, and the plant scram systems also fail. All other systems, including the coolant pumps and balance-of-plant, are assumed to continue normal operation. The control rod withdrawal is assumed to insert 0.3β of reactivity linearly in 15 seconds of time, where β is the effective delayed neutron fraction. The reactivity insertion leads to a power increase, which raises the fuel, coolant, and structural temperatures. These temperature increases bring reactivity feedbacks due to the fuel Doppler effect, fuel and cladding axial thermal expansion, coolant density decrease, radial core dilation by structural thermal expansion at the above-core load pad plane, and thermal expansion of the control rod drivelines. The net reactivity, which is the sum of the assumed reactivity insertion and the feedbacks, rises initially with the inserted reactivity, but soon peaks and falls as the negative feedbacks counter the only positive feedback from coolant density reduction. The net reactivity eventually decreases to near zero, and in the long term, begins a slow, low-amplitude, negative-to-positive oscillation as the reactor adjusts to the heat rejection provided by the steam generators.

For the ULOF sequence, it is assumed that all power for the primary and intermediate coolant pumps and the steam generator feedwater pumps is lost and the reactor scram systems fail. The accident sequence is driven by the loss of forced coolant flow in a reactor operating initially at full power. The rapid flow decrease at full power leads to an equally rapid reactor temperature increase. However, the KALIMER-150 design incorporates six special subassemblies called Gas Expansion Modules (GEMs) that are designed to introduce negative reactivity in the event of a loss of coolant flow. Each GEM subassembly consists of the hexcan of a regular fuel subassembly that is sealed at the top and open to the inlet plenum at the bottom, and is initially filled with an inert gas. As the pumps raise the inlet plenum pressure, the gas in the GEM is compressed and the coolant level rises. As the inlet plenum pressure drops with the coolant flow coast down, the coolant level falls and introduces a low density region that enhances neutron leakage and inserts negative reactivity. In the KALIMER-150 design, the six GEM subassemblies are located in a high leakage region on the core periphery and account for about -2β of reactivity depending on the core state. The GEM reactivity provides a negative shutdown margin in the ULOF sequence.

For the ULOHS sequence, it is assumed that feedwater to the steam generators is completely lost, leaving the air cooling of the reactor vessel as the only heat sink. Further, it is assumed that the reactor scram systems fail to operate. With full reactor power being transferred to the coolant, the cold legs of the primary and intermediate coolant systems heat, and the reactor inlet temperature rises. This introduces multiple reactivity effects, but the overall inlet temperature coefficient is negative, and the rising inlet temperature reduces reactor power.

Reactivity Feedback Effects

The KALIMER-150 conceptual design exhibits superior inherent, passive safety performance, as measured by the peak transient reactor temperatures (fuel, cladding, coolant) during the accident sequences. The safety margin is the difference between component temperatures corresponding to failure or irreversible upsets (the safety limits), and the peak temperatures attained in the transient. Examples of phenomena associated with safety limits include sodium boiling, cladding failure, or fuel melting. Safety margins in accident sequences are optimized when transient temperatures are minimized. The primary safety mechanism in unprotected accident sequences is the net negative reactivity associated with elevated temperatures, which acts to decrease reactor power and limit accident consequences. So, the key to enhancement of safety margins in unprotected accident sequences is to increase the negative reactivity feedbacks (or decrease the positive reactivity feedbacks) associated with reactor temperature changes.

Baseline Analysis Results

The baseline analyses show that in the accident sequences considered, the most important inherent reactivity feedbacks are associated with fuel Doppler, coolant density, fuel and cladding axial expansion, radial core expansion, and control rod driveline thermal expansion. Temperatures for the fuel, cladding, reactor coolant, and subassembly hexcans determine these reactivity feedbacks. The baseline analyses were performed with the customary single-pin-per-subassembly thermal-hydraulic models in SASSYS-1 and SSC-K.

The reactor power history for the UTOP accident sequence in KALIMER-150 calculated by SASSYS-1 is shown in Fig. 16. The reactor power peaks at about 150% and then slowly decreases to seek equilibrium with the available heat sink provided by the coolant system heat capacity and the heat rejection by the steam generators. The power rise is driven by the assumed control rod withdrawal, and the reactor responds with negative reactivity feedbacks triggered by elevated fuel and coolant temperatures. The negative feedbacks reduce the net reactivity and lower the reactor power to eventual equilibrium with the heat removal.

The baseline results calculated by SASSYS-1 for the ULOF accident sequence in KALIMER-150 are depicted in Fig. 17, which shows the reactor power and flow response. As the flow decays, the GEMs introduce negative reactivity, which causes the reactor power to decrease. In the KALIMER-150 design, the GEM reactivity dominates the net reactivity in the ULOF sequence and overwhelms the feedback reactivities.

Figure 18 shows the KALIMER-150 reactor power in response to the ULOHS accident initiator. As the inlet temperature rises due to the loss of heat removal, the reactor responds with negative reactivity feedbacks that reduce the reactor power.

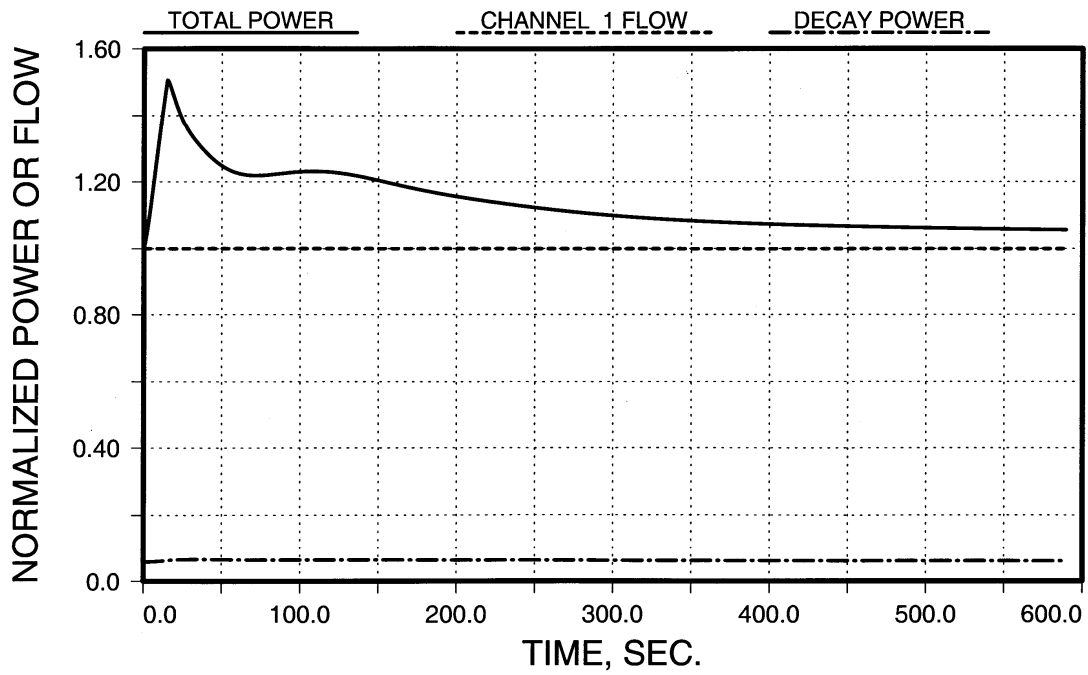


Fig. 16. Unprotected Transient Overpower Accident Power History.

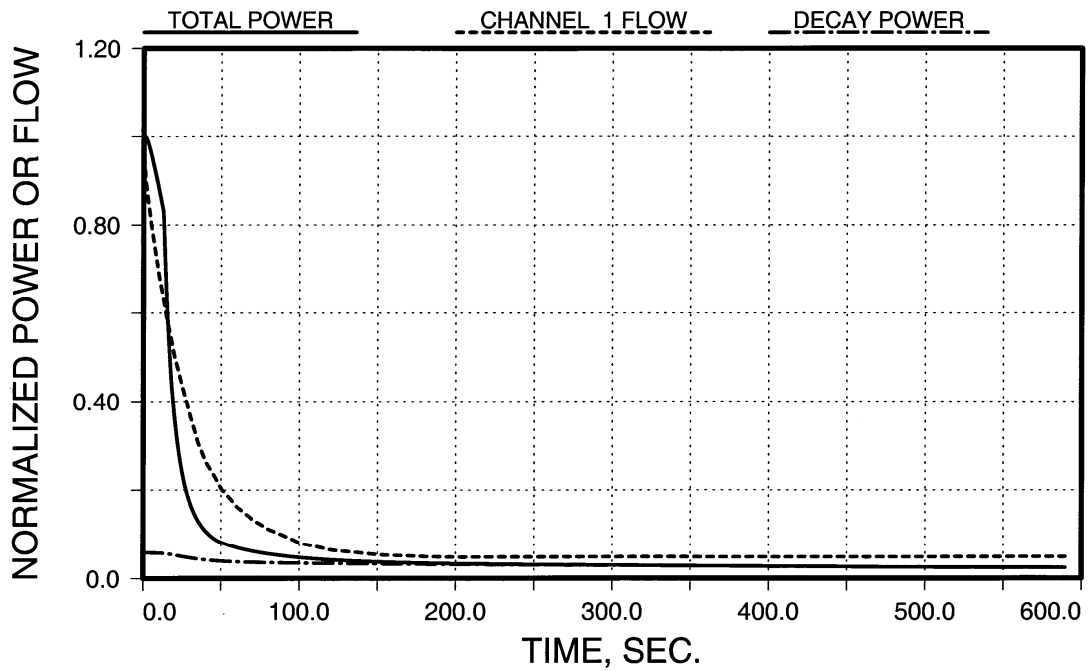


Fig. 17. Unprotected Loss of Flow Accident Power and Flow History.

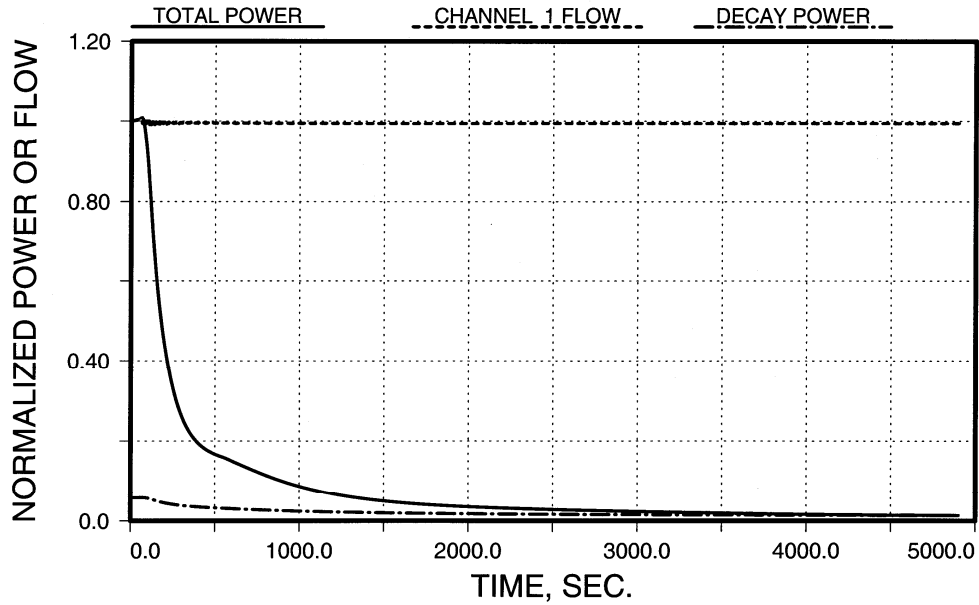


Fig. 18. Unprotected Loss-of-Heat-Sink Accident Power History.

The peak temperatures of the fuel, cladding and coolant in the hottest subassembly, and the average coolant temperatures at the core outlet for the above sequences, are summarized in Fig. 19. Results obtained with SASSYS-1 are compared with early SSC-K results (1.2), and with revised SSC-K calculations (1.3) that employ modeling assumptions (consistent material properties and improved thermal-hydraulic and reactivity feedback models) equivalent to the SASSYS-1 calculations. Figure 19 also shows the KALIMER-150 acceptance safety criteria based on ASME Service Level D limits. The results show that the SASSYS-1 and SSC-K baseline calculations agree, and that the peak temperatures for the unprotected, beyond-design-basis accident sequences are within the design basis acceptance limits.

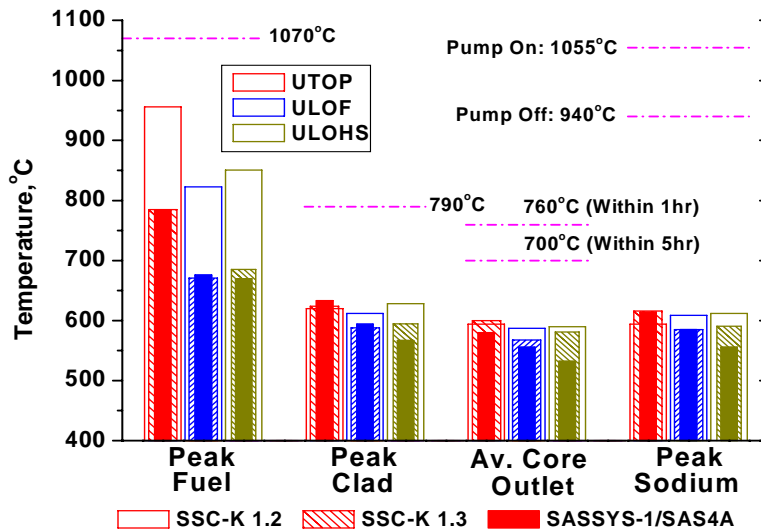


Fig. 19. Summary of Peak Temperatures Calculated by SASSYS-1 and SSC-K.

Enhanced Analysis Application

For the enhanced analysis, the three-dimensional subassembly thermal-hydraulic model developed in Task 1 was used to represent the driver fuel, internal blankets, and radial blankets of the KALIMER-150 design. For the 271 pin driver fuel subassembly model, sixty coolant channels were used to allocate a unique coolant channel to each row of pins in each 60° sector of the subassembly. For the 127 pin blanket fuel subassembly model, forty-two coolant channels were used to allocate a unique coolant channel to each row of pins in each 60° sector of the subassembly. (Thirty-nine axial segments were employed in the channel models for all analyses, both single- and multiple-pin subassembly models). This level of detail is appropriate for demonstrating the multidimensional aspects of transient heat transfer and fluid dynamics effects in safety analysis, and is consistent with available design data for intra-subassembly pin power and coolant flow specifications. The three-dimensional model has the capability to model each individual pin and coolant sub-channel within the subassembly.

In the whole-core model, like subassemblies, i.e. subassemblies with similar initial power, flow, and irradiation exposure, have been grouped into a total of fourteen subassembly types. There are six subassembly types, each with sixty channels, for the driver fuel. There are three subassembly types, each with forty-two channels, for the internal blanket fuel. And, there are five subassembly types, each with forty-two channels, for the radial blanket fuel. Consequently, there are a total of 696 channels in the multiple-pin model for the 126 subassemblies in the KALIMER-150 reactor. This compares to a total of 4 channels in the baseline analyses.

The analyses for the unprotected transient overpower (UTOP), unprotected loss of flow (ULOF), and unprotected loss of heat sink (ULOHS) sequences were performed with the multiple-pin subassembly core model, with all other modeling assumptions the same as were employed for the baseline analyses with the single-pin model.

Figures 20 and 21 compare the power and reactivity components for the UTOP case. The curves labeled 'MP' are the multiple-pin results, as compared to the baseline single-pin results. Figure 20 shows that the peak reactor power for the single-pin result is slightly higher than the multiple-pin results, as a consequence of the slightly higher net reactivity (about 0.11\$ versus 0.10\$) shown in Fig. 21 at 15 sec. Close examination of the component reactivities indicates that the difference between the single- and multiple-pin results is due to a slight difference in the core radial expansion reactivity (Fig. 21) during the reactivity insertion. The core radial expansion reactivity in this transient is coming from the heating and thermal expansion of the hexcan load pads at the above-core axial location. The multiple-pin model is providing a slightly faster heating rate for the structure at the load pad location, yielding the early difference in the reactivity feedback. At later times, from 50 sec. to 300 sec., the difference in the radial expansion is evident. However, the difference is slight, and does not provide a significant difference between the single-pin and multiple-pin results.

Figures 22 and 23 compare the power and reactivity components for the ULOHS case. Figure 22 shows that the power is slightly different for the two cases from about 200 sec. to around 1500 sec. Figure 23 indicates this is due to the slight difference in the net reactivity beginning at about 200 sec., but the net reactivities are nearly identical after 500 sec. Examination of the

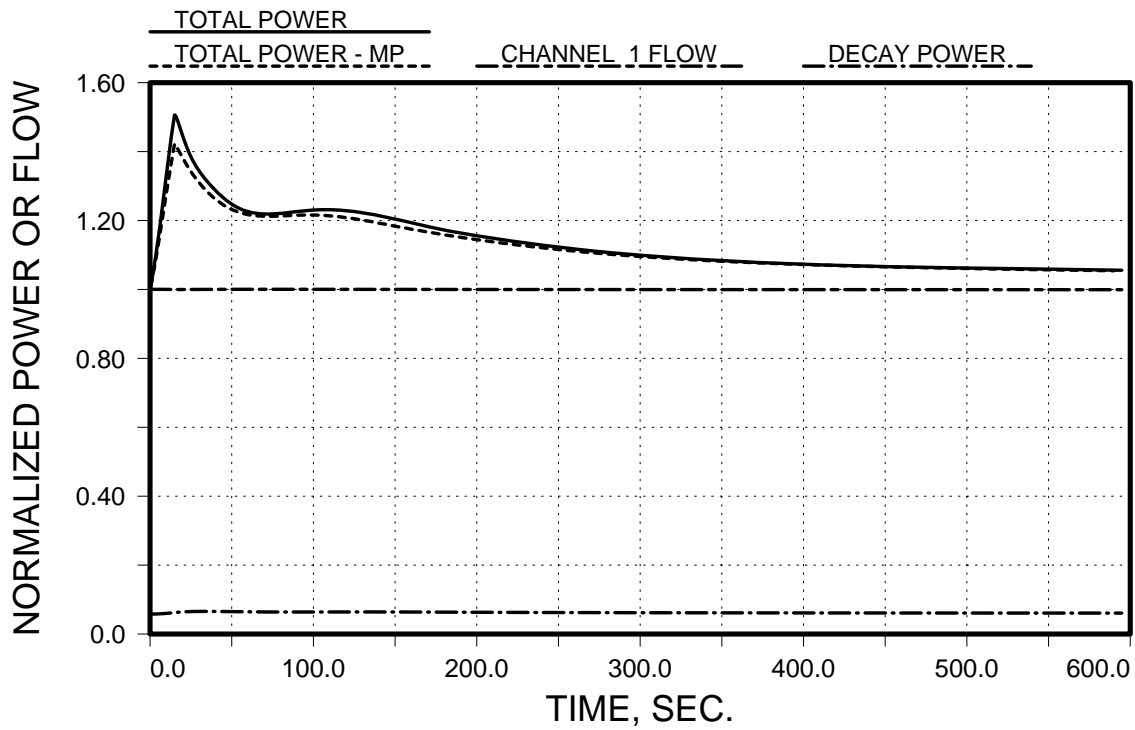


Fig. 20. UTOP Case Power Comparison.

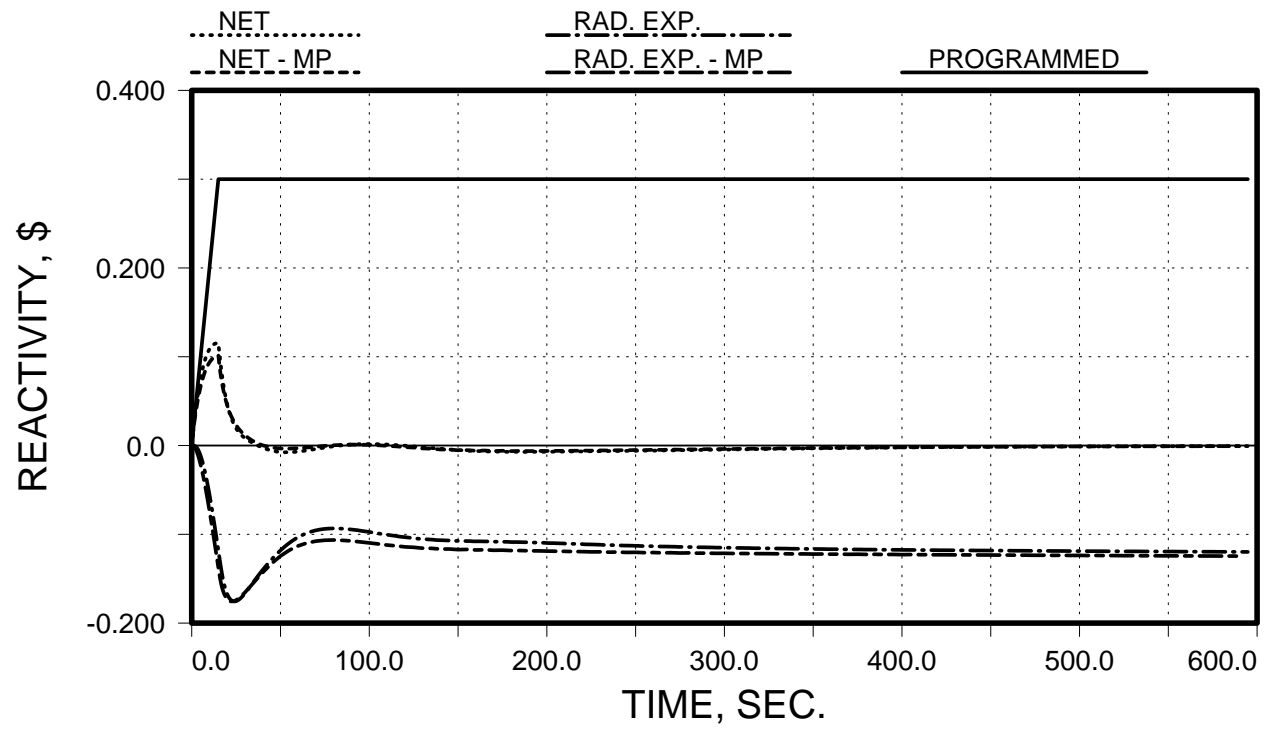


Fig. 21. UTOP Case Core Radial Expansion Comparison.

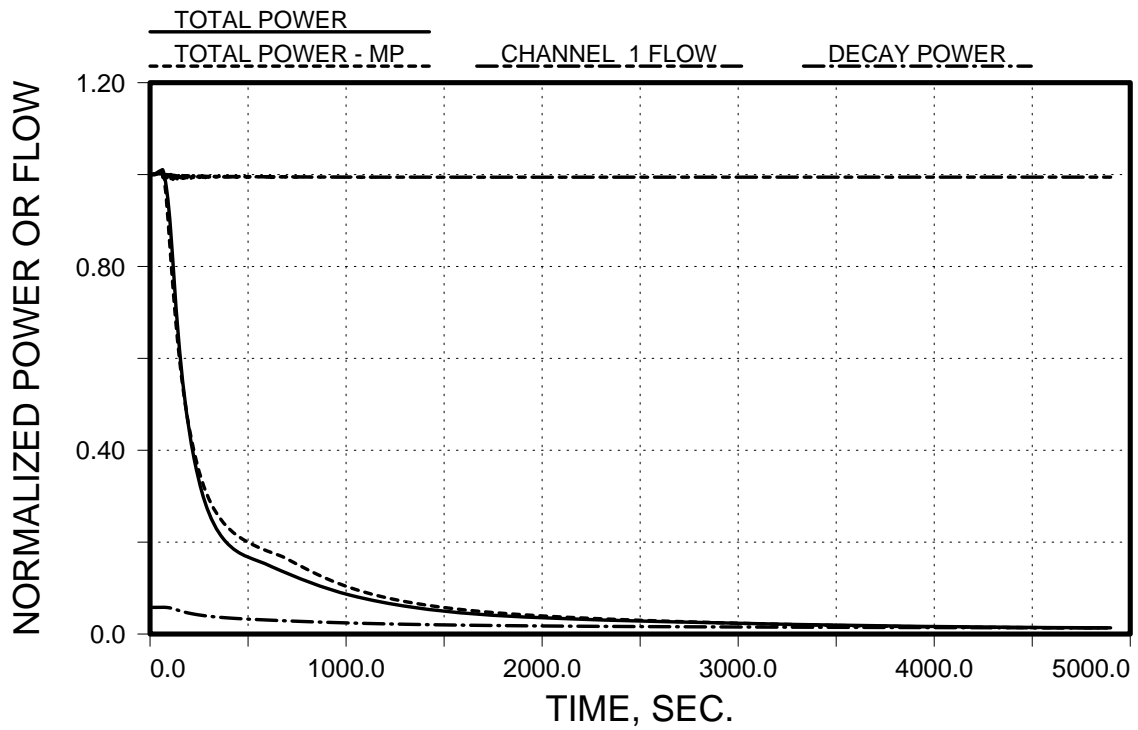


Fig. 22. ULOHS Case Power Comparison.

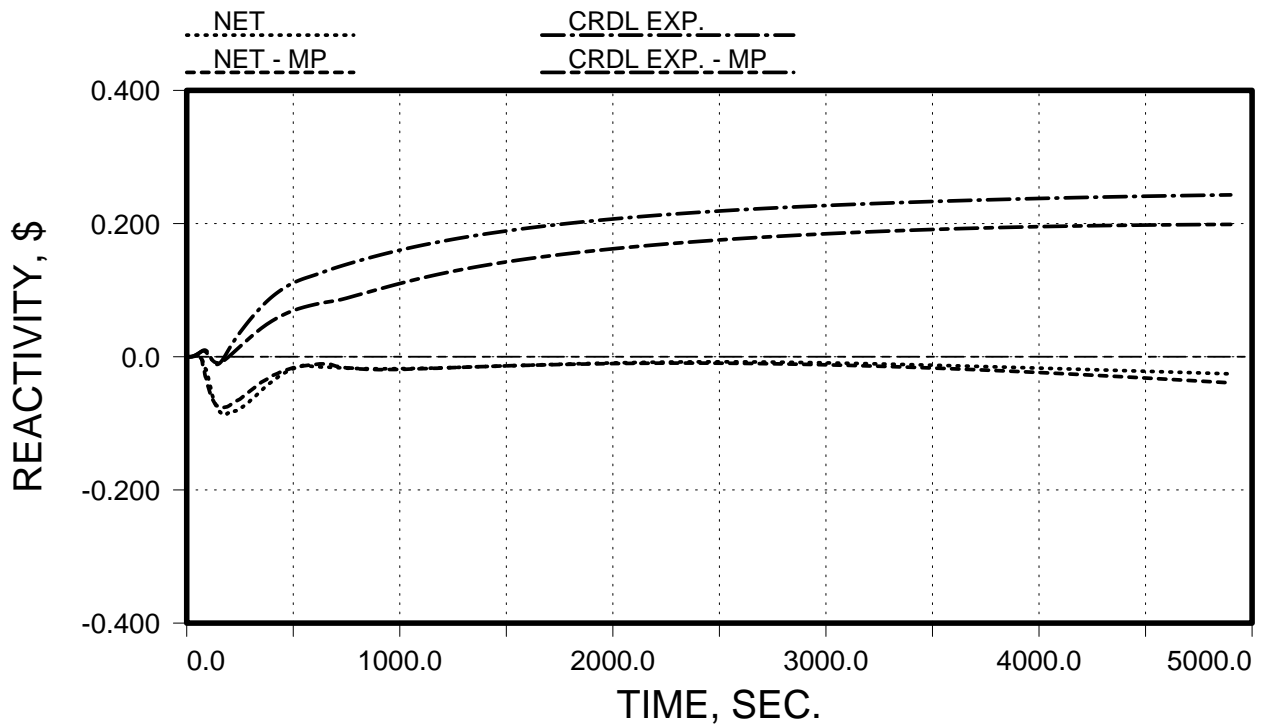


Fig. 23. ULOHS Case Control Rod Driveline Expansion Reactivity Comparison.

Component reactivity traces indicates that there are distinguishable differences in the reactivity components after 500 sec., but these differences cancel in the sum as indicated by the close comparison of the net reactivity. Perhaps the largest difference is in the control rod driveline reactivity shown in Fig. 23, which in this case is being dominated by thermal expansion of the reactor vessel due to elevation of the primary system cold leg temperature. This temperature is determined mainly by the ex-core thermal hydraulic model and only indirectly, through the reactivity/power/temperature coupling, by the core channel modeling.

In summary, the results from the enhanced modeling capability are nearly identical to the single-pin modeling results. Consideration of these comparisons has led to the conclusion that this similarity is due to the fact that the pin power and flow initial conditions were assumed to be the same for the two cases. This has given a measure of coherence to the results, building on the condition that the unprotected sequences are driven by reactivity feedbacks that are calculated similarly for the two cases. The results point out that increased detail in the thermal-hydraulic analysis must be matched by increased detail in the reactivity feedback modeling, especially the radial core expansion model, in order to provide distinguishable differences. The comparison provides increased confidence in both the single-pin and multiple-pin results, since they compare so closely with each other.

Enhanced Safety Design Features

It is possible to identify certain key safety features that can provide greater safety margins through changes in mechanical design. One example is the possibility of greater negative reactivity feedback for a given temperature change in unprotected accident sequences. The baseline KALIMER-150 analyses provided insights indicating that minor revision of the core restraint system design and the control rod driveline design could provide such effects.

The core restraint system is designed to provide a negative overall power coefficient in normal operating conditions by causing controlled dilation of the core subassemblies with increasing coolant temperature. In unprotected accident sequences, coolant and structural temperatures usually exceed normal operating conditions. Modification of the design to provide additional negative feedback in beyond-design-basis conditions would provide greater safety margins in unprotected accidents. (It is important to note that proposed design changes must maintain and preserve design-basis performance). Adjustment of load pad elevations and thicknesses, and of clearances at restraint rings can be made to provide beneficial bending of hexcans for beyond-design-basis temperature gradients, resulting in enhanced negative reactivity feedback in unprotected accidents. The proposed design change is to alter the core restraint design to provide additional negative reactivity feedback in over-power and over-temperature conditions.

In the analyses, this change was modeled as a 50% increase in the reactivity feedback coefficient associated with radial core expansion. Because of the nonlinear nature of the transient response, the impact of this change is considerably less than 50% in the radial core expansion feedback, as shown in the UTOP transient analysis result in Fig. 24. As the figure shows, the radial core expansion becomes more negative by about 20%, but the net reactivity is only slightly reduced during the power ascension. The reactor power traces for the reference and modified cases are

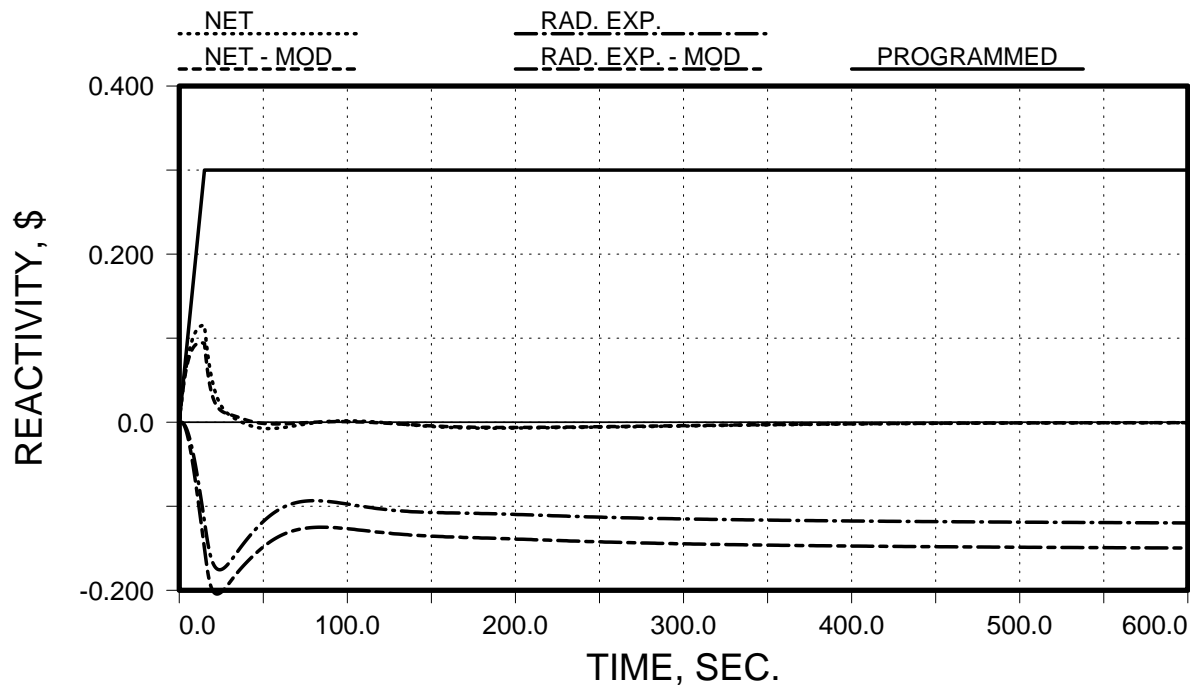


Fig. 24. UTOP Radial Expansion Reactivity Feedback for Core Restraint Modification.

Shown in Fig. 25, where it is seen that the peak power is slightly reduced in the early phase of the transient. This power reduction corresponds to a 16°C reduction in the coolant temperature at the time of the peak power.

The impact of the same design change in the ULOHS sequence is a radial core expansion feedback that is about 20% increased compared to the baseline calculation. The impact of this design change in the transient reactor power is a slight reduction, giving an 11°C lowering of the coolant temperature at 5000 sec.

The ULOF results for this design change are similar to the baseline results, due to the dominance of the GEM reactivity over the feedback reactivity.

A second, slowly-acting negative feedback is provided by thermal expansion of the control rod drivelines. To realize this effect, it is necessary to transport heat from the reactor to the drivelines. Dispersal of coolant in the hot pool above the reactor tends to delay heating of the drivelines. In most accident transients, the benefit of this effect could be increased by reducing the time delay for driveline expansion. This can be accomplished by ducting core outlet flow to enhance flow over control rod drivelines, and to decrease the effective mass of the drivelines to cause faster-acting response to core outlet temperature changes in accident sequences. The proposed design change is to alter the above-core coolant flow and control rod driveline design to accelerate driveline thermal expansion in response to coolant outlet changes. In addition, by supporting the core and the control rod drivelines from a common reference, the vessel expansion contribution to the control rod expansion feedback reactivity is eliminated. In the analyses, the effects of these changes were modeled by neglecting the vessel expansion component and by increasing the effective control rod driveline expansion by 50%. The impact

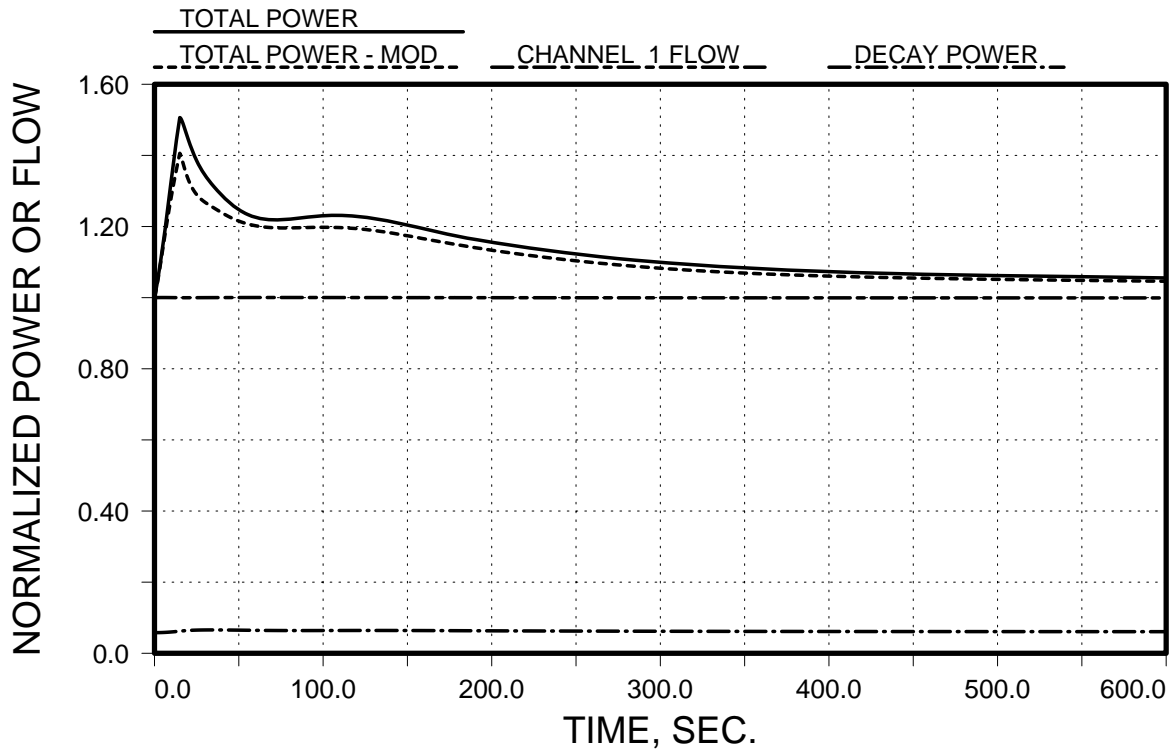


Fig. 25. UTOP Reactor Power for Core Restraint Modification.

Of these changes, in addition to the core restraint modification, is shown in Fig. 26, which shows that for the UTOP case, the two modifications yield a more negative long term reactivity feedback. Figure 27 shows the transient reactor power for this case and demonstrates the reduction in power due to the reactivity enhancement. The long term UTOP coolant temperatures are lower by 26°C compared to the baseline temperatures.

The long term coolant temperatures in the ULOHS transient for the case of the core restraint and CRDL modifications are lower than the baseline temperatures by 33°C.

These analyses have indicated that small improvements in passive safety margins can be gained by simple changes to the KALIMER-150 design. However, the analyses make evident that the overall passive safety performance of the design is established by the basic design selections of 1) sodium coolant, 2) pool-type primary system arrangement, and 3) metallic fuel. These design features give the reactor its inherent self-protecting reactivity feedback response in unscrammed accident sequences, and enable the reactor to remove residual decay heat by natural coolant circulation.

Planned Activities

The reported activities complete the scope planned for Task 2.

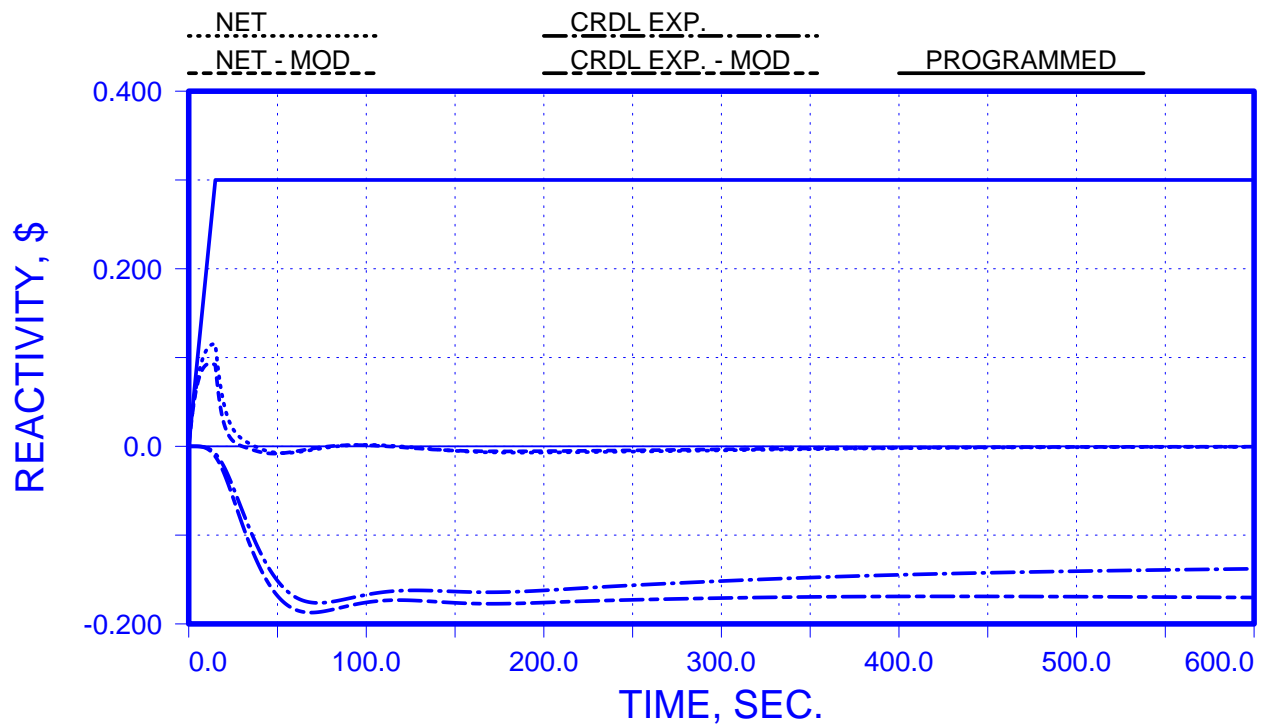


Fig. 26. UTOP Control Rod Driveline Reactivity Feedback for Core Restraint and CRDL Modification.

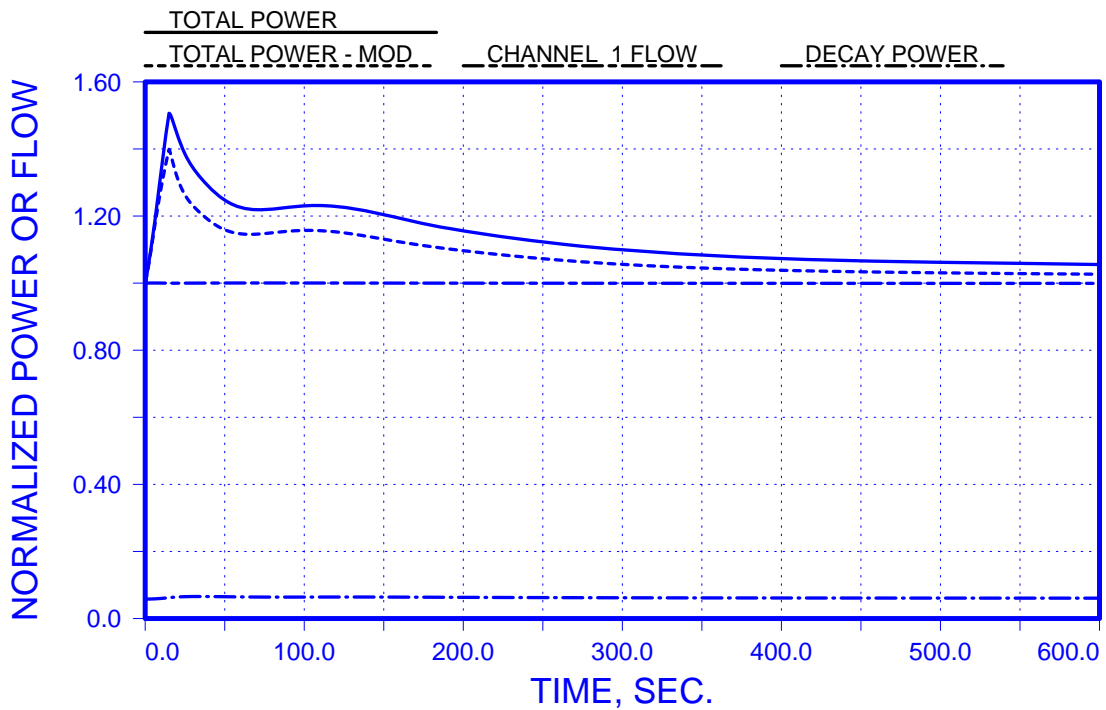


Fig. 27. UTOP Reactor Power for Core Restraint and CRDL Modification.

Narrative

Task 3: Safety Implications of Advanced Technology Power Conversion and Design Innovations and Simplifications

Research Objective

The objectives of this task are to identify and assess by means of analysis the implications for plant safety of proposed specific approaches for reducing capital and operating costs of next generation sodium-cooled fast reactors: i) utilizing an advanced power conversion technology consisting of a gas turbine Brayton cycle using supercritical carbon dioxide (S-CO₂) as the working fluid instead of the traditional Rankine water/steam cycle; and ii) incorporating design innovations including modular sodium-to-supercritical carbon dioxide heat exchangers that enable the traditional intermediate heat transport circuit to be eliminated.

Research Progress Overview

In 2003, an investigation [4] was made of the supercritical CO₂ Brayton cycle efficiencies that are possible when coupled to a sodium-cooled reactor, with and without an intermediate heat transport loop (Milestone 3.1). A study [4] of innovative sodium-to-CO₂ heat exchangers was completed (Milestone 3.2), and conceptual designs [9] of heat exchangers were developed (Milestone 3.3). A conceptual design [9] of a full supercritical CO₂ Brayton cycle was developed (Milestone 3.4). Concepts [4,12] for overpressure protection of the reactor primary system were developed (Milestone 3.5). All results were reported in the first annual report [6] (Milestone 3.6). In 2004, the first version of a plant cycle analysis computer code [14] was completed (Milestone 3.7), and a set of safety-related accident sequences [19] was identified (Milestone 3.8). An initial list of system and equipment modifications [19] was made for improvement of system performance (Milestone 3.9). Results of progress were reported in the second annual report [19] (Milestone 3.10). In the final year of the project, a consequence analysis of heat exchanger pressure boundary failure [21] was completed (Milestone 3.11), as was an assessment [22] of safety-related events (Milestone 3.12). A final assessment [25] of equipment and system changes needed for safety improvements were completed (Milestone 3.13). Final year results were reported in the 2005 annual report [25] (Milestone 3.14)

Supercritical CO₂ Cycle Performance without IHTS

The advantages of the S-CO₂ Brayton cycle include significantly improved cycle efficiency relative to a Rankine steam cycle, reduced plant footprint due to fewer, simpler, and smaller-sized components, as well as reduced capital and operating costs and plant staffing requirements from radical plant simplification and elimination of costly Rankine cycle components.

It has been demonstrated that a S-CO₂ Brayton cycle can be coupled to the KALIMER-150 sodium-cooled fast reactor. Figure 28 provides an illustration of the coupled reactor and S-CO₂ Brayton cycle. In this case, the intermediate heat transport system (IHTS) has been eliminated through the use of modular in reactor sodium-to-S-CO₂ heat exchangers (HXs). The specific

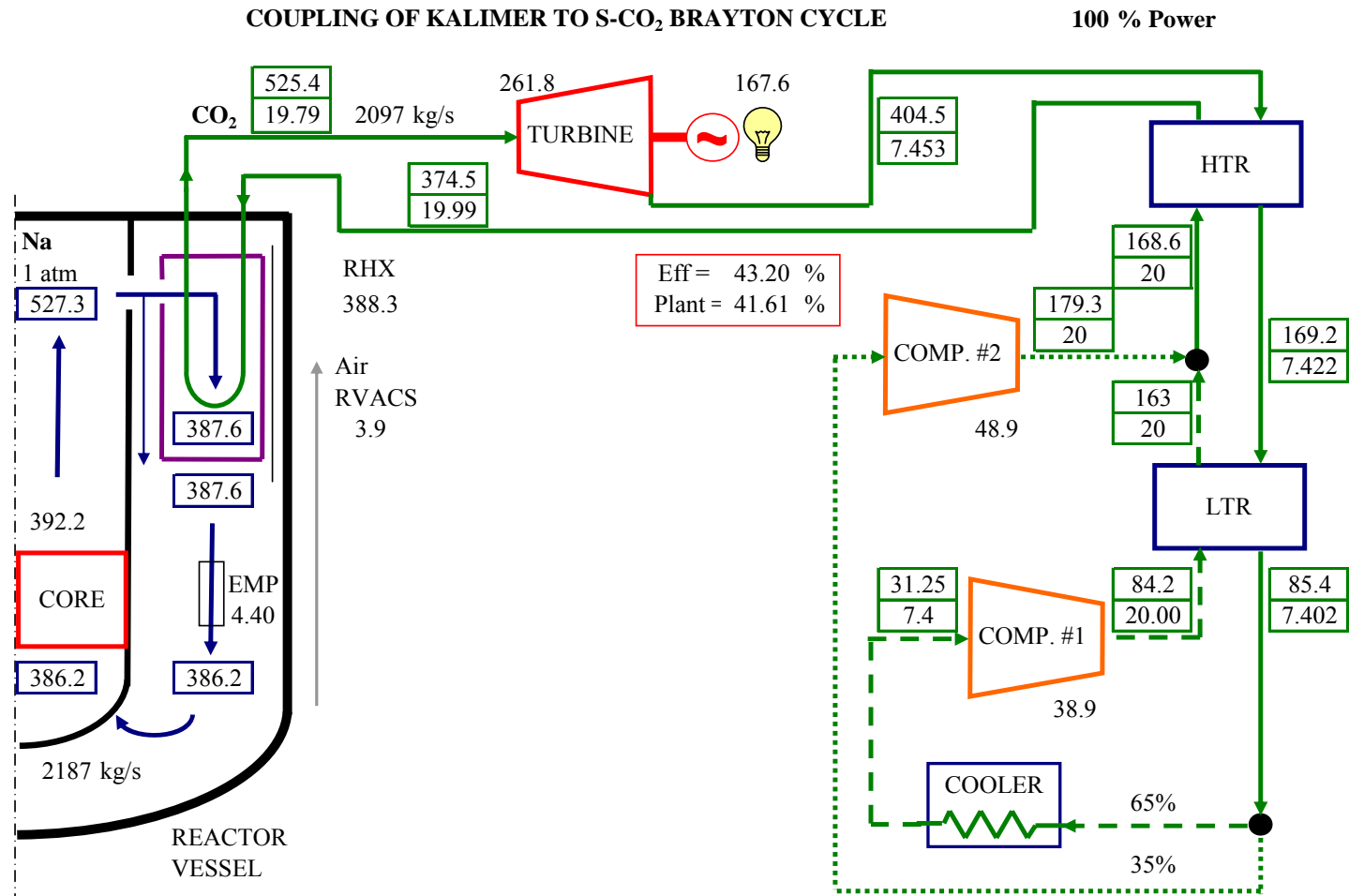


Fig. 28. Schematic Illustration of Temperature and Pressure Conditions for KALIMER-150 Coupled to a Supercritical Carbon Dioxide Gas Turbine Brayton Cycle Power Converter.

temperatures and pressures shown on the figure relate to the case where the primary sodium inlet temperature is assumed to remain unchanged at the current nominal value of 386°C.

For the assumed conditions, the cycle efficiency is about 43 percent. The cited plant efficiency is less because of in-house loads that include the four primary coolant electromagnetic pumps (EMPs). A key contributor to the high cycle efficiency is the low amount of work that is required to compress the S-CO₂ immediately above the critical temperature. This reflects the high S-CO₂ density near the critical point ($\rho_{\text{crit}} = 468 \text{ Kg/m}^3$) which reduces the Pdv work. The S-CO₂ densities are comparable to ordinary liquids such as water ($\rho = 998 \text{ Kg/m}^3$) rather than, say, helium ideal gas in a gas-cooled reactor plant ($\rho \sim 4 \text{ Kg/m}^3$). Thus, as the low end of the cycle, the S-CO₂ temperature and pressure are close to the CO₂ critical temperature (30.98 °C) and pressure (7.37 Mpa). At the high end, the compressed CO₂ pressure is taken to be 20 Mpa. Raising the pressure above this value results in diminishing returns in further gains in cycle efficiency.

The high S-CO₂ density also results in relatively small sizes for the turbine and compressors. For example, the turbine consists of only four stages and is about 0.8 meter in length and 1.2 meter in diameter without the casing from theoretical calculations.

The expanded S-CO₂ that exits the turbine passes through two recuperators (i.e., regenerative heat exchangers) within which a portion of the remaining S-CO₂ thermal energy is utilized to preheat compressed S-CO₂ before it is returned to the modular heat exchangers immersed in the sodium liquid metal primary coolant; this further contributes to the cycle efficiency. The specific heat of supercritical S-CO₂ is dependent upon pressure such that the value at 20 Mpa is significantly larger than that at 7.4 Mpa at the temperatures following compression of the S-CO₂ exiting the cooler. In order to preheat the S-CO₂ effectively, it is necessary to split the S-CO₂ flow such that only a portion (65 percent) passes through the cooler/heat exchanger where heat is rejected from the cycle. This colder flow stream is preheated in the low temperature recuperator. The remainder of the flow is directly compressed and merged with the colder flow stream prior to passing through the high temperature recuperator. For this reason, the cycle is sometimes called a “recompression cycle.” The differences in the specific heats at the two pressures are lower at the temperatures encountered in the high temperature recuperator.

A computer code was developed that determines the steady state behavior of the KALIMER sodium-cooled reactor coupled to a S-CO₂ Brayton cycle plant. The code incorporates deterministic models that calculate the primary sodium temperatures and flow rate as well as the temperatures and pressures around the S-CO₂ balance of plant circuit together with the S-CO₂ flow rate. The code calculates the primary sodium flow rate and temperature rise through the core, given the dimensions of the four in-reactor sodium-to-S-CO₂ heat exchangers. Other models calculate the changes in S-CO₂ conditions as the supercritical fluid passes through the turbine and each of the two compressors. Each of the two recuperators is assumed to be either a shell-and-finned-tube heat exchanger or a compact Printed Circuit Heat Exchanger (PCHE) similar to the type manufactured by Heatric Division of Meggitt (UK) Ltd. In a PCHE, the S-CO₂ streams flow through alternating rows of semicircular channels that are chemically etched into plates which are diffusion bonded together to form a block with embedded channels. The recuperator design is assumed to incorporate headers that enable strictly counterflow heat

exchange between the hot and cold streams. A deterministic multicell calculation of steady state temperature profiles and fluid conditions is carried out for sodium and S-CO₂ in the in-reactor HXs, the hot and cold CO₂ streams inside each recuperator, as well as S-CO₂ and water in the cooler.

The code determines the Brayton cycle efficiency and the overall plant efficiency that is calculated by subtracting the power required to energize the four primary electromagnetic pumps plus other on-site needs. The sodium core inlet temperature is specified by the user.

Heat Exchanger Design

In coupling the S-CO₂ Brayton cycle to KALIMER, each of the four intermediate heat exchangers was replaced by an in-reactor sodium-to-S-CO₂ heat exchanger. The key in achieving a successful coupling is for the heat exchanger to heat the S-CO₂ to the highest temperature possible, since the cycle efficiency directly depends upon the maximum S-CO₂ temperature that enters the turbine. Thus, a heat exchanger configuration was sought that maximizes the number of tubes and interfacial area for heat transfer but at the same time fits into the available volume inside of the reactor vessel.

Each heat exchanger is assumed to be kidney shaped. A counter-flow configuration is assumed in which the S-CO₂ flows upwards through straight circular stainless steel tubes while the sodium flows downwards over the exterior of the tubes. The design configuration of the HX is shell and tube type. The tubes of the HX are straight shape as shown Figure 29.

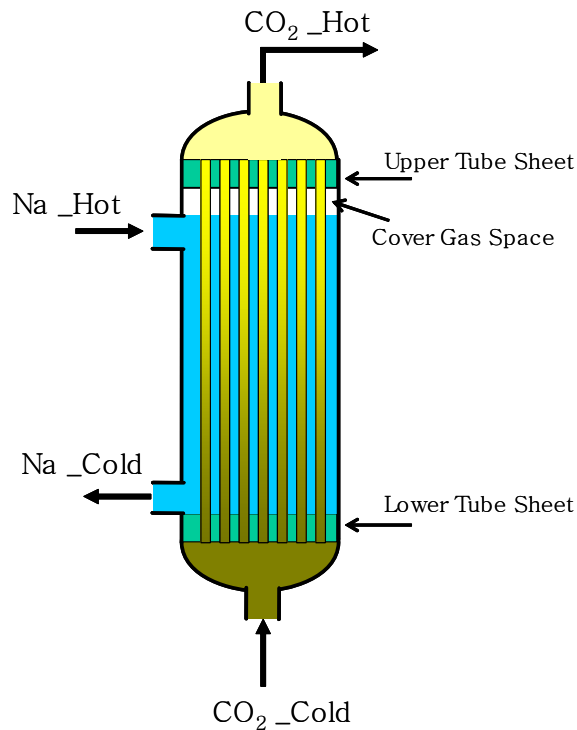


Fig. 29. Design Concepts of Sodium-to-Supercritical CO₂ Heat Exchanger

The tube height is taken to be 6.43 meters. The reference tube inner and outer diameters are 0.25 and 0.45 cm respectively. A tube pitch-to-outer diameter ratio of 1.2 is assumed. The heat exchanger outer and inner diameters are, respectively, 6.82 and 4.24 meters. A gap of 1.4 meters exists between successive heat exchanger; and an electromagnetic pump is located situated inside each gap. A structural wall separates the heat exchangers from the pumps.

The reference sodium core inlet temperature is taken to be the nominal value of 386.2°C, the same as for the current design coupled to an IHTS which is coupled to a Rankine steam cycle. For this assumption, the results shown in Fig. 28 are calculated.

The frictional pressure drop for sodium flow through the heat exchangers is less than that for the current IHXs. Consequently, the primary sodium flow rate is greater (2187 versus 2143 kg/s) and the core outlet temperature is lower (527.3 versus 529.8°C). The S-CO₂ is heated to 525.4°C, only 2°C less than the core outlet temperature. For this value, a resulting Brayton cycle efficiency of 43.2% is calculated. Subtracting the power for the primary coolant pumps (4.4MW), a plant efficiency of 41.6% is obtained. There are also other needs for on-site power. For the current KALIMER design, the other on-site needs are 2.0 % of the nominal core power. However, this value also includes the power requirements of the Rankine steam cycle and, therefore, represents an overestimate for KALIMER with a S-CO₂ Brayton cycle.

A large number of other calculations were performed to investigate the effects of specific design changes on Brayton cycle efficiency. The first variation was to increase the diameter of the in-reactor HX tubes. Increasing the tube diameter by a factor of two would decrease the efficiency only slightly. This indicates that the reference HX design provides more than adequate heat exchange area. The number of tubes could be reduced thereby decreasing the volume occupied by the heat exchanger. However, if the tube inner diameter were to be further increased to 1.0 cm, then a significant drop in efficiency of almost 1% would be the consequence. This reflects the reduction in the maximum S-CO₂ temperature from 525 to 504°C.

Next, the sodium core inlet temperature was increased by 20, 40, and 60°C. This has the direct effect of raising the core outlet temperature by about the same value. It is observed that a 1% gain in efficiency is achieved for each 20°C incremental increase in the core outlet temperature. Thus, if it were possible to raise the outlet temperature by 20 or 40°C a significant gain in plant efficiency could be realized. Increases in temperature would need to be evaluated in relation to the margins for potential fuel-cladding interaction and service of in-vessel structures.

An additional study was performed to evaluate the trends in sodium-to-CO₂ shell-and-tube heat exchanger sizes for changes in the system design parameters. The results of this study are given in Appendix C of the 2003 annual report.

The PCHEs are nominally assumed to have semicircular channels only 1 mm in diameter. For this size channel, the recuperator channel length is only 3 meters. Thus, the volume occupied by the recuperators is small. Current PCHEs such as those that are used in offshore oil recovery, utilize channels that are about 2 mm in diameter. It is found that for such a diameter, a recuperator channel length of about 6 meters would be needed in the S-CO₂ Brayton cycle.

Pressure Relief System Design

In Fig. 28, heat exchangers are immersed in the sodium primary coolant; an intermediate heat transport circuit typical of traditional sodium-cooled reactors coupled to a Rankine steam cycle has been eliminated. Of significant safety concern are the potential consequences of rupture of the boundary between the high pressure CO₂ and the lower pressure sodium. For example, a pressure relief system must be provided to relieve the pressurization of the reaction vessel and closure head, in the event of a heat exchanger tube rupture. Design concepts are developed for pressure relief systems in plant designs both with and without an IHTS.

Design concept with IHTS

A Sodium Water Reaction Pressure Relief System (SWRPRS) could be used as the pressure relief system for KALIMER with IHTS. The SWRPRS is a system to prevent the IHTS from being over pressurized in the accident of sodium water reaction. The system is composed of pipe routed from the steam generator to the environment through the sodium dump tank and separator. The piping is plugged by a rupture disk to prevent sodium leakage during normal operation. If the pressure of the IHTS exceeds the set pressure of the rupture disk, the IHTS is protected by the explosion of the rupture disk. The schematic drawing of SWRPRS is as shown Fig. 30.

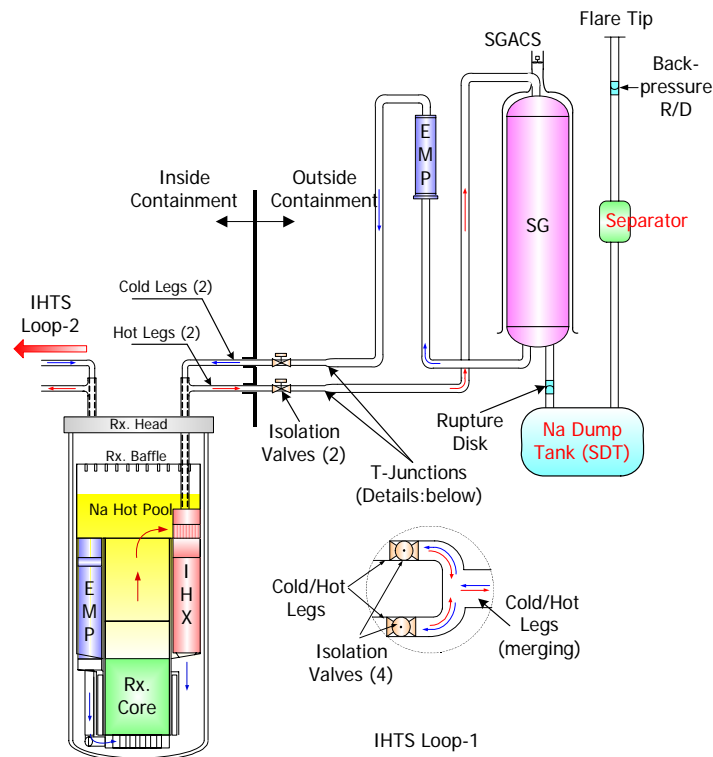


Fig. 30. Schematic Drawing of SWRPRS for KALIMER-150.

Design concept without IHTS

The pressure relief system for KALIMER without IHTS shall be designed to accommodate all the effluents from the high pressure system such as the supercritical CO₂ system. When sodium is used for the primary system coolant for a supercritical CO₂ plant but IHTS is not used, there may be two kinds of approaches to satisfy the requirements above mentioned. The first one is to increase the design pressure of the reactor vessel to cover the peak pressure which is expected to occur at the breach of the interface between primary and secondary system. However, if the design pressure of the reactor vessel is assigned to be the same as the one of the CO₂, then the reactor vessel wall is very thick and the performance of the Passive Safety Decay Heat Removal System (PSDHRS) is deteriorated. Therefore it may not be a feasible approach.

Another approach is to install pressure suppression tanks. A very similar design concept is adopted in the BREST-300 reactor system as shown in Fig. 31. The BREST-300 reactor is a lead cooled reactor where heated water is used as secondary coolant. In the case of interface break, the injected steam is drawn into the suppression pool where the high temperature steam is condensed to maintain the primary pressure within limited values for specified times.

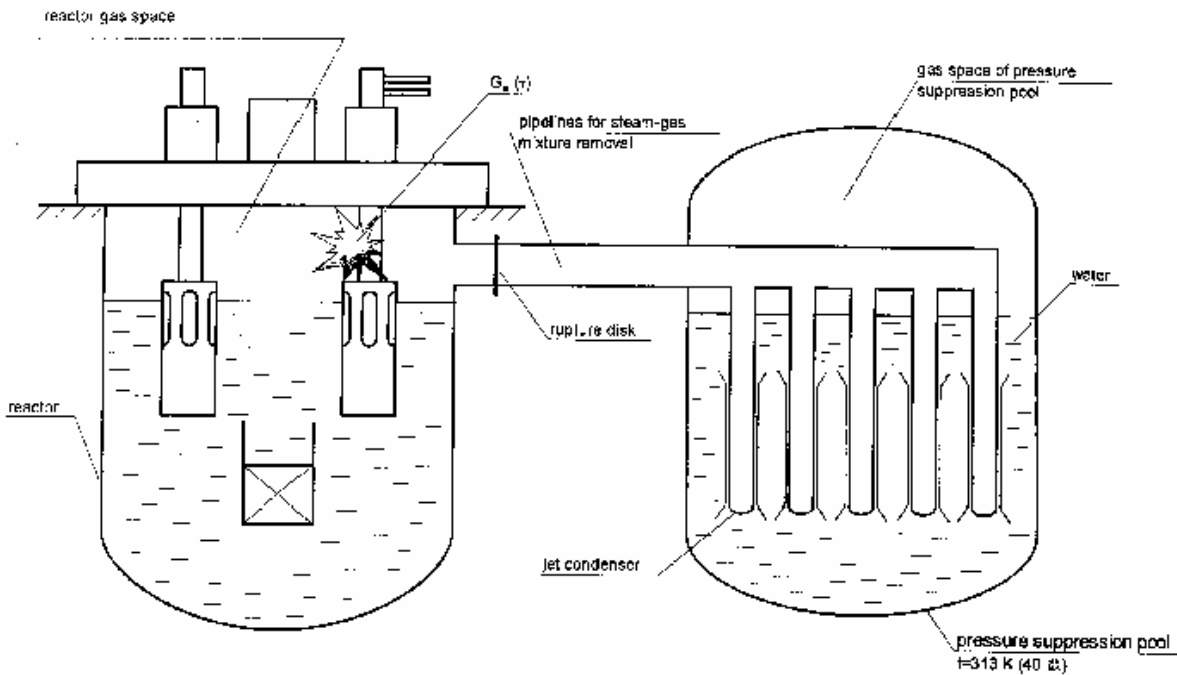


Fig. 31. Design Concept of Pressure Relief System for BREST-300.

The pressure relief system for KALIMER-150 without IHTS could be considered on the similar concept of BREST-300 for overpressure protection from the secondary system where the design pressure of KALIMER-150 reactor is almost similar to atmospheric pressure. However, since the operating pressure of the secondary system is almost 20Mpa and the coolant is non condensable gas, it is not feasible to adopt the design concept used in BREST-300.

Therefore, a filtered venting system could be one of the feasible approaches for pressure relief system. The system uses a Power Operated Relief Valve (PORV) which is installed in the

secondary system and actuates on the signal of interface breaks such as rapid pressure spike of primary system. The system is composed two physically separated loops. Each loop has two power operated serial and parallel valve ash shown in Fig. 32.

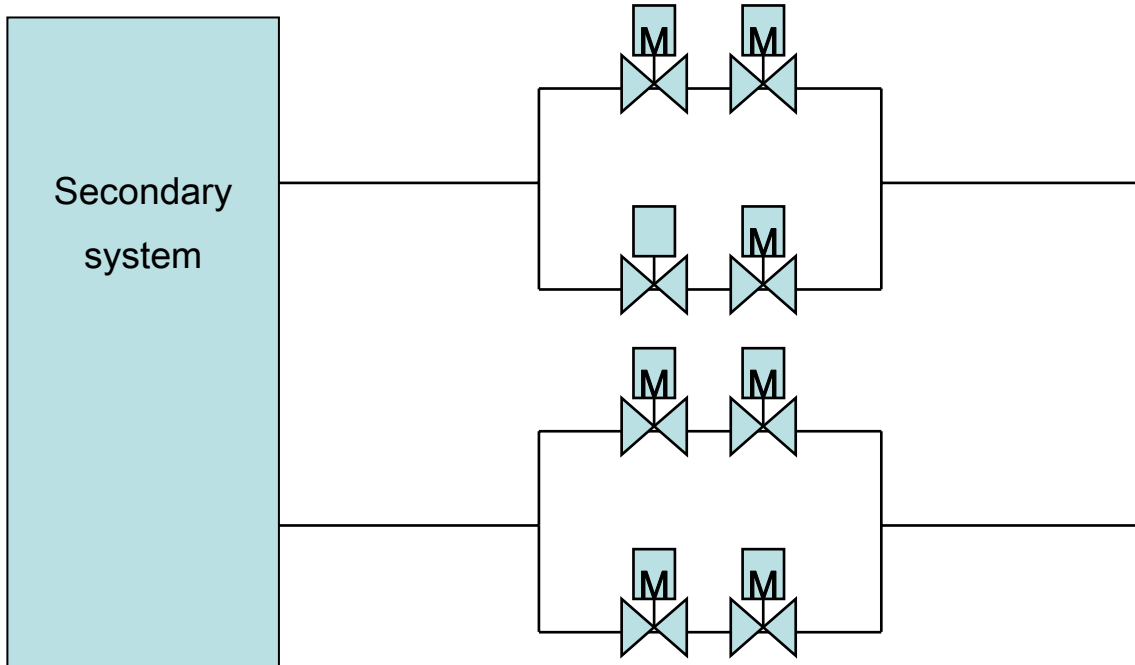
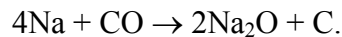
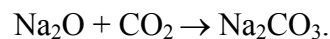


Fig. 32. Design Concept of Pressure Relief System for KALIMER-150 without IHTS

The blowdown flow rate of CO₂ into sodium depends upon the flow area through the tube. Thus, a smaller tube diameter is effective in limiting the flowrate. Of additional concern, is the potential for CO₂ void to be transported to the core. An escape path can be provided for the CO₂ to rise to the free surface of the sodium pool. As the CO₂ rises through the sodium, chemical reactions could take place. The reactions would occur at the transient interface between the substances. Experiment studies with liquid sodium metal at temperatures between 110 and 200°C exposed to carbon dioxide gas at low pressure (less than atmospheric) suggest that liquid sodium can react with carbon dioxide. Sodium first reacts with carbon dioxide to form sodium oxide and elemental carbon,



Then, in the presence of excess CO₂, the sodium oxide would further react with CO₂ to produce sodium carbonate,



It is not known whether the above reaction sequence would still be valid for high pressure blowdown and intermixing of CO₂ in a sodium pool at 530°C. Thermodynamic calculations of the reaction equilibrium for the reactor-relevant conditions would be extremely useful. If the

above reaction sequence is assumed to be correct, there should be no gas generation, although there might be heat generation. Thus, explosion hazards such as the sodium-water reaction would appear to be extremely unlikely. However, the reaction sequence involves solid reaction products (i.e., carbon and sodium oxides and carbonates), forming particulate matter and/or crust which might tend to clog in coolant flow channels. Following a HX tube rupture, it might be necessary to remove the solid contaminants from the sodium.

Thus, it has been demonstrated that a S-CO₂ Brayton cycle can be coupled to KALIMER with a consequent gain in plant efficiency and a compact balance-of-plant footprint. The case in which the IHTS has been eliminated has been investigated. Future investigations of the case in which an IHTS is retained are needed.

Coupled KALIMER-150/S-CO₂ Brayton Cycle Plant Configuration Studies

An investigation was carried out demonstrating that the S-CO₂ Brayton cycle can be coupled to the KALIMER-150 sodium-cooled fast reactor with an intermediate heat transport system (IHTS). The design point of the S-CO₂ Brayton cycle is selected to obtain maximum efficiency through a sensitivity study of the cycle efficiency with respect to the compression ratio of compressor and the turbine inlet temperature. A maximum pressure of 20 Mpa and a compression ratio of 2.7 are assumed as reference conditions for which a turbine inlet temperature of 517.0 °C provides a maximum efficiency. Figure 33 provides an illustration of the coupled reactor and S-CO₂ Brayton cycle through sodium-to-S-CO₂ heat exchangers (HXs) in the operating conditions of the primary heat transport system (PHTS) and the IHTS of KALIMER-150.

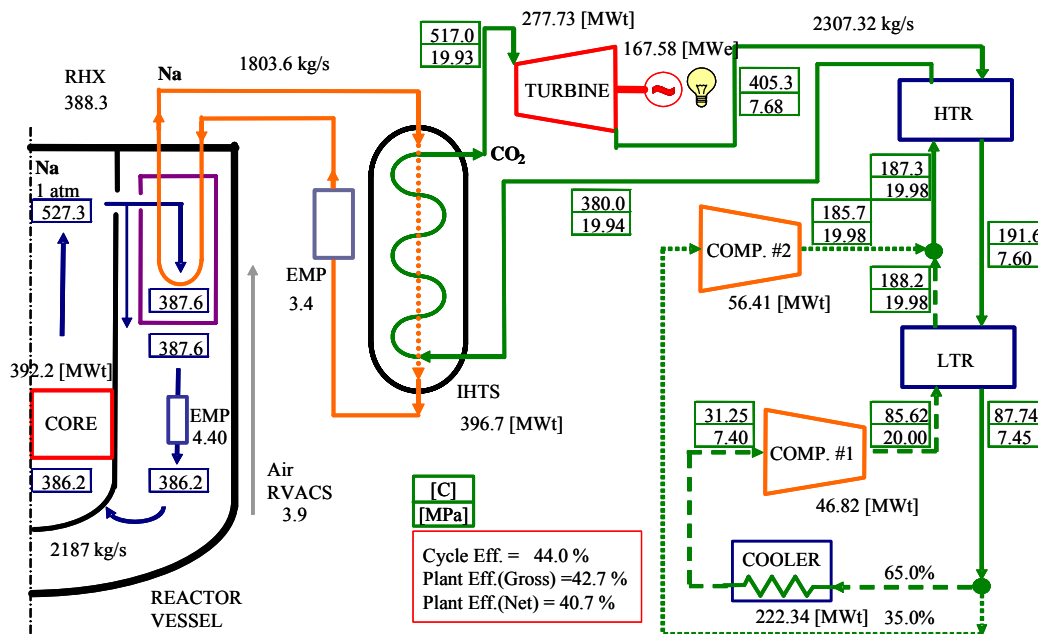


Fig. 33. Schematic of S-CO₂ Brayton Cycle Coupled to KALIMER-150.

A computer code was developed that determines the steady state behavior of a S-CO₂ Brayton cycle plant coupled to KALIMER-150. The code determines the Brayton cycle efficiency and the overall plant efficiency. A resulting Brayton cycle efficiency of 44.0 % is calculated. Subtracting the power for the primary coolant pumps (4.4MW) and intermediate pumps (3.4MW), a plant efficiency of 40.7 % is obtained.

A sensitivity study of the cycle efficiency with respect to the compression ratio of compressors and the turbine inlet temperature was carried out. Figure 34 shows the dependency of the cycle efficiency on two key parameters. The maximum efficiency is calculated for a design point of the turbine inlet temperature of 550°C and a compression ratio of 3.7; that is, for a maximum pressure of 27.4 Mpa. However, there is no experience with component design and operation at such conditions. A maximum pressure of 20 Mpa, i.e., a compression ratio of 2.7, was therefore selected for the cycle design condition. For the compression ratio of 2.7, the optimal design point is calculated at a turbine inlet temperature of 517°C. A temperature-entropy diagram of the S-CO₂ Brayton cycle is presented in Fig. 35. For the optimal operating conditions, the cycle efficiency is about 44 percent.

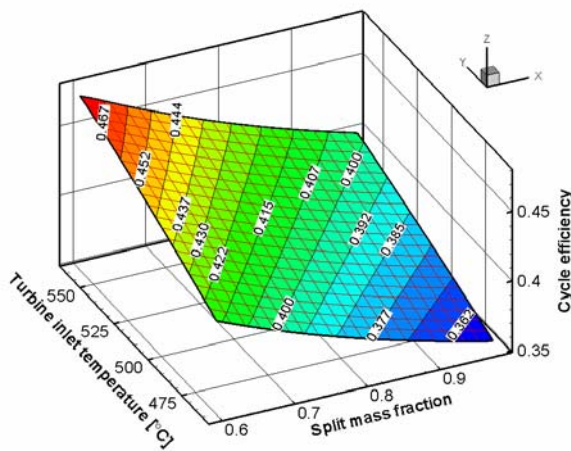


Fig. 34. Cycle Efficiency Dependencies.

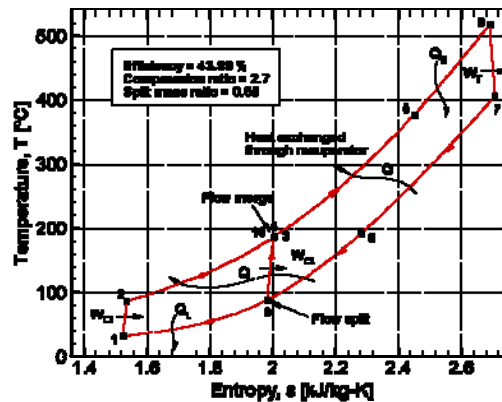


Fig. 35. T-s Diagram for the Cycle.

An investigation was carried out of different plant heat transport configurations to assess the potential gain in efficiency from incorporation of the S-CO₂ Brayton cycle. In all cases, the core outlet and inlet temperatures are held fixed at 550 and 386°C, respectively. The primary and intermediate electromagnetic pumps are assumed to deliver the driving heads required to maintain the primary inlet and outlet temperatures. The IHX and HX tube diameters, tube heights, tube spacing, and number of tubes are optimized to maximize the cycle efficiency subject to the constraint that in-vessel IHXs and HXs must fit within the volume available inside of the KALIMER-150 reactor vessel. For the case in which an IHTS is incorporated, a S-CO₂ Brayton cycle efficiency of 42.0 % is calculated. When the IHTS is eliminated and Na-to-CO₂ HXs are installed inside of the reactor vessel, a lower cycle efficiency of 41.2 % is calculated. The limitation on size of the in-vessel HXs limits their performance resulting in lower

efficiencies compared with the case incorporating an IHTS. It is possible to achieve efficiencies exceeding those with an IHTS by utilizing larger HXs located outside of the reactor vessel and coupled to it with piping segments. A cycle efficiency of 42.3 % is calculated. However, the configuration incorporating ex-vessel HXs represents a departure from the traditional Na pool reactor concept. On the basis of the results as well as safety-related considerations, it has been decided to retain an IHTS.

Cycle/Plant Efficiency Optimization Study

In order to take advantage of the greater Brayton cycle efficiency at higher temperatures, the S-CO₂ temperature at the turbine inlet should be as high as possible. This temperature, however, is limited by the intermediate sodium temperature at the Na-CO₂ heat exchanger (HX) and the HX performance. The sodium temperature, in turn, is limited by the primary sodium temperature at the intermediate heat exchanger (IHX) inlet, which is equal to the core outlet temperature, and the performance of the IHX. Since the primary sodium core inlet and outlet temperatures are considered fixed, the secondary sodium temperature (and, therefore, CO₂ temperature) could be increased by enhancing the performance of the IHX. The simplest way to increase the IHX performance is to increase the heat transfer area by using as much space as is available inside the reactor vessel. For this reason, kidney-shaped heat exchangers were selected for the IHXs. Figure 36 illustrates the cross-sectional area of the kidney-shaped heat exchangers compared to the original circular IHX design. The use of kidney-shaped IHXs with their greater heat transfer area enables the sodium IHX outlet temperature to be raised to 524°C (compared to 511°C before).

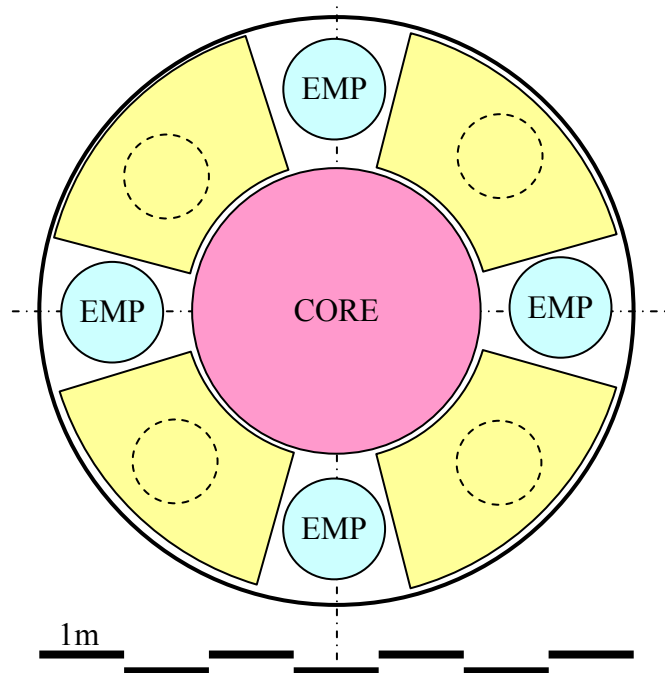


Fig. 36. IHX Design Comparison.

The design analysis code was modified to model frictional pressure drops around each of the primary and intermediate Na circuits. Major pressure drops in the primary circuit include the core, a core inlet orifice, and the shell side of an in-vessel heat exchanger. The Novendstern model was used for the wire wrapped fuel pins. The pressure drops on the shell and tube sides of the heat exchanger were obtained from the ASTEED code, which was developed by KAERI for the thermal hydraulic performance analysis of shell-and-tube type heat exchangers. In an intermediate circuit, the pressure drop on shell side of the Na-CO₂ heat exchanger was also obtained from the ASTEED code. Table 3 shows the summary of pressure drops and required pumping power in the each of the primary and intermediate Na circuits.

Table 3. Pressure Drops and Required Pumping Power

Primary Na circuit		Intermediate Na circuit	
Core and orifice, kPa	675	Tube side of IHX, kPa	9
Rest of circuit, kPa	125	Shell side of Na-CO ₂ HX, kPa	14
Shell side of IHX, kPa	5	Total, kPa	23
Total, kPa	805	Pumping power, MW	0.1
Pumping power, MW	4.0		

The Na-CO₂ HXs were also optimized to increase the HX performance. For example, four heat exchangers were used instead of two steam generators. The total effect from optimizing the IHX and Na-CO₂ HX designs is to increase the CO₂ temperature at the turbine inlet (HX outlet) from 460°C to about 517°C. Figure 37 shows the temperature distribution for the systems as well as the Brayton cycle efficiency. The gross efficiency (which takes into account the calculated pumping requirement for sodium) is 41%.

Na-CO₂ Heat Exchanger Design Optimization

A design method was developed for sizing of a segmented, baffled Na-CO₂ heat exchanger (See Appendix B of the 2004 annual report). Through application of the method, design data of the Na-CO₂ heat exchanger were calculated in parametric sensitivity studies. For the design of the HX, some design limitations were assumed such as pressure drops of the tube and shell sides and the aspect ratio of the HX. The pressure drop of the tube side was stipulated to be 0.4 Mpa such that it is the same as for the steam generator (SG) in KALIMER-150, and the pressure drop on the shell side was set as 0.2 Mpa to reduce the heat transfer area. The aspect ratio of the HX was set as 6.0 to assure a mechanically reasonable design shape. The Table 4 summarizes the Na-CO₂ heat exchanger design results which meet the requirements stated above.

Overpressure Protection System Development

Design concepts for the overpressure protection (OP) systems were developed for the cases with and without an IHTS. The overpressure protection system with IHTS involves installation of a rupture disk on the reactor head through which all the secondary CO₂ is discharged to the containment dome that is filled with inert N₂ gas. The required volume of the containment is calculated with respect to the assumed maximum containment pressure. Comparing the size of

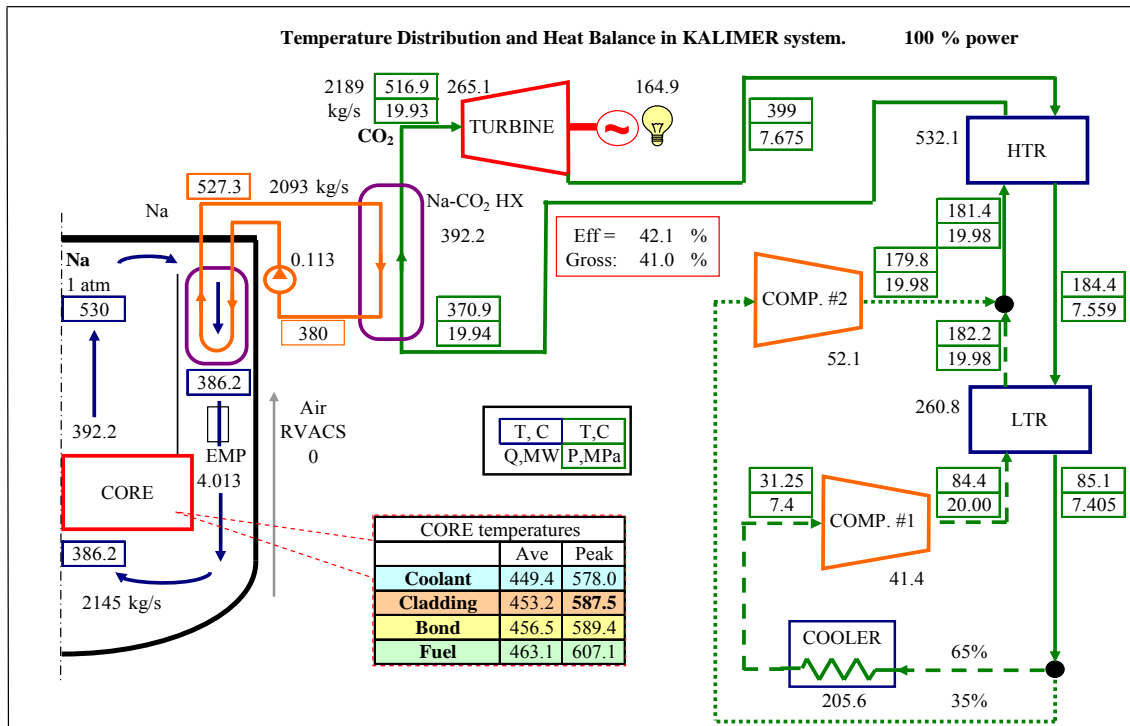


Fig. 37. KALIMER-150 Coupled to the S-CO₂ Brayton Cycle with Optimized HXs.

Table 4. Design Summary of Na-CO₂ Heat Exchanger

Parameter	Values	Parameter	Values
Thermal duty, MW	198.35	No. of tubes	6240
Na Inlet Temp. °C	511	Tube I.D. / O.D., m	0.01/0.016
Na Outlet Temp. °C	339	Tube length, m	13.04
Na Flow Rate, kg/sec	901.8	HX shell O.D., m	2.0
CO ₂ Inlet Temp. °C	330	Tube Arrangement	Triangle
CO ₂ Outlet Temp. °C	460	No. of Baffles	12
CO ₂ Flow Rate, kg/sec	1243.7	Baffle Cut, %	25
Shell side ΔP, Kpa	165	Pitch/Tube O.D.	1.5
Tube side ΔP, Kpa	325	Surface Area, m ²	4088.5

the containment dome with those of other reactors, the calculated required volumes lie in a reasonable range. For the case with an IHTS, the SWRPRS (sodium-water reaction pressure relief system) can be used as the overpressure protection system of the IHTS. For evaluation of the performance of the system, the pressure of the steam generator (SG) shell side is calculated with respect to the number of broken tubes and modeling of choked flow in the tube ends. The SG shell pressure is kept below 0.17 Mpa for the case of 10 ruptured tubes. Detailed design concepts for the overpressure protection systems are presented in Appendix C of the 2004 annual report.

Assessment of HX Failure Consequences

A system transient analysis computer code for long term behavior for HX boundary failure was developed and the transient pressure behavior in the Na-CO₂ heat exchanger and IHTS were evaluated. To simplify tube rupture phenomena in Na-CO₂ heat exchanger, it is assumed that all CO₂ gas merged into the cover gas region. And the Na-CO₂ reaction effect was disregarded in the simulation, since it is known that the reaction rarely occurs in the operating conditions of KALIMER.

Through the calculations, the temperature behaviors of heat exchanger and overpressure protection system were analyzed for single-tube failure as shown in Figure 38. A sensitivity study of system pressure behavior on rupture disk set pressure and drain pipe diameter were performed. The system pressure transients after the Na-CO₂ boundary failure and the actuation of rupture disk is depicted in Figure 38. The analysis shows that the designed overpressure protection system can accommodate the postulated heat exchanger boundary failure. This analysis also is able to cover the activity 3.11 of “Assess HX failure consequences of the S-CO₂ system coupled with KALIMER-150 for the case with IHTS”.

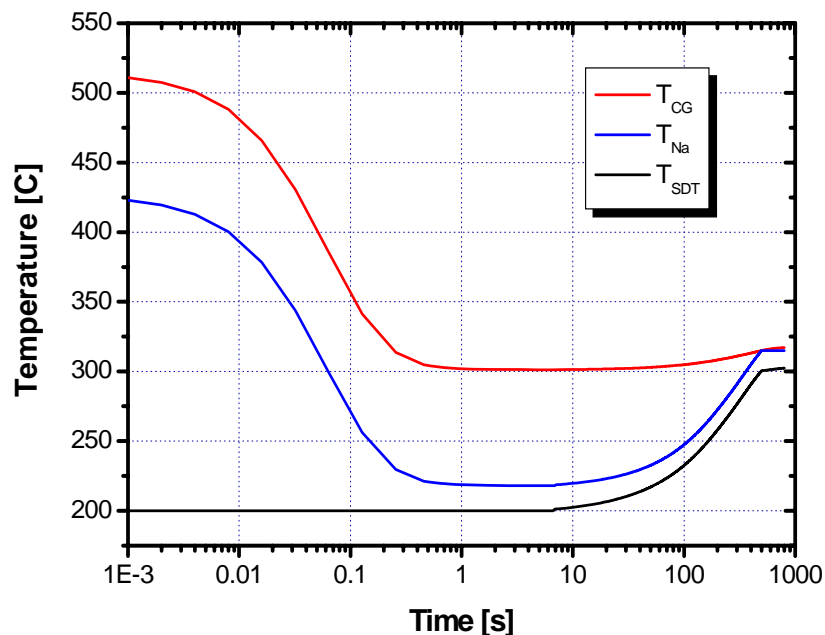


Fig. 38. Temperature Behaviors of SG and OPS.

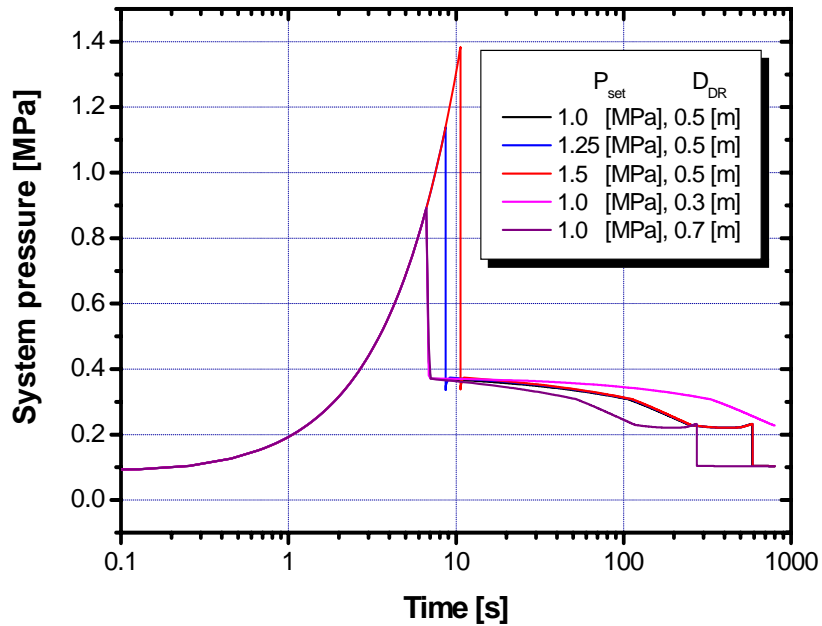


Fig. 39. System Pressure Behavior with Rupture Disk Set Pressure Variations.

Overpressure Protection System Conceptual Design

A conceptual design was presented for overpressure protection system against the boundary failure event of Na-CO₂ Heat exchanger. Because CO₂ rarely react with the liquid sodium below 600°C, only the over-pressurization of IHTS should be considered. The design concept of the system is consisted of sodium drain pipe, tank, rupture disk and separator as shown Fig. 40. The number and the type of pressure relief devices of the system were decided as a single rupture disk which was installed in the bottom Na-CO₂ heat exchanger through the DIER's decision tree methodology.

The design concept was evaluated to determine design data for the case of various numbers of broken tubes for maintaining the integrity of Na-CO₂ heat exchanger and IHTS system. The analyses were done by a one-dimensional computer code which simulates steady state behavior of HX. The critical flow rate and the system pressure of HX calculated with the assumption that the primary system volume and secondary system volume are large enough and the expansion process is isentropic. The pressure distribution in HX is obtained with the consideration of pressure loss in the abrupt expansion and contraction of pipe system of HX. Through the calculation of the pressure difference between upstream and downstream of the broken tube, the choking condition in the broken tube of HX is discriminated. And then, the corresponding leak flow rate was calculated.

The flow rate of supercritical CO₂ was evaluated in various numbers of broken tubes. Because the pressure of downstream of rupture tube is lower than the critical pressure, the choking flow occurs in the end of broken tube as depicted in Figure 41. The HX shell pressure and the leak mass flow rate increase with respect to the increasing number of broken tubes. Choking

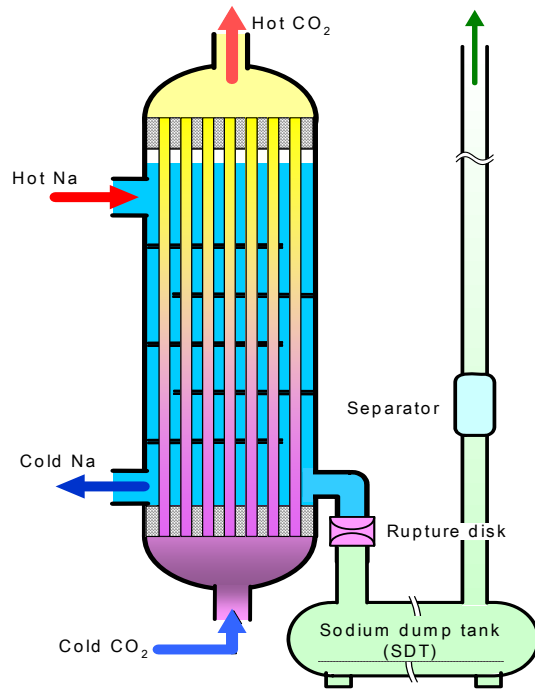


Fig. 40. Design Concept of Overpressure Protection System for KALIMER-150 Coupled with S-CO₂ Brayton Cycle Power Conversion System.

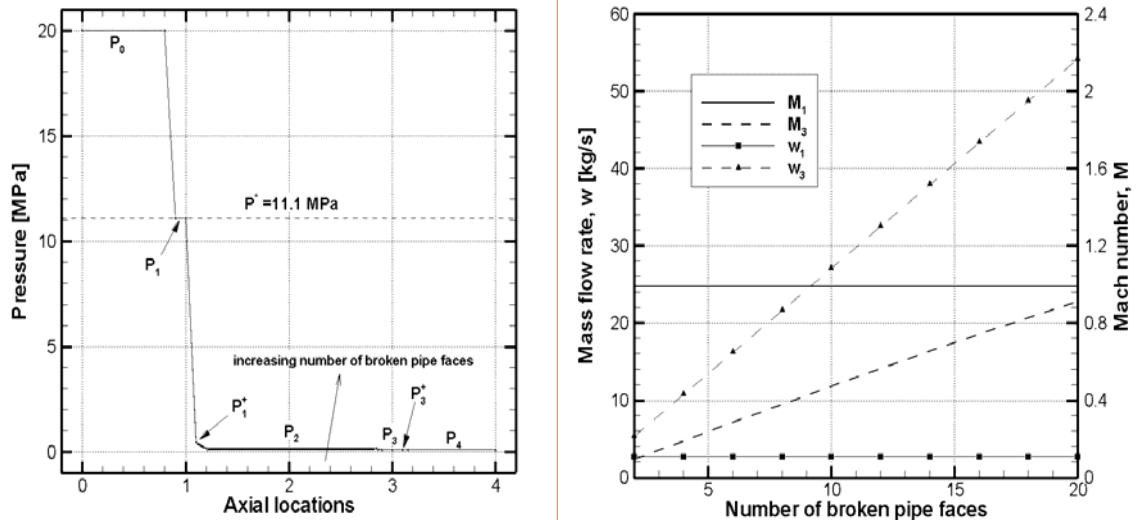


Fig. 41. Pressure Distributions in Axial Locations and Mass Flow Rates and Mach Numbers in Broken Pipe and Drain Pipe.

phenomena do not occur in the drain pipe of sodium due to the large pressure drop in the broken pipe.

Through the analysis, the maximum shell pressure in Na-CO₂ HX is less than 0.18 Mpa in the case of 10 DEGB (double ended guillotine break). The detailed design data of an overpressure protection system were established as shown in Table 5. To set up the design pressure of the OPS, the maximum pressure in the IHTS piping in the range of the allowable stress of the component materials must be estimated. The maximum pressure is the upper limit of the set pressure of the rupture disc. And the maximum pressure on the disc which can occur in the operational transient and operational events should be the lower limit of the set pressure, so the disc doesn't rupture in an operating condition. Between the two limits, the design pressure should be determined with a sufficient margin to satisfy the safety and economic requirements. The maximum pressure in operational transient is 0.75 Mpa and the allowable fluid pressure is 2.79 Mpa.

Table 5. Overpressure Protection System Design Summary.

Item	Design data	Remarks
Number of tube breaks for design basis	1 DEGB	
Rupture disk set pressure [Mpa]	1.0	
Drain pipe diameter [m]	0.51	same with hot leg
Sodium dump tank volume [m ³]	150	

Gas Turbine Performance Analysis

Gas turbine performance analysis methodology using CFD code was developed. Turbine performance analysis methodology was established using CFX computer code. At given geometry, detailed flow field and temperature field were calculated as shown in Fig. 42.

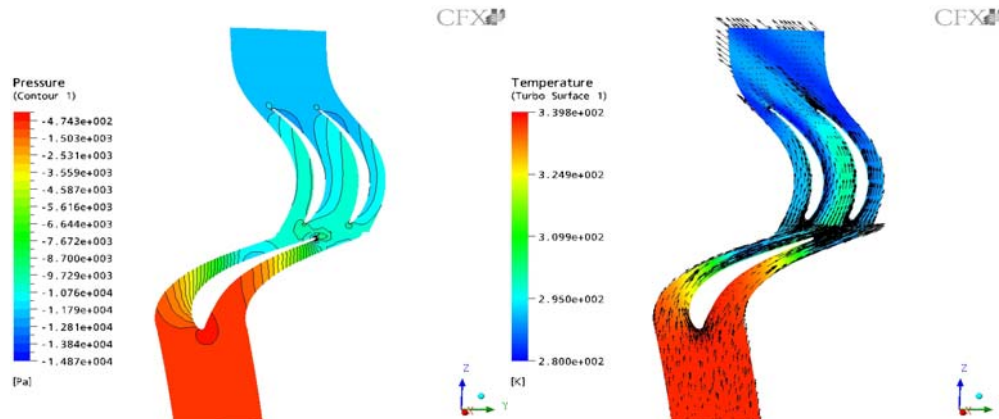


Fig. 42. Pressure and Temperature Distribution and Velocity Vectors in 1-Stage Stator and Rotor of Turbine.

Turbine characteristics for various inlet and outlet conditions were estimated. And, the choking phenomena and condition in turbine blade were investigated. In Figure 43, when the pressure ratio increases, choking occurs in the case that the pressure ratio exceeds 3. The maximum efficiency was obtained at a pressure ratio of 2. The available range of turbine efficiency for system design was presented (~90%).

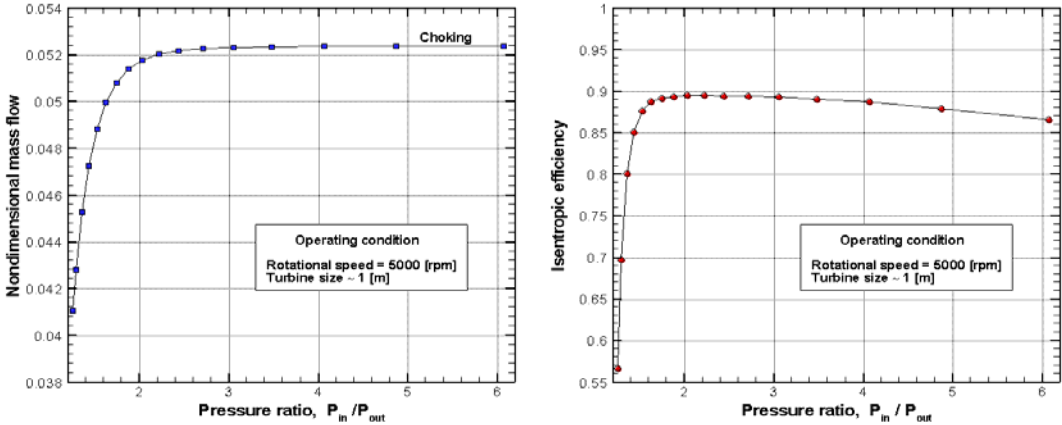


Fig. 43. Performance Curve of a Turbine.

Planned Activities

The reported activities complete the technical work scope planned for Task 3.

Narrative

Task 4: Post-Accident Heat Removal and In-Vessel Retention

Research Objective

The goal of this task is to develop test plans for measurement of phenomenological data describing freezing of molten metallic fuel, melt relocation and interaction with steel structure, and intermixing of high-pressure CO₂ and sodium. These phenomena are relevant for very low probability accident sequences involving core melting or failure of barriers that might challenge containment integrity. The data to be measured is needed for assessment of accident consequences and the establishment of containment requirements.

Research Progress Overview

In 2003, a test plan [11] for measurement of phenomenological data for freezing of molten metallic fuel was prepared (Milestone 4.1). In 2004, a test plan [18] was written for measurement of data describing molten fuel relocation and interaction with steel structures (Milestone 4.2). In 2005, a test plan [29] for characterization of mixing and interaction of high-pressure CO₂ and liquid sodium was produced (Milestone 4.3).

Task 4.1 Test Plan for Measurement of Metallic Fuel Liquidus/Solidus and Mobilization Temperatures

For Task 4.1, preliminary test plans have been developed for two different tests, one for determination of the solidus/liquidus temperature and another for determination of the mobilization temperature of a metallic fuel/steel mixture. For both of these tests, various alloy samples of fuel/steel mixtures will be prepared in a high-temperature furnace with a high-purity inert atmosphere (e.g. helium). These samples will consist of U, Zr, Ce, Fe, Cr, Ni and Mo. Ce is used as surrogate for Pu. The metal fuel (e.g. U-10 wt% Zr alloy) and stainless steel components will be mixed in powder form and heated and melted in a refractory crucible (e.g. yttria). The sample compositions could be determined using SEM/EDS methods.

For the test for determination of the liquidus/solidus temperature, the standard differential thermal analysis (DTA) method will be employed. As defined by the International Confederation for Thermal Analysis, it is a “technique for recording the difference in temperature between a substance and a reference material against either time or temperature as the two specimens are subjected to identical temperature regimes in an environment heated or cooled at a controlled rate”.

Basically, a DTA apparatus consists of four components: 1) Sample holder-measuring system, which comprises the thermocouples and sample containers, 2) Furnace-heat source having a large uniform temperature zone, 3) Temperature programmer-to supply energy to the furnace in such a manner as to ensure a reproducible (and preferably linear with time) rate of change of temperature, and 4) Recording system-method of indicating and/or recording the e.m.f from the differential and temperature measuring thermocouples. The DTA technique now is such a

routine laboratory procedure that a number of DTA instruments are commercially available. For tests envisioned in this activity, the sample temperature would not likely exceed 1500°C. Some of the commercially available DTA instruments designed for high temperature are expected to be suitable for the planned tests.

In a typical DTA measurement, a cylindrical sample of the fuel-steel mixture alloy about 5 mm high and 5 mm in diameter will be cleaned and placed in the DTA crucible and mounted on the sample thermocouple in the DTA system. An identical crucible containing platinum will be mounted on the reference thermocouple. The furnace will be lowered into position and the system will be pumped and flushed several times with high-purity helium. The system will finally be filled with high-purity helium to a pressure slightly above ambient. Samples will be heated to approximately 1500°C. A number of heating and cooling cycles will be completed and data will be recorded (Data from the initial heating/cooling cycle may be discarded). Measurements will be made at heating/cooling rates of 5-10 K/min.

A typical DTA curve consists of the temperature difference between the test and reference materials plotted against time or temperature. The DTA curve normally contains one or more exothermic and/or endothermic peaks, which are indicative of phase transitions. Generally, solidus temperatures are determined on heating and liquidus temperatures are determined on cooling. A simple DTA curve taken from previous ANL work [L. Leibowitz et al., "Solidus and Liquidus Temperatures in the Uranium-Plutonium-Zirconium System", *Journal of Nuclear Materials*, 154 (1988) 145-153] is shown in Fig. 44, which gives a portion of a heating/cooling cycle run at 10 K/min for a sample of U-19.5 Pu-3.3 Zr (atomic %) alloy. Fig. 44 indicates that the solidus for this alloy is 996°C while the liquidus is 1050°C.

The planned test matrix for determination of the solidus/liquidus temperature is based on the following sequence: 1) Calibration tests that periodically measure the melting point of high-purity material (e.g. aluminum and gold) to ensure that accurate temperatures are being obtained, 2) Baseline tests for fuel components, i.e. U-Ce-Zr alloys for comparison with available data for U-Pu-Zr alloys, and 3) Main tests for fuel-steel mixtures in various proportions.

For the test for determination of the mobilization temperature, a thermal gravimetric method will be employed. This method is based on measurement of a weight loss that occurs as the sample alloy contained in a narrow tube is heated and becomes molten and starts to flow under gravity. Measurements will provide insight into the overall mobility of the sample as a function of temperature.

A schematic diagram of the apparatus is shown in Fig. 45. Briefly, it consists of 1) a narrow, refractory (e.g. yttria) tube ("sample holder tube") hung from a tantalum wire which is connected to a microbalance, 2) an electric furnace surrounding the sample tube, 3) a temperature control device, 4) a catch cup underneath the sample holder tube, and 5) a steel enclosure for the furnace and catch cup. (During the test, this steel enclosure will continually be purged with an inert gas such as Argon).

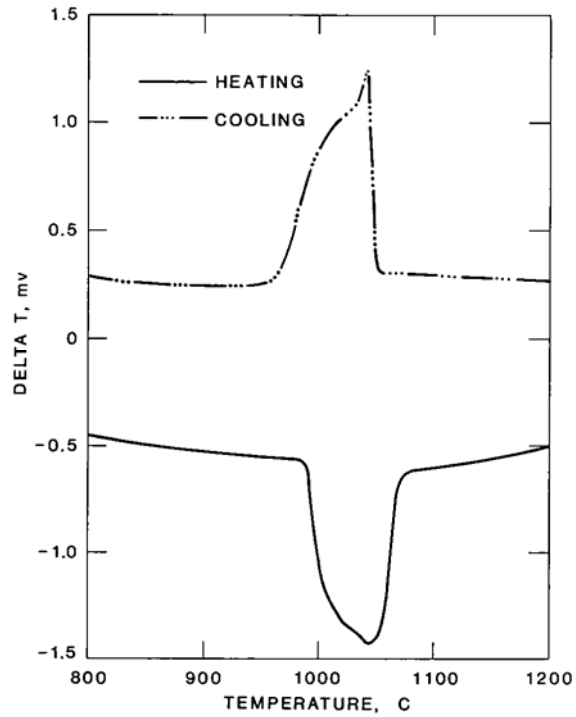


Fig. 44. Heating and Cooling DTA Curves at 10 K/mm for U-19.5 Pu-3.3 Zr (at. %) Alloy. (L. Leibowitz et al.)

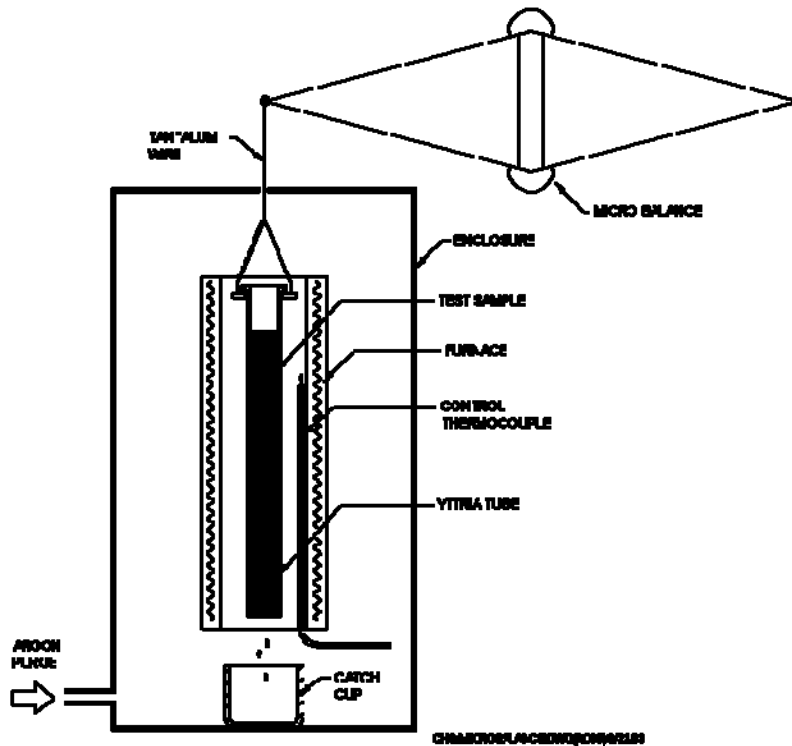


Fig. 45. Thermal Gravimetric Method for Determination of Mobilization Temperature.

A typical test procedure will consist of the following steps: 1) Load the sample holder tube with a fuel/steel mixture of desired compositions while blocking the bottom end of the tube (e.g. with a piece of refractory sheet), 2) place the sample holder tube with the bottom end blocked in the furnace and melt the fuel-steel mixture sample, 3) Remove the sample holder tube from the furnace when the sample has frozen and cooled to room temperature and remove the refractory sheet blocking the bottom end of the sample holder tube, 4) Re-place the sample holder tube containing the sample (once molten and frozen) in the furnace and suspend it from a tantalum wire which is connected to a microbalance. The microbalance measures the combined weight of the sample holder tube and sample alloy. 5) Place a refractory dish (“catch cup”) underneath the sample holder tube so that melt flowing out of the bottom end of the tube under gravity may be collected, and 6) Heat the furnace in a pre-determined mode and monitor the temperature increase and weight loss of the sample holder tube and sample alloy as a function of time. The sample temperature may be increased linearly with time or at a variable rate.

The mobilization temperature of the sample alloy may be determined by noting the temperature at which the combined weight of the sample and holder tube begins to decrease. In addition, the time-history of the weight loss at a given temperature would provide insight into the overall mobility of the sample at that temperature. To extract quantitative information on the sample mobility, modeling efforts would be required. Specifically, a model describing the behavior of transient flow of melt in a narrow tube under gravity is needed. If the sample is heated to a temperature between the solidus and liquidus, the sample would most likely contain a “mushy” zone where the solid and liquid phases co-exist. This mushy zone may exhibit a non-Newtonian behavior, which would need to be taken into consideration in the modeling efforts.

The planned test matrix for determination of the mobilization temperature would be very similar to that for determination of the solidus/liquidus temperature. Initially, calibration tests using high-purity material (e.g. aluminum and gold) will be conducted to see if the mobilization temperature coincides with the melting point of the high-purity material. Data on the transient flow behavior of the high-purity material will be collected and compared to the model predictions. These calibration tests will be followed by the baseline tests employing fuel alloys and the main tests employing fuel-steel mixture alloys.

Task 4.2 Test Plan for Measurement of Metallic Fuel and Fuel/Steel Alloy Freezing Behavior

An effort has been made by KAERI to establish the requirements for the tests investigating molten fuel relocation behavior upon injection into the coolant channel. Preliminary test requirements have been developed by KAERI for two different tests, one for investigating the relocation and freezing behavior of fuel melt in steel channels and the other for looking into the possible inter-metallic chemical interaction of the fuel melt with steel structures. Test requirements developed are made of the general requirements that are in general nature or applied to both types of the tests as well as those specific to each type of tests. Some of the major items constituting the requirements include test objectives and scope, test facilities, protection, test data required, test material and composition, test variables and their ranges, measurements, data acquisition and control, and post test analysis.

With input from KAERI regarding the testing requirements, a preliminary test plan has been developed for investigations of relocation and freezing behavior of molten fuel in coolant channels and possible chemical interactions of molten fuel with steel. This preliminary test plan is described below.

Two different types of tests are described here. The first type is concerned with the transient freezing and plugging behavior of molten fuel flowing in coolant channels (“Freezing/Plugging Test”) whereas the second type investigates aspects of the intermetallic chemical interaction between molten fuel and solid steel (“Chemical Interaction Test”). Depending on the melt temperature, the molten fuel/steel chemical interaction may play a role in the first type of tests and will be considered in the post-test examination. Thus the chemical interaction test will be useful in the analysis and interpretation of the results of the Freezing/Plugging Test. In addition, the Chemical Interaction Test is expected to provide significant information relevant to the development of in-vessel retention concepts for KALMER. A single test apparatus will be employed for the two types of tests.

As shown schematically in Fig. 46, the overall test apparatus consists of a fuel melt furnace vessel, melt delivery system, test section, catch pan and containment vessel. Each component of the apparatus is described below.

The melt furnace vessel serves for both melting the fuel alloy and injecting the molten fuel into the test section. It is a flanged, 304 stainless steel pipe (e.g. nominal 8 inch, schedule 10) and is mounted on the top plate of the containment. The inside surfaces of the vessel are insulated (e.g. alumina sleeve with an air gap). The fuel alloy is inductively heated to melting and then to test temperature in a crucible sealed within the melt furnace vessel. The crucible is designed for melt masses up to 5 kg. Various crucible materials may be considered, including graphite and ceramics such as MgO. The crucible may be coated with a thin layer of yttria paint to protect it from chemical attack by the molten fuel alloy. The bottom of the crucible has a tapered opening that can accommodate a plug, which may be of the same material as the crucible or other ceramics (e.g. zirconia). The fuel is heated and melted with the plug firmly placed in the bottom opening of the crucible. This plug is removed pneumatically with a pull rod from the crucible opening, thus permitting the downward injection of the fuel melt into the test section. Type K thermocouples are mounted in the gas space inside the vessel and inside the melt in the crucible. A pressure transducer is mounted on the vessel to monitor the vessel pressure.

The melt delivery system directs the fuel melt from the crucible in the furnace vessel to the test section. It comprises a ceramic drop tube inside the furnace vessel, adapter tube below the furnace vessel and funnel. The drop tube is located directly below the crucible inside the furnace vessel. The adapter tube is a doubly-flanged, stainless steel tube that connects the furnace vessel to the top of the containment. The bottom end of the adapter is located inside the containment and closed by a steel diaphragm held in place by flanges. The diaphragm is made of cold-rolled type 302 stainless steel and its thickness is in the range of 0.001 – 0.002 inch. The steel diaphragm forms part of the pressure-containment boundary of the furnace vessel/adapter tube system. It is designed to fail quickly upon contact by melt flowing out of the crucible. The funnel is located directly below the bottom of the adapter tube and receives the melt that flows from the crucible and directs it into the flow channel of the test section.

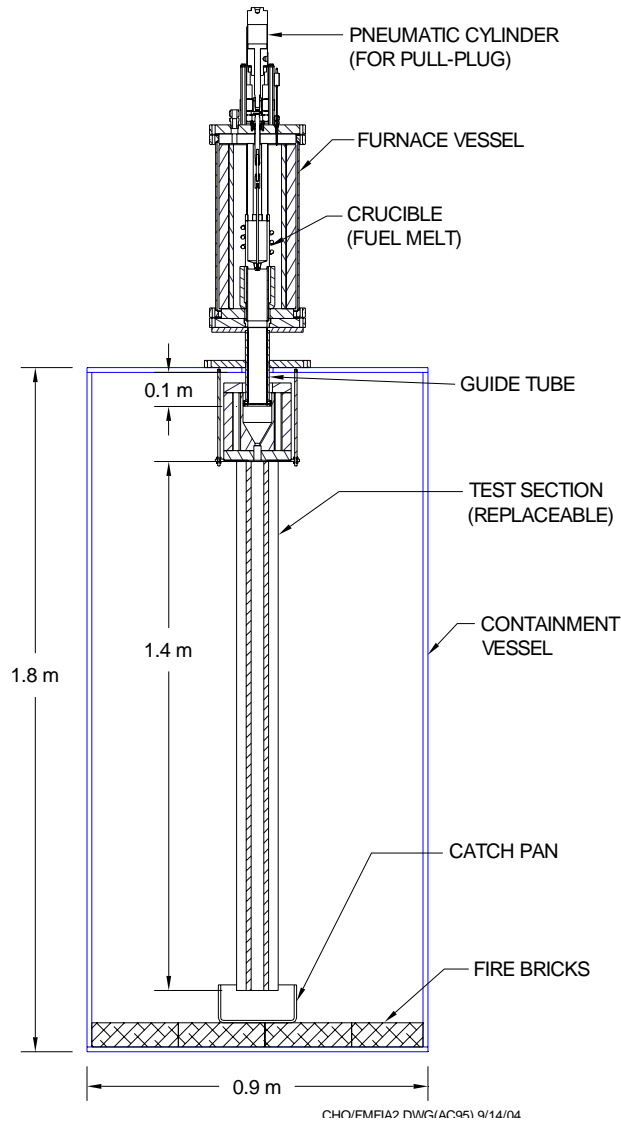


Fig. 46. Fuel Melt Freezing and Interaction Apparatus.

The catch pan is a tray which is placed below the bottom of the test section. It is designed to collect any melt material that may flow out of the bottom of the test section. The catch pan may be made of a ceramic or graphite if necessary.

The body of the containment vessel is a 1.8-m long section of a 0.91-m O.D., 25 mm thick carbon steel pipe. The electrical and mechanical penetrations, such as those for heating wires and Argon purging, are through the top and bottom covers of the vessel. Also, the containment vessel is equipped with sight ports for visual inspection of the inside of the vessel. The inside bottom surface of the vessel is lined with fire bricks for protection from possible splashing of the melt.

For the freezing/plugging test, three different flow channel geometrics will be employed for the test section. The first flow channel geometry is a circular tube made of stainless steel. The I.D. of the tube will be 4.0 mm, corresponding to the hydraulic diameter of the KALIMER -600 coolant channel. This circular tube geometry will be used to obtain baseline data for modeling purposes. The second flow channel geometry is a rectangular tube made from stainless steel. Its internal dimensions will be 4.0 mm by 8.0 mm. The 4.0- mm opening corresponds to the subassembly duct wall gap. The purpose of this rectangular tube geometry is to obtain data pertinent to melt flow through the gaps between subassemblies. The third flow channel geometry is a 3-pin bundle contained in a stainless steel, fluted tube. The pin may be a solid rod or circular tube made of stainless steel. The pin diameter and the flow area will correspond to those of KALIMER-600. The cross sections of the three flow channel geometrics are shown in Fig. 47. For all these flow geometrics, the test section height will be the same at about 1.4 m.

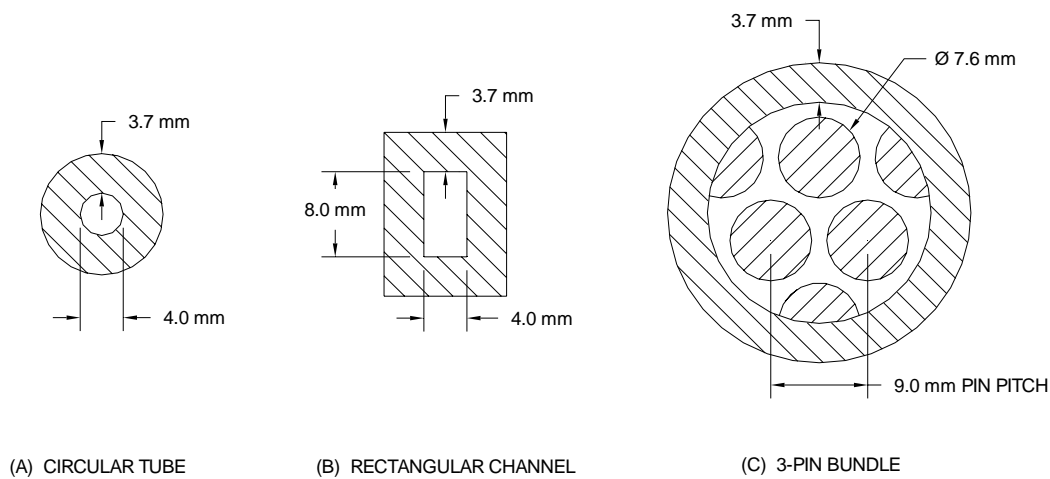


Fig. 47. Cross-Section of Freezing/Plugging Test Section.

For the chemical interaction test, the test section consists of a steel cylinder divided into two compartments by a circular steel disc in between. As shown in Fig. 48, the test section may be assembled by clamping a circular steel disc between two pipe sections (e.g. 3-inch nominal, schedule 80). The bottom of the test section will be closed while the top will be open for molten fuel entry. Both the upper and lower compartments of the test section will be instrumented with a thermocouple and a conductivity probe. The upper compartment conductivity probe will detect the arrival of fuel melt at the circular steel disc while the lower compartment conductivity probe will detect the penetration of fuel melt through the steel disc due to chemical interactions. The time delay in the probe signal between the two compartments would correspond to the time of fuel penetration through the steel disc. The inner surface of the steel cylinder (i.e. two compartments) will be protected from possible chemical interactions by a ceramic (“mullite”) sleeve inserted in the cylinder as shown in Fig. 48. Thus, fuel-steel chemical interactions will be limited to the steel disc. The thickness of the steel disc would be in the range of 1.0-5.0 mm. If the thickness is much smaller than 1.0mm, the steel disc might fail under the load of the melt weight at high temperature. A thermocouple will be attached at the bottom of the steel disc to measure the temperature history during the fuel-steel interaction including the penetration of the steel disc.

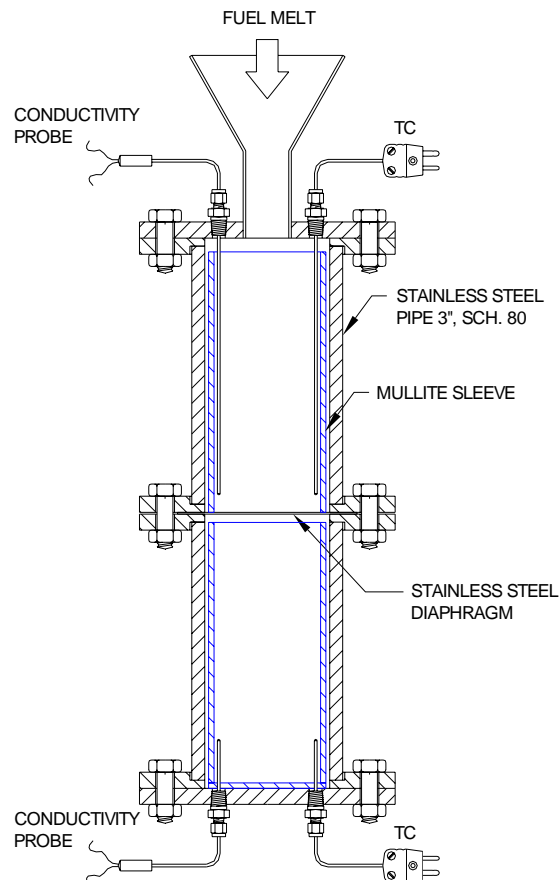


Fig. 48. Chemical Interaction Test Section.

The test matrix for the freezing/plugging test will consider the following parameter ranges. Three different fuel alloys, namely 1) pure uranium, 2) uranium-zirconium alloy and 3) KALIMER fuel with Pu replaced by Ce will be used for the melt material. Two different melt superheats (e.g. 50° and 100°C) will be considered for the melt temperature. Two different initial temperatures (e.g. 300° and 500°C) will be employed for the test section flow channel. For the melt injection, gravity flow as well as pressure-driven flow will be utilized.

The test matrix for the chemical interaction test will consider the following parameter ranges. Two types of melt materials will be employed. The first type is based on fuel components only while the second type involves mixtures of fuel and steel components. The steel disc material and thickness will be varied. The disc material will be 304/316 stainless steel as well as HT-9 steel. The disc thickness will be in the range of 1.0 – 5.0 mm. Two different melt superheats (e.g. 25° and 50°C) will be considered for the melt temperature. The test section temperature will vary from sodium inlet temperature to sodium boiling point.

Task 4.3 Test Plan for Measurement of CO₂/Sodium Mixing Consequences in Pool Geometry

Technical Issues

For the CO₂-sodium mixing and interaction, three technical issues to be addressed have been identified. These are; 1) heat exchanger pressurization, 2) CO₂ gas bubble entrainment in the primary sodium flow, and 3) damage to heat exchanger tubes (“wastage”). The first two issues are safety-related while the third issue would likely have an operational and economic impact. The second issue would not arise unless the heat exchanger involves the primary coolant sodium.

Primary information needs are concerned with the nature and extent of the sodium CO₂ chemical reaction. Available data seems to indicate that the chemical reaction between sodium and CO₂ would likely produce sodium oxide, sodium carbonate, carbon, and perhaps, carbon monoxide (note that none of these are explosive compounds). Also, thermodynamic consideration would suggest that the heat of the sodium-CO₂ reaction would be comparable to that of the sodium-steam reaction (of the order of 20-60 Kcal per mole of sodium), depending on the reaction sequence assumed. However, information on the kinetics of the sodium CO₂ reaction is virtually non-existent. The overall reaction rate would also depend on the extent of sodium-CO₂ mixing. Thus, experiments at conditions relevant to situations of interest (e.g. pressure and temperature) are needed.

Apparatus

It is planned to employ a single apparatus to conduct three different types of experiments. The apparatus will consist of a test section and associated components (e.g. CO₂ gas supply tank, CO₂ gas injection device, sodium vapor trap, aerosol collection device, sodium reservoir tank and instrumentation), as indicated in Fig. 49.

The test section is a 2.0 m long section of a 4 inch, schedule 80, type 316 stainless steel pipe. It is instrumented with an array of thermocouples along its length, inserted through the bottom flange. A pressure transducer is connected to the top of the test section. The test section is heated by a set of band heaters clamped around the outside wall of the test section. The CO₂ gas injection device is inserted into the test section through the top flange. The CO₂ injection device is a standard gas sparger, the sparger hole size being in the range of 0.5 – 1.0 mm. It is shown schematically in Fig. 50. The test section is filled with sodium and heated by the band heaters. The CO₂ gas is injected into the sodium column near the bottom of the test section. Depending on the type of an experiment to be conducted, three different designs for the CO₂ gas injection device will be employed, as described below. The top of the test section is closed except for a ½ inch O.D. tube that carries the CO₂ gas/sodium vapor mixture to a sodium vapor trap/aerosol collection system before exhausting to the environment.

An assembly drawing of the test section is shown in Fig.51.

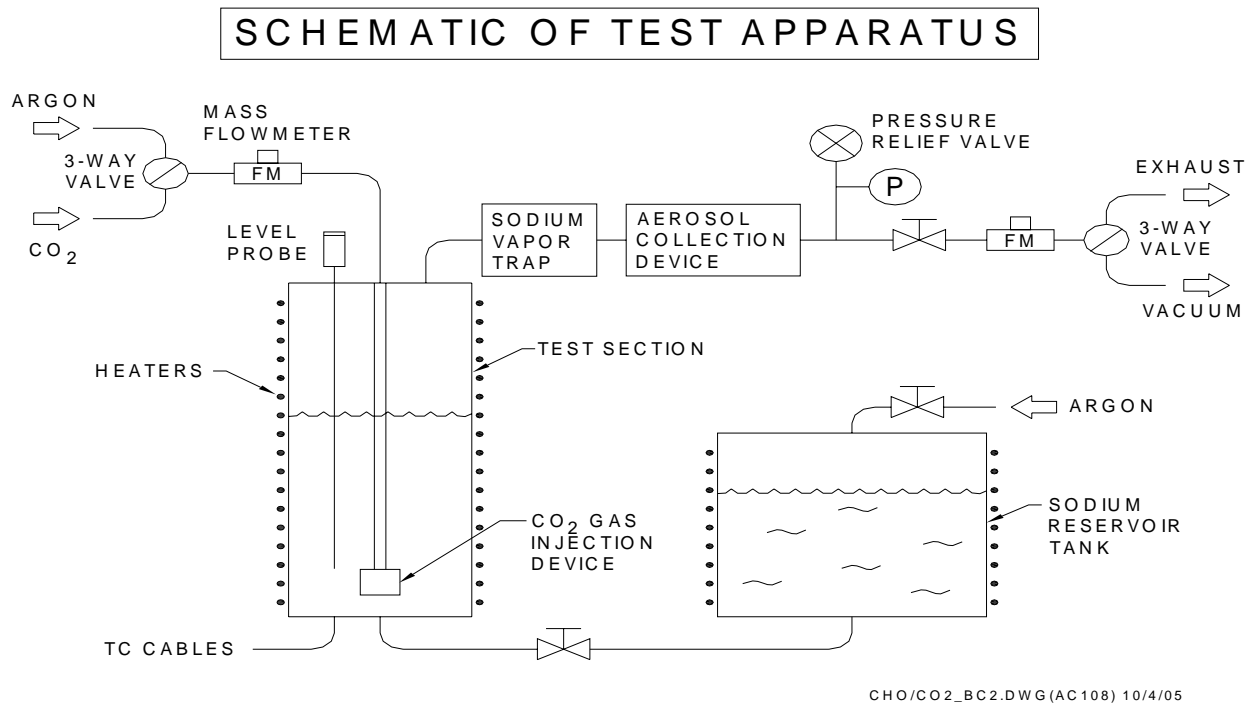


Fig. 49. Schematic of Test Apparatus

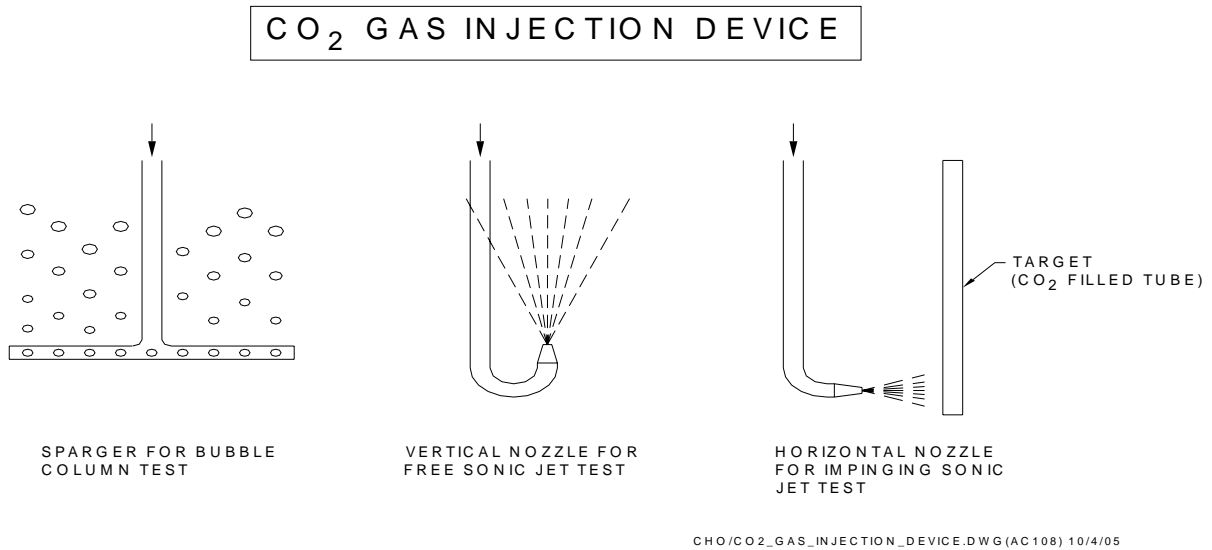


Fig. 50. CO₂ Gas Injection Device.

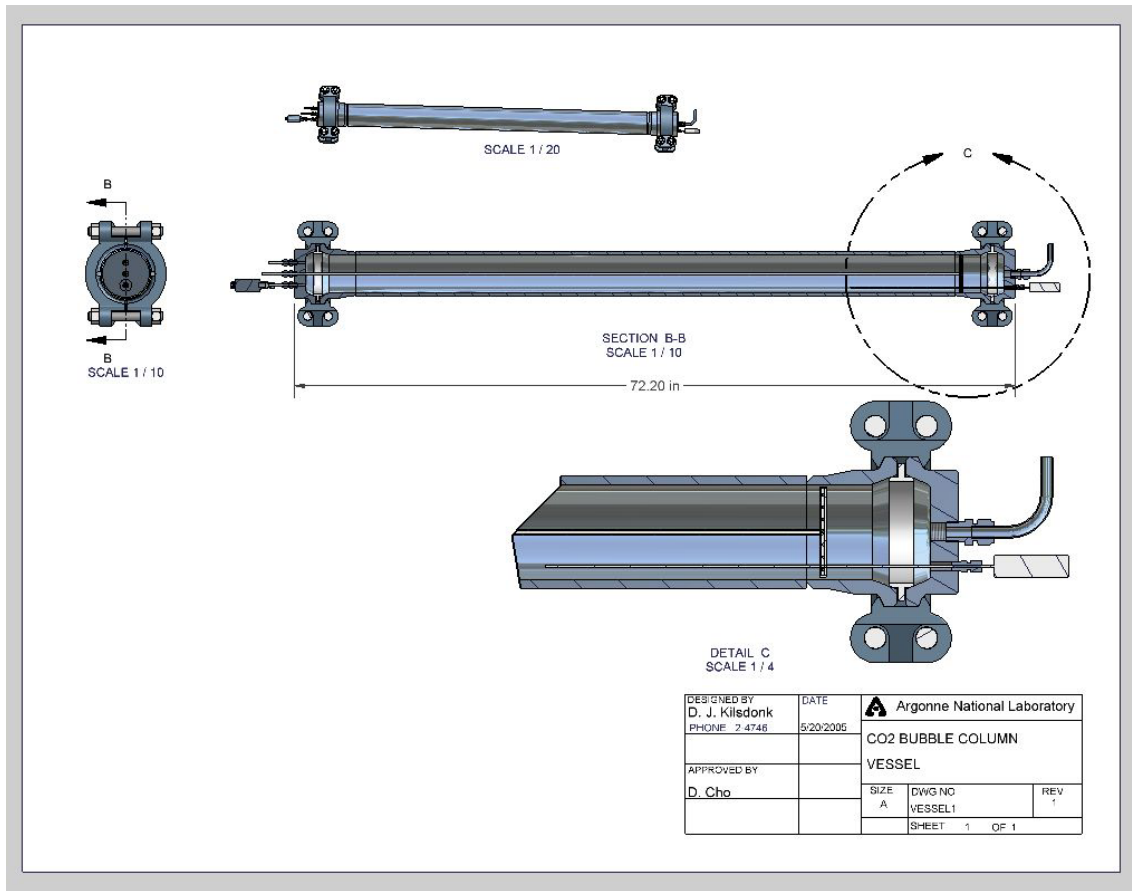


Fig. 51. Assembly Drawing of Test Section.

The apparatus will be employed to conduct the following three types of experiments.

1. Bubble Column Experiment: The experiment will involve bubbling of CO₂ gas in a column of liquid sodium at various temperatures and pressures. Baseline data on the reaction heat release as well as product species will be obtained for modeling purposes. The CO₂ injection device will be a standard gas sparger, the sparger hole size being in the range of 0.5 – 1.0 mm. Measurements will be relevant to issues associated with the CO₂ bubble entrainment in a sodium flow.
2. Free Sonic Jet Experiment: The experiment will involve vertical, upward injection of CO₂ gas in the sodium pool. The CO₂ gas pressure will be such that the flow at the injection nozzle will be choked, i.e. sonic. The CO₂ gas injection device will be a single vertical nozzle. Measurements relevant to the pressurization issue will be made.
3. Impinging Sonic Jet Experiment: The experiment will involve horizontal injection of CO₂ gas in the sodium pool. The CO₂ gas pressure will be such that the flow at the injection nozzle will be choked, i.e. sonic. The CO₂ gas injection device will be a single horizontal nozzle. A CO₂-filled tube will be located next to the injection nozzle so that the CO₂ gas jet will impinge upon the tube. The distance from the

nozzle to the neighboring tube will be in the range of several millimeters. Measurements relevant to the wastage issue will be made.

Test Plan

The test plan report consists of five sections; Introduction and Background, Objectives, Exploratory Capsule Test, Main Test Approach, and Main Test Description.

The test plan describes three types of experiments that will address the various issues associated with failure of the sodium-CO₂ heat exchanger boundary. The first type (“Bubble Column Test”) will provide baseline data on the Na-CO₂ reaction behavior as well as measurements relevant to the issue of CO₂ gas bubble containment in sodium flow. The second type (“Free Sonic Jet Test”) will provide measurements relevant to the issue of pressurization of the Intermediate Heat Transport System due to failure of the sodium-CO₂ heat exchanger boundary. The third type (“Impinging Sonic Jet Test”) will provide measurements relevant to the wastage issue including self-wastage damage and damage propagation.

A preliminary test matrix for each of the three types of experiments was developed. Generally, the sodium temperature will range from 200°C to 500°C. For the Bubble Column Test, the test section pressure will nominally be 0.1 Mpa. For the Free Sonic Jet Test as well as for the Impinging Sonic Jet Test, the CO₂ gas pressure in the feeding tube will range from 1.0 to 10.0 Mpa.

Exploratory Capsule Test

A concept for an exploratory test for preliminary assessment of the nature and extent of the sodium-CO₂ chemical reaction was developed. This test concept, which involves using a static capsule, was reviewed by KAERI. Also, KAERI developed a plan for conducting the static capsule test as part of defining the ultimate testing requirements.

ANL and KAERI jointly finalized the design of the exploratory capsule test that will provide preliminary data on the sodium-CO₂ chemical reaction to be utilized for the development of the main testing requirements. KAERI developed a detail plan for conducting the static capsule test to explore the nature and extent of the sodium-CO₂ chemical reaction. The plan includes detailed drawings of the test apparatus as well as test specifications. ANL reviewed the apparatus assembly drawings and testing procedures prepared by KAERI. Purchase orders have been made for the long-lead items of equipments and instruments.

The exploratory capsule test, which is currently being conducted at KAERI, provides preliminary information on the nature and extent of the sodium-CO₂ chemical reaction. This information will be utilized for the refinement of the main testing requirements.

Planned Activities

The reported activities complete the scope planned for Task 4.

Table 6. Project Task/Milestone/Deliverable Summary.

Task No.	Task Activity Description	Deliverable	Milestone Date Plan/Actual
1.0	Task 1. Computational Methods for Analysis of Passive Safety Design Features		
1.1	Document the project activities, organization responsibilities, and schedule. Prepare a project definition document to be updated as the project proceeds.	Report	Mar'03/Mar'03
1.2	Specify the model design specifications, including capabilities and interface data requirements (input and output). Prepare a model design specification document, to be updated as model revisions occur.	Report	Sep'03/Sep'03
1.3	Specify the model formulation, including phenomenological equations and numerical solution strategies. Prepare a model formulation specification document, to be updated as model revisions occur.	Report	Mar'04/Mar'04
1.4	Specify the computer code architecture, programming language, and data management techniques. Prepare a code architecture specification document, to be updated as model revisions occur.	Report	Sep'04/Sep'04
1.5	Implement the model as a computer code module. Perform initial proof testing as code implementation proceeds	Report	Jun'05/Jun'05
1.6	Prepare code documentation report, including final model design specifications, model formulation, numerical solution strategies, input data specification, and user guide.	Report	Jun'05/Jun'05
1.7	Perform code verification with multiple test problems. Prepare a code verification document containing objectives, problem definition, input data, and test problem results.	Report	Dec'05/Dec'05
1.8	Maintain an archive of all documentation, computer source code, verification problem input and output data	Report	Dec'05/Dec'05

Table 6. Project Task/Milestone/Deliverable Summary (cont.).

Task No.	Task Activity Description	Deliverable	Milestone Date Plan/Actual
2.0	Task 2. Comparative Analysis and Evaluation of Innovative Design Features		
2.1	Document the project activities, organization responsibilities, and schedule. Prepare a project definition document to be updated as the project proceeds.	Report	Mar'03/Mar'03
2.2	Specify the conceptual reactor designs to be considered in the safety evaluations. Document the designs in progress reports with sufficient detail to provide input data for safety analyses	Report	Jun'03/Jun'03
2.3	Identify the state-of-the-art computational methods to be used for the safety analyses, and specify the schedule and computational role for the advanced modeling developed in Task 1.	Report	Dec'03/Dec'03
2.4	Assemble required input data, and format the input data for use by the computational methods identified in Task 2.3.		Mar'04/Mar'04
2.5	Identify the transient scenarios to be analyzed for evaluation of safety design features. Specify the criteria to be applied for evaluation of merit.	Report	Mar'04/Mar'04
2.6	Perform baseline safety analyses of transient scenarios using state-of-the-art computational methods and document analysis results in progress reports.	Report	Dec'04/Dec'04
2.7	Perform safety analyses of transient scenarios including innovative design features for enhanced safety margin quantification. Employ both state-of-the-art and advanced modeling.		Dec'05/Dec'05
2.8	Document reactor design features and safety analysis results in a final project report.	Report	Dec'05/Dec'05

Table 6. Project Task/Milestone/Deliverable Summary (cont.).

Task No.	Task Activity Description	Deliverable	Milestone Date Plan/Actual
3.0	Task 3. Safety Implications of Advanced Technology Power Conversion and Design Innovations and Simplifications		
3.1	Complete investigation of cycle conditions and efficiencies for supercritical CO ₂ gas turbine power conversion systems coupled to sodium-cooled fast reactors with or without an intermediate heat transport circuit		May'03/May'03
3.2	Complete investigation of innovative concepts for sodium-to-supercritical CO ₂ modular heat exchangers		Jun'03/Jun'03
3.3	Complete development of conceptual designs for innovative sodium-to-supercritical CO ₂ heat exchangers		Nov'03/Nov'03
3.4	Complete development of conceptual designs for supercritical CO ₂ gas turbine Brayton cycle power conversion components and systems coupled to sodium-cooled fast reactors. Complete evaluation of component and cycle efficiencies. Complete development of control strategies for power conversion system.		Dec'03/Nov'03
3.5	Evaluate the design concepts of supercritical CO ₂ gas turbine Brayton cycle power conversion components and systems for the overpressure protection of primary system from the failure of the barrier between primary and CO ₂ systems.		Jun'03/Jun'03 Mar'04/Mar'04
3.6	Complete draft joint annual report contributions for first twelve months.	Report	Dec'03/Dec'03
3.7	Complete development of plant analysis computer code capability to model and analyze accidents involving the supercritical CO ₂ gas turbine Brayton cycle power conversion system conceptual designs.		Jul'04/Jul'04
3.8	Complete identification of set of accidents and initial analyses of accidents involving supercritical CO ₂ gas turbine Brayton cycle power conversion system.		Dec'04/Dec'04

Table 6. Project Task/Milestone/Deliverable Summary (cont.).

Task No.	Task Activity Description	Deliverable	Milestone Date Plan/Actual
3.9	Complete initial identification of needs for system or equipment modifications, revised control strategies, additional equipment, or new systems to assure or improve safety and complete initial analyses of their effectiveness.		Dec'04/Dec'04
3.10	Complete draft joint annual report contributions for second twelve month period.	Report	Dec'04/Dec'04
3.11	Complete analyses of consequences of heat exchanger boundary failure.		Mar'05/Mar'05
3.12	Complete analyses of accidents involving supercritical CO ₂ gas turbine Brayton cycle power conversion system and complete assessment of implications of system behavior for plant safety.		Jun'05/Jun'05
3.13	Complete identification of needs for system or equipment modifications, revised control strategies, additional equipment, or new systems to improve safety and complete analyses of their effectiveness.		Dec'05/Dec'05
3.14	Complete draft joint annual report contributions for third twelve months.	Report	Dec'05/Dec'05
4.0	Task 4. Post Accident Heat Removal and In-Vessel Retention		
4.1	Test Plan for the determination of liquidus/solidus and mobilization temperature for fuel/steel mixtures consisting of U, Zr, Fe, Cr, Ni, Mo, and Ce (Ce mocks up Pu).	Report	Dec.'03/Nov'03
4.2	Test Plan for Components and Materials Evaluation Loop (CAMEL) tests investigating molten fuel relocation behavior upon injection into coolant channels under sodium flow conditions.	Report	Dec'04/Dec'04
4.3	Test plan for the evaluation of the consequences of blowdown and intermixing of CO ₂ in a sodium pool.	Report	Dec'05/Dec'05

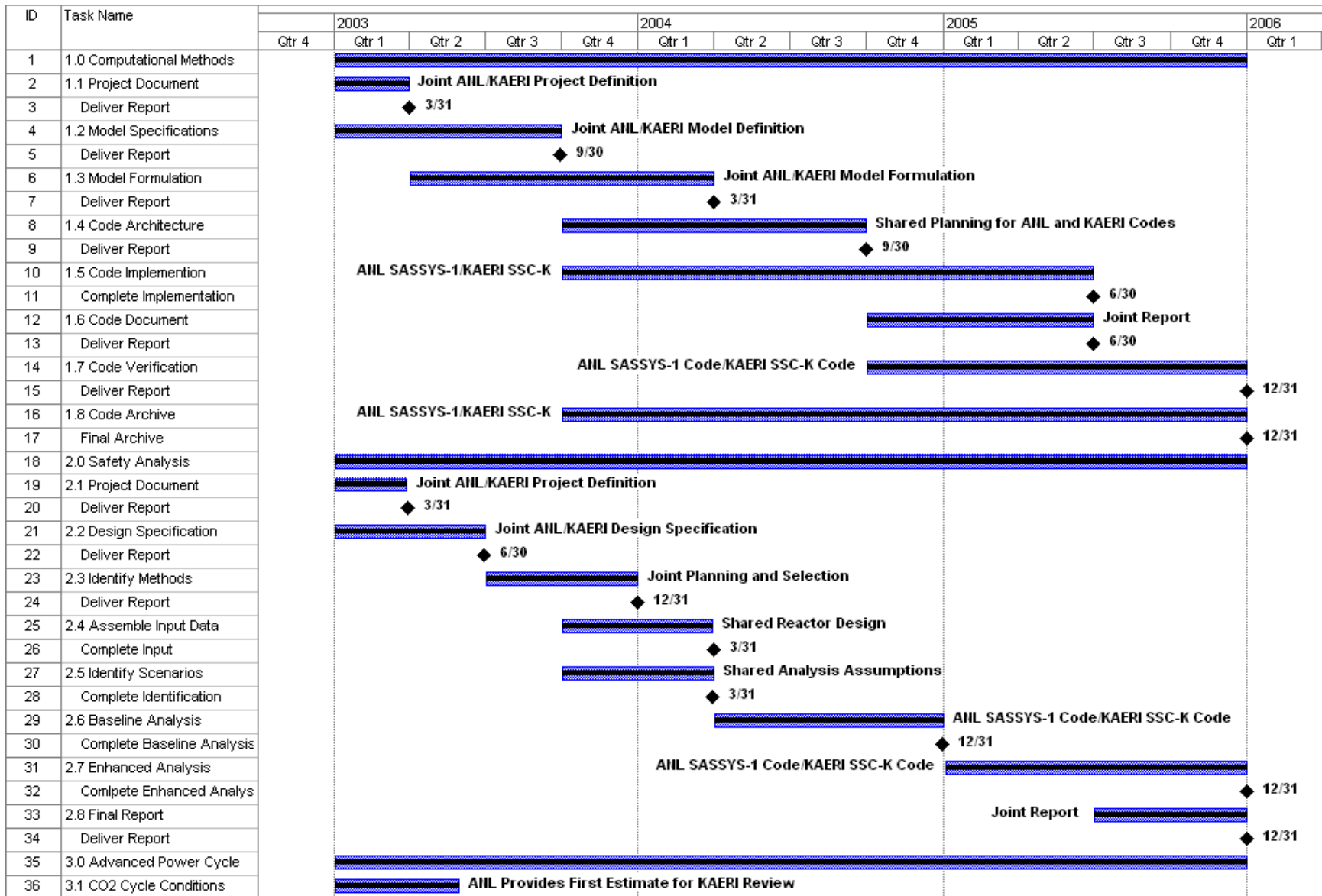


Fig. 52. Project Schedule Gantt Chart.

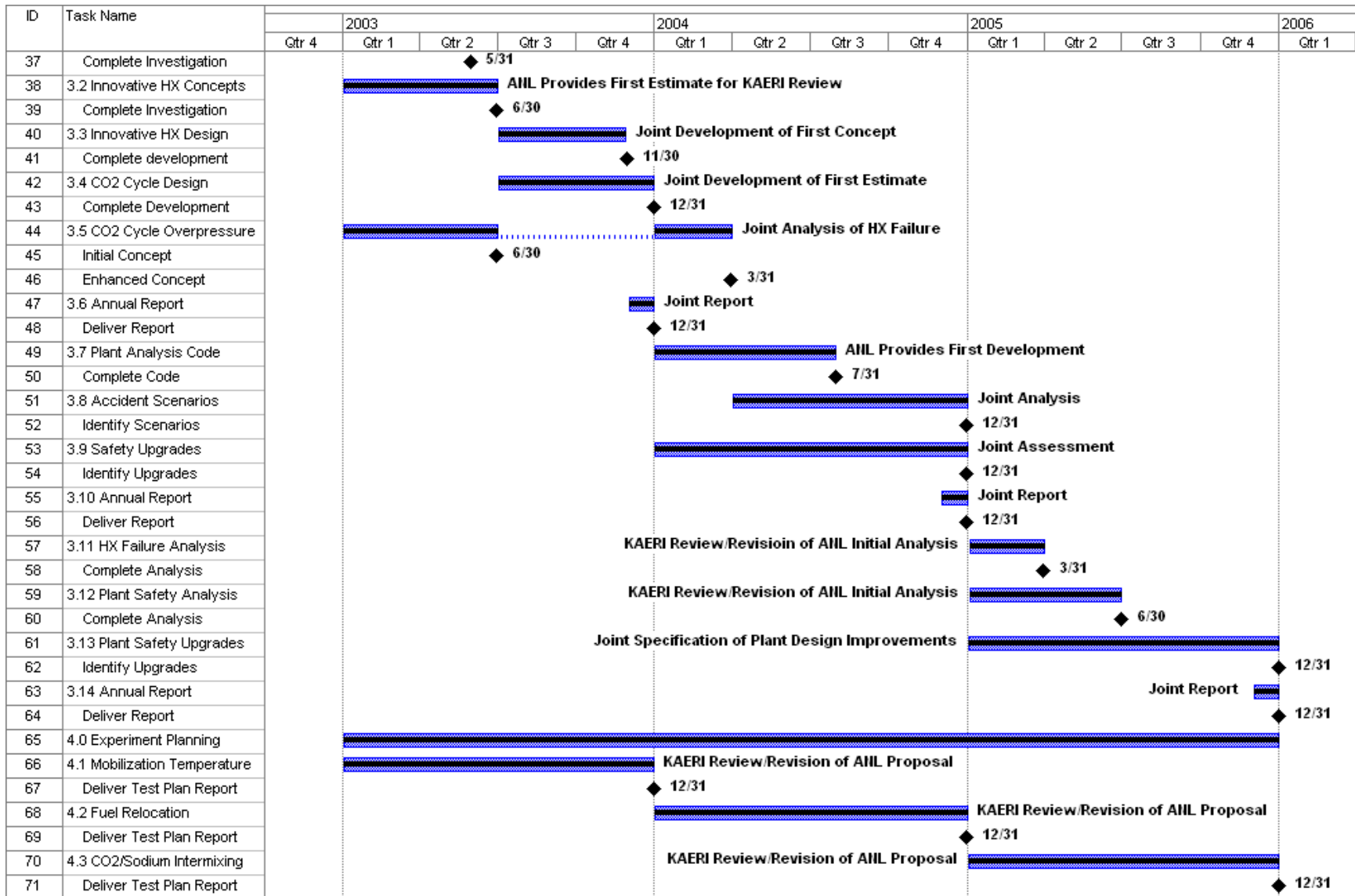


Fig. 52. Project Schedule Gantt Chart (cont.).

Project Publications

- A) F. E. Dunn, D. Hahn, H. Jeong, K. Ha, and J. E. Cahalan, *Whole Core Sub-Channel Analysis for LMR Passive Safety Analysis*, 14th Pacific Basin Nuclear Conference, Honolulu, Hawaii, March 21-25, 2004.
- B) H. Y. Jeong, K. S. Ha, Y. B. Lee, D. Hahn, F. E. Dunn, and J. E. Cahalan, *Evaluation of Thermal Conduction between Two Subchannels with a Computational Fluid Dynamics Code*, Proceedings of CHT-04, ICHMT International Symposium on Advances in Computational Heat Transfer, Norway, April 19-24, 2004.
- C) J. E. Cahalan, D. Hahn, W. Chang, and Y. Kwon, *Passive Safety Optimization in Liquid-Metal Cooled Reactors*, NUTHOS-6 International Topical Meeting on Nuclear Reactor Thermal Hydraulics, Operation and Safety, Nara, Japan, October 4-8, 2004.
- D) F. E. Dunn, J. E. Cahalan, D. Hahn, and H. Jeong, *Detailed Sub-Channel Treatment for Whole Core LMR Analysis*, NUTHOS-6 International Topical Meeting on Nuclear Reactor Thermal Hydraulics, Operation and Safety, Nara, Japan, October 4-8, 2004.
- E) H. Jeong, K. Ha, Y. Lee, D. Hahn, F. Dunn, J. Cahalan, *Evaluation of Turbulent Mixing Between Subchannels with a CFD Code*, NUTHOS-6 International Topical Meeting on Nuclear Reactor Thermal Hydraulics, Operation and Safety, Nara, Japan, October 4-8, 2004.
- F) J. J. Sienicki, D. H. Cho, A. V. Moisseytsev, S. Kim, and D. Hahn, *Thermal Hydraulic Feasibility of Supercritical Carbon Dioxide Brayton Cycle Power Conversion for the KALIMER-150 Sodium-Cooled Fast Reactor*, NUTHOS-6 International Topical Meeting on Nuclear Reactor Thermal Hydraulics, Operation and Safety, Nara, Japan, October 4-8, 2004.
- G) F. E. Dunn, J. E. Cahalan, D. Hahn, and H. Jeong, *Whole Core Sub-Channel Analysis in LMR Systems Codes, Current Status*, American Nuclear Society Meeting, San Diego, CA, June, 2005.
- H) Y. M. Kwon, W. P. Chang, Y. B. Lee, D. Hahn, and J. E. Cahalan, *Comparative Analysis for Evaluating Passive Safety Design Features of the KALIMER-150*, American Nuclear Society Meeting, San Diego, CA, June, 2005.
- I) H. Y. Jeong, D. Hahn, F. E. Dunn, and J. E. Cahalan, *Constitutive Relations for the Whole Core Sub-Channel Analysis Code*, American Nuclear Society Meeting, San Diego, CA, June, 2005.
- J) F. E. Dunn, J. E. Cahalan, D. Hahn, and H. Jeong, *Verification of Whole Core Sub-Channel Analysis in LMR Systems Codes*, American Nuclear Society Meeting, Washington, D.C., November, 2005.

References: Project Technical Reports

- 1) Proposal, International Nuclear Energy Research Initiative, Field Work Proposal 24452, Passive Safety Optimization in Liquid Sodium-Cooled Reactors, December, 2002.
- 2) International Nuclear Energy Research Initiative Project 2003-002-K, Passive Safety Optimization in Liquid Sodium-Cooled Reactors, *Quarterly Technical Progress Report*, January-March 2003.
- 3) International Nuclear Energy Research Initiative Project 2003-002-K, Passive Safety Optimization in Liquid Sodium-Cooled Reactors, *Project Definition Document* (Milestone Deliverable Tasks 1.1 and 2.1), March 2003.
- 4) International Nuclear Energy Research Initiative Project 2003-002-K, Passive Safety Optimization in Liquid Sodium-Cooled Reactors, *Quarterly Technical Progress Report*, April-June 2003 (Milestones 3.1, 3.2, 3.5), June 2003.
- 5) International Nuclear Energy Research Initiative Project 2003-002-K, Passive Safety Optimization in Liquid Sodium-Cooled Reactors, *Conceptual Reactor Design for Safety Evaluations* (Milestone Deliverable Task 2.2), June 2003.
- 6) International Nuclear Energy Research Initiative Project 2003-002-K, Passive Safety Optimization in Liquid Sodium-Cooled Reactors, *Annual Progress Report*, January-December 2003 (Milestone Deliverable Task 3.6), September 2003.
- 7) International Nuclear Energy Research Initiative Project 2003-002-K, Passive Safety Optimization in Liquid Sodium-Cooled Reactors, *Model Design Specifications for the Three Dimensional Fuel Subassembly Thermal Hydraulic Model* (Milestone Deliverable Task 1.2), September 2003.
- 8) International Nuclear Energy Research Initiative Project 2003-002-K, Passive Safety Optimization in Liquid Sodium-Cooled Reactors, *2003 Annual Review Presentation*, Seoul, November 6, 2003.
- 9) International Nuclear Energy Research Initiative Project 2003-002-K, Passive Safety Optimization in Liquid Sodium-Cooled Reactors, *Quarterly Technical Progress Report*, October-December 2003 (Milestones 3.3, 3.4), December 2003.
- 10) International Nuclear Energy Research Initiative Project 2003-002-K, Passive Safety Optimization in Liquid Sodium-Cooled Reactors, *State-of-the-Art Computational Methods for Safety Analysis* (Milestone Deliverable Task 2.3), December 2003.
- 11) International Nuclear Energy Research Initiative Project 2003-002-K, Passive Safety Optimization in Liquid Sodium-Cooled Reactors, *Test Plan for Determination of Liquidus/Solidus and Mobilization Temperature for Fuel/Steel Mixtures* (Milestone Deliverable Task 4.1), December 2003.
- 12) International Nuclear Energy Research Initiative Project 2003-002-K, Passive Safety Optimization in Liquid Sodium-Cooled Reactors, *Quarterly Technical Progress Report*, January-March 2004 (Milestones 2.4, 2.5, 3.5), March 2004.
- 13) International Nuclear Energy Research Initiative Project 2003-002-K, Passive Safety Optimization in Liquid Sodium-Cooled Reactors, *Model Formulation Specification for the Detailed Sub-Channel Model* (Milestone Deliverable Task 1.3), March, 2004.
- 14) International Nuclear Energy Research Initiative Project 2003-002-K, Passive Safety Optimization in Liquid Sodium-Cooled Reactors, *Quarterly Technical Progress Report*, April-June 2004 (Milestone 3.7), June, 2004.

- 15) International Nuclear Energy Research Initiative Project 2003-002-K, Passive Safety Optimization in Liquid Sodium-Cooled Reactors, *Quarterly Technical Progress Report*, July-September, 2004.
- 16) International Nuclear Energy Research Initiative Project 2003-002-K, Passive Safety Optimization in Liquid Sodium-Cooled Reactors, *Code Architecture Specification for the Detailed Sub-Channel Model*, (Milestone Deliverable Task 1.4), September, 2004.
- 17) International Nuclear Energy Research Initiative Project 2003-002-K, Passive Safety Optimization in Liquid Sodium-Cooled Reactors, *Baseline Safety Analysis of Transient Scenarios* (Milestone Deliverable Task 2.6), December, 2004.
- 18) International Nuclear Energy Research Initiative Project 2003-002-K, Passive Safety Optimization in Liquid Sodium-Cooled Reactors, *Test Plan for Investigations of Relocation and Freezing Behavior of Molten Fuel in Coolant Channels and Possible Chemical Interactions of Molten Fuel with Steel* (Milestone Deliverable Task 4.2), December, 2004.
- 19) International Nuclear Energy Research Initiative Project 2003-002-K, Passive Safety Optimization in Liquid Sodium-Cooled Reactors, *Annual Progress Report*, January-December 2004 (Milestones 3.8, 3.9, 3.10), December, 2004.
- 20) International Nuclear Energy Research Initiative Project 2003-002-K, Passive Safety Optimization in Liquid Sodium-Cooled Reactors, *2004 Annual Review Presentation*, Rockville, MD, January 26, 2005.
- 21) International Nuclear Energy Research Initiative Project 2003-002-K, Passive Safety Optimization in Liquid Sodium-Cooled Reactors, *Quarterly Technical Progress Report*, January-March 2005 (Milestone 3.11), March, 2005.
- 22) International Nuclear Energy Research Initiative Project 2003-002-K, Passive Safety Optimization in Liquid Sodium-Cooled Reactors, *Quarterly Technical Progress Report*, April-June 2005 (Milestone 1.5, 3.12), June, 2005.
- 23) International Nuclear Energy Research Initiative Project 2003-002-K, Passive Safety Optimization in Liquid Sodium-Cooled Reactors, *Code Documentation Report for the Three Dimensional Fuel Subassembly Thermal Hydraulic Model* (Milestone Deliverable Task 1.6), June, 2005.
- 24) International Nuclear Energy Research Initiative Project 2003-002-K, Passive Safety Optimization in Liquid Sodium-Cooled Reactors, *Quarterly Technical Progress Report*, July-September 2005, September, 2005.
- 25) International Nuclear Energy Research Initiative Project 2003-002-K, Passive Safety Optimization in Liquid Sodium-Cooled Reactors, *Annual Progress Report*, January-December 2005 (Milestones 3.13, 3.14), November, 2005.
- 26) International Nuclear Energy Research Initiative Project 2003-002-K, Passive Safety Optimization in Liquid Sodium-Cooled Reactors, *2005 Annual Review Presentation*, Jeju, Korea, November 8-9, 2005.
- 27) International Nuclear Energy Research Initiative Project 2003-002-K, Passive Safety Optimization in Liquid Sodium-Cooled Reactors, *Code Verification Report for the Three Dimensional Fuel Subassembly Thermal Hydraulic Model* (Milestone Deliverable Task 1.7), December, 2005.
- 28) International Nuclear Energy Research Initiative Project 2003-002-K, Passive Safety Optimization in Liquid Sodium-Cooled Reactors, *Enhanced Safety Analysis of Transient Scenarios* (Milestone Deliverable Task 2.7), December, 2005.

- 29) International Nuclear Energy Research Initiative Project 2003-002-K, Passive Safety Optimization in Liquid Sodium-Cooled Reactors, *Test Plan for Investigations of Intermixing Behavior of CO₂ and Sodium* (Milestone Deliverable Task 4.3), December, 2005.
- 30) International Nuclear Energy Research Initiative Project 2003-002-K, Passive Safety Optimization in Liquid Sodium-Cooled Reactors, *Final Report*, (Milestone 1.8, Milestone Deliverable 2.8), December, 2005.



Nuclear Engineering Division

Argonne National Laboratory
9700 South Cass Avenue, Bldg. 208
Argonne, IL 60439-4842

www.anl.gov



UChicago ►
Argonne_{LLC}

A U.S. Department of Energy laboratory
managed by UChicago Argonne, LLC